Characterization of PSI-mediated vacuolar transport through genomic and proteomic approaches

Sofia de Oliveira Santos
Master's degree in Cell and Molecular Biology
Faculty of Sciences of the University of Porto, Biology Department
2023

Supervisor
Cláudia Pereira, Researcher and Invited auxiliary professor, GreenUPorto, FCUP

Co-supervisor
Susana Pereira, Associate professor, GreenUPorto, FCUP

U.PORTO
FACULDADE DE CIÊNCIAS
UNIVERSIDADE DO PORTO

Dedicado aos meus pais e avós

Acknowledgments

“Your work is going to fill a large part of your life, and …to do what you believe is great work…is to love what you do…and you’ll know when you find it ”

Steve Jobs

Esta foi talvez a melhor, mas também a experiência mais desafiante dos últimos anos. Todo este trabalho não teria sido possível sem as pessoas que estiveram comigo ao longo deste ano e a quem gostaria de agradecer.

Primeiro, queria agradecer ao professor Pissarra por me ter acolhido no laboratório e por estar sempre disponível para nos ajudar.

Segundo, à minha orientadora, Cláudia. Obrigada pela liberdade desde o primeiro dia não só na condução deste projeto, mas também no dia a dia do laboratório. Por todo o conhecimento partilhado e acima de tudo pela tua disponibilidade, mesmo quando já nada parecia resultar. Foste incansável.

À professora Susana pelo apoio e por ter sempre uma palavra de carinho. Obrigada pela disponibilidade e ajuda nesta fase final. À professora Ana pela simpatia e ao professor Jorge por estar sempre disponível para nos ajudar no laboratório.

Ao Miguel, apesar das nossas discórdias, sem dúvida que foste a pessoa que mais me aturou no lab. Obrigada por tudo aquilo que me ensinaste, pelo desafio em entrar no mundo das interações e por estares sempre disponível para me ajudar.

A todas as amizades que fiz no lab. Ao João, obrigada por ajudares a cuidar das minhas plantinhas. À Ana, à Inês e à Diana por serem as minhas “labmates” e por todas as nossas conversas entre experiências. À Tatiana obrigada por toda a ajuda e dicas. À Jessy pelos nossos cafezinhos e pela amizade. Obrigada pelas dicas de organização.

À Catarina pela amizade e pelo apoio. Obrigada por estares sempre disponível para mais uma aventura e mal posso esperar pela próxima revenge. À Diana acho que foste a pessoa que mais aturou o meu mau feitio quando saía do laboratório depois de um dia em que nada parecia ter funcionado. Obrigada pela amizade que criámos nos últimos anos e um dia ainda irei a Amarante, prometo. À Amandine, pela amizade e conselhos.

À minha madrinha por todos os conselhos e pela ajuda nesta fase final.

Ao meu avô Manuel com quem aprendi a querer saber mais e mais, por todas as nossas viagens juntos e por seres a minha maior inspiração. À minha avó Lurdes

pelo apoio incondicional. Continuarei sempre a ser a vossa neta burra, depois da Cecília, claro.

Aos meus pais por me permitirem estudar aquilo que mais gosto, pelo apoio e por aturarem o meu mau feitio.

Ao Lano pela amizade e, acima de tudo, por ouvires as minhas reclamações. Já podemos ir a Paris.

Ao Poly e à Brie, por todos os miminhos, escrever foi mais divertido com vocês.

Resumo

O *Plant-Specific Insert* (PSI) é um domínio aminoacídico presente em algumas proteinases aspárticas (APs) de plantas, que é clivado durante processo de maturação das mesmas. Estudos *in vivo* mostraram que este domínio está associado ao correto endereçamento vacuolar das APs. O PSIs da cardosina A (PSI A) e da cardosina B (PSI B), duas APs de cardo, medeiam diferentes rotas de endereçamento para o vacúolo. O PSI A medeia uma via não convencional, independente do Golgi, em que as proteínas são diretamente levadas do Retículo Endoplasmático (ER) para o vacúolo. No entanto, o PSI B segue a via clássica ER – Golgi – Vacúolo. Nos últimos anos, novas vias não convencionais de endereçamento foram descobertas, e os estudos focam-se agora em caracterizar os mecanismos subjacentes às mesmas. Além disso, a dimerização dos PSIs pode ser um pré-requisito para o transporte mediado por este domínio, dado que um pH ácido promove a elicidade da estrutura do PSI e favorece a sua atividade através da dimerização. Este trabalho pretende caracterizar os determinantes moleculares envolvidos no trânsito mediado pelos PSIs, envolvendo estudos de genómica e proteómica. Deste modo, recorremos a mutantes de *Arabidopsis thaliana* da família de SNAREs SYP2 caracterizados por apresentarem defeitos no trânsito vacuolar. Um atraso no crescimento e no desenvolvimento das plantas das linhas mutantes foi observado e, através de Microscopia Eletrónica de Transmissão, foram identificadas alterações da estrutura de alguns organelos. Adicionalmente, para perceber se as alterações no trânsito vacuolar das linhas mutantes interferiam com o endereçamento de proteínas e/ou com o trânsito, o PSI A e PSI B, fundidos com a proteína fluorescente mCherry, foram expressos de forma transitória em plântulas das linhas mutantes. Através de Microscopia Confocal, verificou-se que o PSI A e o PSI B apresentaram defeitos no endereçamento vacuolar, na ausência de dois genes *SYP2*. Estudámos também o processo de dimerização do PSI A e PSI B ao testar a sua interação em diferentes condições de pH. Como tal, usámos uma estratégia combinada com recurso a técnicas *in vitro* (Co-imunoprecipitação e ensaios de *pull-down*) e *in vivo* (*Yeast Two-Hybrid* e 2in1 rBiFC). Os resultados obtidos mostram que os PSIs formam homo- e hetero- dímeros de forma dependente do pH. Além disso, os resultados sugerem ainda que uma sequência na região C-terminal do PSI A poderá ser responsável pela sua dimerização. Em suma, este trabalho apresenta novos dados sobre as vias seguidas pelos PSIs e a sua dimerização dependente do pH.

Palavras-chave: Plant-Specific Insert, SNAREs, 2in1 rBiFC, Protein-Protein Interactions, Co-immunoprecipitação, Pull-down assay, ER-Vacuole Sorting

Abstract

The Plant-Specific Insert (PSI) is a unique 100 amino acid domain present in some plant aspartic proteinases (APs), that is cleaved out during their maturation process. Several reports from *in vivo* studies showed that the PSI domain is associated with the vacuolar targeting of APs. PSI domains from cardosin A and cardosin B, two cardoon APs, are able to sort proteins to the vacuole via different pathways. Cardosin A PSI (PSI A) allows for a Golgi bypass, mediating an unconventional route to the vacuole by sorting proteins directly from the Endoplasmic Reticulum (ER) to the vacuole. In contrast, cardosin B PSI (PSI B) follows the classic ER - Golgi - Vacuole route. In recent years, novel unconventional vacuolar routes have been discovered, and focus has turned towards the characterization of the mechanisms behind those routes. Moreover, PSIs dimerization can be a prerequisite for their mediated transport, as an acidic pH promotes helicity in the PSI structure and favours its activity through dimerization. This study intends to further characterize the molecular determinants involved in PSI-mediated trafficking through genomic and proteomic studies. As so, we used *Arabidopsis thaliana* mutants from the SYP2 family of SNAREs reported to have vacuolar trafficking defects. A delay in growth and development was detected and, through Transmission Electron Microscopy, defects in the organelle organization were identified. Additionally, to assess if the vacuolar defects of the mutated lines interfered with protein sorting and/or trafficking, PSI A and B fused with mCherry tag were infiltrated in the mutants for transient expression. Through Confocal Microscopy, PSI A and PSI were shown to have their vacuolar sorting impaired when two *SYP2* genes were absent. To further increase our knowledge on cardosins PSIs dimerization, we aimed to study the dimerization process of PSI A and PSI B, by testing their interaction, under different pH conditions. A combined approach using *in vitro* (Co-Immunoprecipitation and Pull-down assays) and *in vivo* studies (Yeast-Two hybrid and 2in1 rBiFC) were used. Our results indicate that PSIs form homo- and hetero-dimers in a pH-dependent manner. Furthermore, the results suggest that a sequence in the C-terminal region of PSI A might be responsible for its dimerization. In summary, this work presents new insights regarding the routes followed by PSIs and the pH-dependent dimerization of PSIs.

Keywords: Plant-Specific Insert, SNAREs, 2in1 rBiFC, Protein-Protein Interactions, Co-Immunoprecipitation, Pull-down assay, ER-Vacuole Sorting

Table of Contents

LIST OF TABLES XI

LIST OF FIGURES XIII

LIST OF ABBREVIATIONS XV

1. INTRODUCTION 1

1.1 The endomembrane system 1

Endoplasmic Reticulum 3

Golgi 4

Pre-vacuolar Compartmens and Vacuole 6

1.2 soluble N-ethylmaleimide-sensitive-factor attachment protein receptors (SNAREs) 7

1.3 Vacuolar trafficking 10

Vacuolar sorting machinery 10

Vacuolar Sorting Determinants (VSDs) and Vacuolar Sorting Receptors (VSRs) 11

Pathways to the vacuoles - conventional and unconventional routes 12

1.4. Plant Aspartic Proteinases 15

Cardosins 16

1.5 Plant-Specific Insert 17

PSI-mediated routes 18

1.6 Aims 20

2. MATERIALS AND METHODS 23

2.1. Plant material and growth conditions 23

Development assays 23

2.2. Transmission Electron Microscopy 24

2.3 Vacuum infiltration for transient transformation of *Arabidopsis thaliana* seedlings 25

Seedlings' growth conditions 25

Agrobacterium tumefaciens culture preparation 25

2.4 Constructs generation 26
DNA amplification 27
Cloning 28
Enzymatic Restriction Cloning 28
Gateway Cloning 29
Preparation of chemical competent cells 30
Bacteria heat-shock transformation 31
Bacteria screening 32
Screening for positive clones 32
2.5 Large scale protein production and purification 32
2.6 Protein-protein interactions 34
Yeast Two-Hybrid 34
Co-immunoprecipitation assay 35
Pull-down assay 36
2.7 Polyacrylamide gel electrophoresis (SDS-PAGE) 36
Coomassie and Silver staining 37
Western Blot 38
2.8 Cell imaging: Confocal Laser Scanning Microscopy Analysis 38
2.9 Data processing and statistical analysis 38
3. RESULTS 41
3.1 Characterization of *Arabidopsis thaliana syp2* mutants 41
Phenotypic and developmental analysis 41
Ultrastructural characterization of syp2 lines 43
3.2 Expression of PSIs in vacuolar trafficking defective plants 47
3.3 In-vitro search for PSI-PSI interactions 50
PSI purification from bacteria 50
Cloning 50
Large scale purification 51
In-vitro PSI interactions 56

Pull-down assay 56
Pull-down assay at acidic pH 62
Pull-down assay with PSI A_Y95A/L99A 63
In vivo confirmation of PSI-PSI interactions 66
Y2H 66
2in1 rBiFC 68
Cloning 68
4.DISCUSSION 70
4.1 Characterization of vacuolar defective lines 70
4.2 Definition of trafficking pathways in vacuolar defective plants 72
4.3 In vitro cardoons' PSI-PSI interactions 74
PSI expression and purification 74
PSI-PSI interactions 74
4.4 In vivo cardoons' PSI-PSI interactions 77
5. CONCLUSIONS 79
6. REFERENCES 81
7. ATTACHMENTS 113

List of Tables

Table 1. List of the *Arabidopsis thaliana* lines used. 23
Table 2. List of constructs used. 26
Table 3. List of cDNAs used. 27
Table 4. Component mix for PCR reactions using NZYProof 2× Green Master Mix (NZYTech, Portugal). 28
Table 5. Program for PCR reactions using NZYProof 2× Green Master Mix (NZYTech, Portugal). 28
Table 6. Gateway cloning combinations performed for 2in1 rBiFC constructs. 30
Table 7. Bacteria used to replicate and express each construct and their respective antibiotic and concentration. 31
Table 8. List of primers for sequencing. 32
Table 9. List of experimental matings. 35
Table 10. Parameters and concentration of elution 1 resultant from PSI A and PSI B purification. 56

List of Figures

Figure 1. Overview of the routes of the plant endomembrane system. 2
Figure 2. Two major models for intra-Golgi trafficking. 6
Figure 3. Two distinct types of SNARE complexes containing four αα-helices to drive vesicle fusion events. 8
Figure 4. Exon–intron organization of the *SYP2* genes. 9
Figure 5. Conventional routes to the vacuoles. 13
Figure 6. Unconventional routes to the vacuoles. 14
Figure 7. Domain organization of Cardosin A and B and the sequential processing steps to acquire the mature form. 18
Figure 8 pH-dependent monomer-dimer equilibrium of PSI in solution. 16
Figure 9. Model procedure to obtain a 2in1 rBiFC vector. 30
Figure 10. *Arabidopsis thaliana syp2* mutant seedlings (Col-0), at 15 days after sowing (DAS). 41
Figure 11. *Arabidopsis thaliana* syp2 mutants (Col-0) primary root length measurement (A) and adventitious roots (B). 42
Figure 12. Developmental stages of *Arabidopsis thaliana syp2* mutants (Col-0). 43
Figure 13. Transmission electron micrographs of 15-day-old leaf cells from *Arabidopsis thaliana* wild-type (Col-0) A) to D). 44
Figure 14. Transmission electron micrographs of 15-days-old leaf cells from *Arabidopsis thaliana syp22-3* mutant (Col-0) A) to D). 45
Figure 15. Transmission electron micrographs of 15-days-old leaf cells from *Arabidopsis thaliana syp22-1 syp23* mutant (Col-0) A) to D). 46
Figure 16. Transmission electron micrographs of 15-day-old leaf cells from *Arabidopsis thaliana syp23* mutant (Col-0) A) to D). 47
Figure 17. Subcellular localization of Cardosin PSI A and PSI B fused with mCherry in cotyledon leaves of *Arabidopsis thaliana* wild-type and *syp22-3* and *syp23* mutant plants. 48
Figure 18. Subcellular localization of Cardosin PSI A and PSI B fused with mCherry in cotyledon leaves of *Arabidopsis thaliana* wild-type*, syp22-1 syp23 and syp22-3 syp23* mutant plants. 49
Figure 19. Restriction digestion analysis of pGEX-6p-1-GST-PSI A_Y95A/L99A with XhoI and Bam HI enzymes. 50
Figure 20. Alignment of the sequencing results of pGEX-6p1--GST-PSIA. 51
Figure 21. SDS-PAGE analysis of GST-PSI A-6xHis purification. 52

Figure 22. SDS-PAGE analysis of GST-PSI B-6xHis purification. 53
Figure 23. SDS-PAGE analysis of FLAG-PSI A-6xHis purification. 54
Figure 24. SDS-PAGE analysis of FLAG-PSI B-6xHis purification. 54
Figure 25. SDS-PAGE analysis of GST-PSI A_Y95A/L99A -6xHis purification. 55
Figure 26. SDS-PAGE analysis of PSI-PSI interactions by pull-down assay at pH 7.4 (A) and 6.8 (B). 58
Figure 27. Western Blot analysis to evaluate the presence of FLAG-tagged PSIs at pH 7.4 (A) and 6.8 (B). 59
Figure 28. SDS-PAGE analysis of PSI-PSI interactions by co-immunoprecipitation at pH 4.5 (A) and 3.5 (B). 61
Figure 29. SDS-PAGE analysis of PSI-PSI interactions by pull-down assay at pH 5.0. 62
Figure 30. SDS-PAGE analysis of PSI-PSI interactions by pull-down assay at pH 7.4 (A) and 6.8 (B). 64
Figure 31. Western Blot analysis to evaluate the presence of FLAG-tagged PSIs at pH 7.4 (A) and 6.8 (B). 65
Figure 32. Y2H analysis of PSI-PSI interactions. 67
Figure 33. Restriction digestion analysis of pDONR221-P1P4 with EcoRI and Eco32I enzymes. 68
Figure 34. Alignment of the sequencing results of pDONOR221-P1P4-PSI A. 68
Figure 35. Alignment of the sequencing results of pDONOR221-P1P4-PSI B. 69
Supplementary figure 36. pGEX-6p-1 empty plasmid map. 113
Supplementary figure 37. pDONR221-P1P4 empty plasmid map. 113
Supplementary figure 38. pBiFC-2 CC empty plasmid map. 114
Supplemenyary figure 39. Prey and bait Y2H plasmids 114

List of Abbreviations

2in1 rBiFC	2in1 Ratiometric Bimolecular Fluorescence
AP	Aspartic Proteinase
BiFC	Bimolecular Fluorescence
bp	Base Pair
CCV	Clathrin-Coated Vesicle
CLSM	Confocal Laser Scanning Microscope
Co-IP	Co-Immunoprecipitation
COPI	Coat Protein Complex I
COPII	Coat Protein Complex II
ctVSD	C-Terminal VSD
DAS	Days after sowing
DNA	Deoxyribonucleic acid
DVs	Dense Vesicle
EE	Early Endosome
ER	Endoplasmic Reticulum
ERAD	ER-associated protein degradation
ERGIC	ER–Golgi intermediate compartment
ERMEC	ER Microtubule-related Export Compartments
EYFP	Enhanced Yellow Fluorescent Protein
Fwd	Forward
His	Histidine
IPTG	isopropyl β-D-1-thiogalactopyranoside
LB	Luria Broth
LE	Late Endosome
LV	Lytic Vacuole
MPR	Mannose 6-Phosphate Receptor
MS	Murashige & Skoog
MVB	Multivesicular body
Na-PIPES	1, 4-piperazinediethanesulfonic acid
NASC ID	Nottingham Arabidopsis Stock Centre Identification
OD	Optical Density
ON	Overnight
PAC	Precursor-Accumulating Compartment

PCR	Polymerase Chain Reaction
PM	Plasma Membrane
PPI	Protein-Protein interactions
ppVSD	VSD Dependent on the Physical Structure of Protein
PRE	Presegment
PRO	Prosegment
PSI	Plant-Specific Insert
PSI A	Plant-Specific Insert A
PSI B	Plant-Specific Insert B
PSV	Protein Storage Vacuole
PVC	Pre-Vacuolar Compartment
rBiFC	Ratiometric Bimolecular Fluorescence Complementation
Rev	reverse
RT	Room temperature
SDS-PAGE	Sodium Dodecyl Sulphate–Polyacrylamide Gel Electrophoresis
SNARE	soluble N-ethylmaleimide-sensitive factor attachment protein receptor
ssVSD	Sequence-specific VSD
StAP PSI	*Solanum tuberosum* Aspartic Proteinase PSI
soyAP	*Soybean* AP
T-DNA	Transfer DNA
TEM	Transmission Electron Microscopy
TEMED	N,N,N′,N′ -Tetramethylethylenediamine
TGN	Trans Golgi Network
TMD	Transmembrane Domain
t-SNARE	Target SNARE
v/v	Volume Per Volume
VSD	Vacuolar Sorting Determinant
v-SNARE	vesicle SNARE
VSR	Vacuolar Sorting Receptor
w/v	Weight Per Volume
WT	Wild-type
Y2H	Yeast Two-Hybrid
YFP	Yellow Fluorescent Protein

1. Introduction

1.1 The endomembrane system

The endomembrane system of eukaryotic cells is crucial for the maintenance of key cellular functions, such as cell proliferation and homeostasis (Morita & Shimada, 2014; Surpin & Raikhel, 2004). This system is composed of a well-coordinated and complex network of trafficking routes and membrane-bound organelles. It includes the Endoplasmic Reticulum (ER), the Golgi, the trans-Golgi network (TGN), the Pre-vacuolar Compartment (PVC), the Vacuole, secretory vesicles, endosomes, and the plasma membrane (PM) (Frigerio & Hawes, 2008; Nebenführ, 2002). Although each of these organelles enacts distinct functions, the endomembrane system works as a whole in the synthesis, modification, packaging and transport of proteins and other molecules to their final destinations. The communication between the several compartments of the endomembrane trafficking system is accomplished via membrane-bound transport carriers (vesicles) (Rojo & Denecke, 2008). Therefore, the transport of molecules between compartments entails the formation and budding of membrane vesicles from a donor organelle, their transport, and consequent fusion with a target one (Rothman, 2002).

Two major pathways characterize the endomembrane trafficking in plant cells. First, the secretory pathway, where proteins produced *de novo* are transported from the ER to the Golgi apparatus via coat protein complex II (COPII) vesicles. After being sorted at the TGN/early endosome (EE), proteins are transported to the vacuole via multivesicular bodies (MVB)/PVC/late endosome (LE) or to the PM by clathrin-coated vesicles (CCVs) (Aniento et al., 2022; Okita & Rogers, 1996; Paez Valencia et al., 2016). This pathway is involved in plant development and reproduction. Second, the endocytic pathway, responsible for recycling molecules between the PM and endosomal compartments. Overall, traffic in each of these pathways involves the budding, transport, targeting, tethering, and fusion of transport vesicles to the membrane of the target organelle, ending with the recycling of the endomembrane components (Rojo & Denecke, 2008) (Figure 1). These events are mediated by numerous proteins, protein complexes, and vesicles, among which CCVs, COPII vesicles, coat protein complex I (COPI) vesicles, caveolin vesicles and dense vesicles (DVs) (Béthune & Wieland, 2018; Jahn & Scheller, 2006; Langemeyer et al., 2018; McMahon & Boucrot, 2011; Robinson & Pimpl, 2014; Sun & Brodsky, 2019; Wang et al., 2017; Zhang & Hughson, 2021). The mentioned carriers are essential to ensure the accurate traffic of molecules within the endomembrane system. The transport of molecules between the several compartments

of this system is not unidirectional. It can either be a forward transport, starting at the ER and heading towards the destination organelle, called anterograde transport. Or it can occur backwards, in the opposite direction described, called retrograde transport (Robinson, 2020).

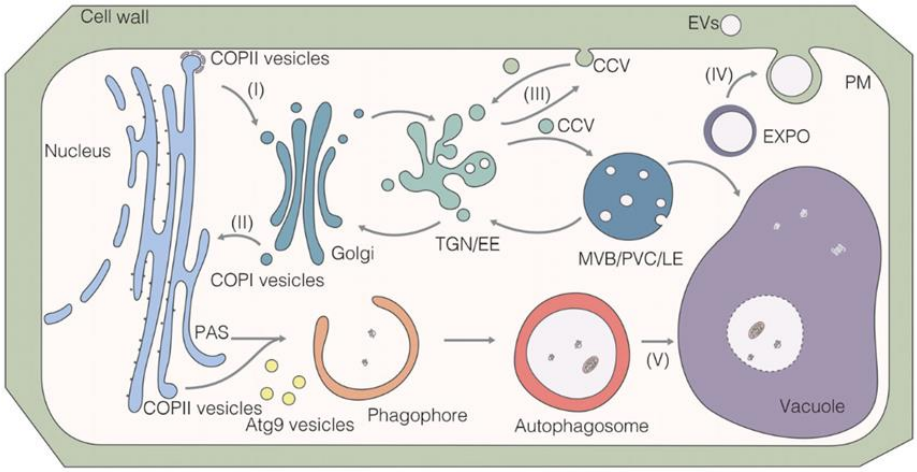

Figure 1. Overview of the routes of the plant endomembrane system. The endomembrane system in plant cells consists of several functionally distinct membrane-bound organelles, including the ER, Golgi, TGN/EE, MVB/PVC, and vacuole. Membrane trafficking in the endomembrane system can be achieved by multiple transport pathways, including (I) COPII-mediated ER–Golgi pathway; (II) COPI-mediated Golgi–ER pathway; (III) CCV-mediated exocytosis/endocytosis pathways; (IV) EXPO-mediated unconventional protein secretion pathway (Wanget al.,2010); and (V) autophagosome-vacuole pathway. ATG, autophagy-related gene; CCV, clathrin-coated vesicle; COPI, coat protein complex I; COPII, coat protein complex II; EE, early endosome; ER, endoplasmic reticulum, extracellular vesicles; EXPO, exocyst positive organelle; LE, late endosome; MVB, multivesicular body; PAS, phagophore assembly site; PM, plasma membrane; PVC, prevacuolar compartment; TGN,trans-Golgi network. Adapted from (Zeng et al., 2023).

More recently, a pathway for cell degradation has been discovered. Autophagy starts with the formation of a double membrane-bound organelle, the autophagosome, which imprisons intracellular molecules that are further degraded at the vacuole (Mizushima et al., 2011; Xie & Klionsky, 2007).

Although the mechanisms that regulate endomembrane trafficking in eukaryotes are highly conserved, plants display some unique mechanisms (Jürgens, 2004). The secretory and biosynthetic pathways of plant cells take part in several processes like stress responses, autophagy, gravitropism and hormone transport (Carter et al., 2004; Surpin & Raikhel, 2004). In recent years, the advances made in the microscopy field led to the discovery of new structures and organelles in plant cells.

Endoplasmic Reticulum

The ER is the point of entry to the endomembrane system, composed of an intricate network of cisternae and tubules, that form closed polygons, and the nuclear envelope (Staehelin, 1997; Stefano et al., 2014). In most cells, this organelle is packed between the PM and the tonoplast. Even though the ER has the ability to rearrange itself, two structurally and functionally different types can be distinguished - the rough and smooth ER. The first has ribosomes attached to its cytosolic surface and is involved in membrane and secretory protein synthesis. The second is ribosome-free, being responsible for Ca^{2+} signalling (Meusser et al., 2005). This heterogeneity enables the ER to perform different functions across different cellular regions (Meldolesi & Pozzan, 1998). The ER is a pleomorphic and dynamic organelle, and besides being the site of protein biosynthesis, folding and modification (Brandizzi et al., 2003), it performs a number of other functions among which lipid biogenesis (Wallis & Browse, 2010), calcium homeostasis (Hong et al., 1999) and protein body formation (Herman, 2008; Huang, 1996).

Plant cells can also have structures derived from the ER that perform specific functions (Chrispeels & Herman, 2000; Okita & Rogers, 1996; Staehelin, 1997) as the protein bodies in the endosperm of maize (*Zea mays*) or rice (*Oryza sativa*) that accumulate seed storage proteins (Herman & Larkins, 1999). One example of an ER-derived structure is the ER bodies found in the order Brassicales (Nakano et al., 2014), which have also been observed in Arabidopsis seedlings (Matsushima et al., 2002) and these structures are thought to be involved in plant defence (Matsushima et al., 2003).

The ER is a dynamic organelle and this feature can be perceived by its connection with the PM, Golgi, mitochondria, peroxisomes, chloroplasts, endosomes (English & Voeltz, 2013; Staehelin, 1997; Stefan et al., 2013; Stefano et al., 2014), and it is hypothesized that the ER contributes to the movement of other organelles (English & Voeltz, 2013). Besides, given its close proximity to the plant cell wall, it is a source of cellular signalling components such as hormone receptors and signalling complexes (Chen, Shen, Prywes, 2002; Friml & Jones, 2010), a sensor for cellular stresses (Chen et al., 2008) and some other unique roles can be highlighted, such as being a reservoir for hormone receptors (Chen, Randlet, et al., 2002; Friml & Jones, 2010) or, even being a storage compartment for proteins during plant growth and defence (Ibl & Stoger, 2012; Yamada et al., 2011).

Misfolded proteins can cause deleterious effects on cells and lead to functional deficiencies. Therefore, it is of the utmost importance for cells to possess quality control

mechanisms. The ER is responsible for monitoring the folding of transmembrane and soluble proteins destined to other cellular organelles or even of those retained at the ER (Claessen et al., 2012). This mechanism allows the export of correct folded proteins to their final destinations, in other words, proteins that have correctly folded into their native conformation (Schröder & Kaufman, 2005a, 2005b). However, the ones that have not acquired a proper folding, or even those that are unfolded, are recognized by chaperones whose function is to assist in the folding of these proteins (Strasser, 2018). Most ER-resident proteins monitor the folding and assembly events (Anelli & Sitia, 2008). Since protein folding is an error-prone process, misfolded proteins are retained in the ER and sent for degradation to the cytosol (Vembar & Brodsky, 2008), or, alternatively, to the lytic vacuole (Schmitz & Herzog, 2004) via ER-associated protein degradation (ERAD) (Meusser et al., 2005). Membrane and soluble proteins that have acquired the correct folding are finally transported to other organelles or outside the cell along the secretory pathway (Vitale & Denecke, 1999).

Golgi

The Golgi apparatus is a key organelle that lies at the junction of both secretory and endocytic pathways. It is composed of flattened stacked sacs named cisternae that form the Golgi stack (Glick & Nakano, 2009). The stacked structure of the Golgi is in close association with the ER (Sparkes et al., 2009), and it is the most striking feature of this organelle, making it easy to identify among the several components in the cytoplasm (Porter, 1961). Cisternae of each Golgi stack are polarized between the *cis*- and *trans*-side (Mellman & Warren, 2000). There are three different types of cisternae: the *cis-cisternae*, turned towards the ER, which represents the point of entry for secretory proteins coming from the ER into the Golgi, the *median-cisternae* and the *trans-cisternae*. Among eukaryotes, there are some differences regarding Golgi structure. In baker's yeast (*Saccharomyces cerevisiae*) there is no Golgi stack and individual cisternae are scattered through the cytoplasm (Suda & Nakano, 2012). In animal cells, Golgi stacks are located around the perinuclear area and appear as a clustered and immobile structure, whereas in plants they are motile and dispersed through the cytoplasm (Ito et al., 2014). However, in animal cells there is a structure that is absent in plant cells termed ER–Golgi intermediate compartment (ERGIC). This is a microtubule-dependent structure crossing at the interface between ER exit sites (ERES) and the cis-Golgi (Appenzeller-Herzog & Hauri, 2006).

Golgi cisternae are structurally and biochemically different, as they contain enzymes that are distributed across a gradient along the stacks (Moore et al., 1991).

The Golgi is viewed as a station for carbohydrate synthesis, in fact, it is involved in the processing of oligosaccharide side chains of secretory/vacuolar glycoproteins and glycolipids (Strasser, 2016) and in the synthesis of cell wall polysaccharides (Meents et al., 2019; Zhang & Staehelin, 1992). Besides, it also participates in the sorting of secretory proteins destined for the vacuole and the recycling of proteins internalized from the PM that are either recycled back to the PM or sent to the vacuole for degradation (Alberts et al., 2002). Inside the Golgi stacks, there is a continuous *cis*- to *trans*- flow of proteins (Dunphy & Rothman, 1985; Moore et al., 1991), during which they acquire post-translational modifications (such as glycosylation, sulfation and phosphorylation). After being modified, proteins reach the TGN, the distribution centre of Golgi-derived cargo, where proteins are sorted into carrier vesicles for subsequent transport to the PM or the vacuoles (Alberts et al., 2002; Glick & Nakano, 2009). The TGN also participates in the trafficking and recycling of endosomal cargoes, thus the name TGN/EE (Viotti et al., 2010). Additionally, the Golgi acts as a membrane frame for adhesion of varied signalling, sorting and cytoskeleton proteins (Altan-Bonnet et al., 2003; De Matteis & Morrow, 2000; Donaldson & Lippincott-Schwartz, 2000).

Proteins enter the cis-Golgi, move along the med-Golgi and exit trough the trans-Golgi (Xiang et al., 2013). However, intra-Golgi trafficking is still a matter of great debate and focuses has been on how cargoes are transported through the cisternae stacks. There are two major models proposed. One is the vesicular transport model (stable compartments) and the other is the cisternal maturation model (Figure 2). In the cisternal maturation model, Golgi cisternae themselves are viewed as transient cargo carriers coming from the ER that gather at the cis-Golgi. Cisternae nature change as they mature, and they move forward towards the TGN. In this model, COPI vesicles recycle resident Golgi proteins by retrograde transport (Boncompain & Weigel, 2018; Glick & Nakano, 2009). This model is supported by data that showed that cargoes larger than COPI vesicles are able to travel across Golgi stacks (e.g., scales of algae) and transported forward without being packed into COPI vesicles (Becker et al., 1995; Brown et al., 1970; Melkonian et al., 1991). On the other hand, in the vesicular transport model, the Golgi stack is viewed as a stable compartment, with a set of resident proteins and cargoes travelling from one cisterna to another via anterograde COPI vesicles (Rothman & Wieland, 1996). This model seems to offer an explanation for the polarity of the Golgi since Golgi stacks are viewed as distinct sub-organelles (Dunphy & Rothman, 1985; Farquhar, 1985). Besides, studies reported the existence of COPI vesicles around the Golgi (Farquhar, 1985; Orci et al., 1986). Also, a cell-free reconstitution assay in the 1980's reported that vesicular transport between cisternae was mediated by COPI

vesicles (Rothman & Wieland, 1996). Notably, further studies are needed to comprehend the mechanisms behind intra-Golgi transport, since the levels to which the different models explain it are also very different.

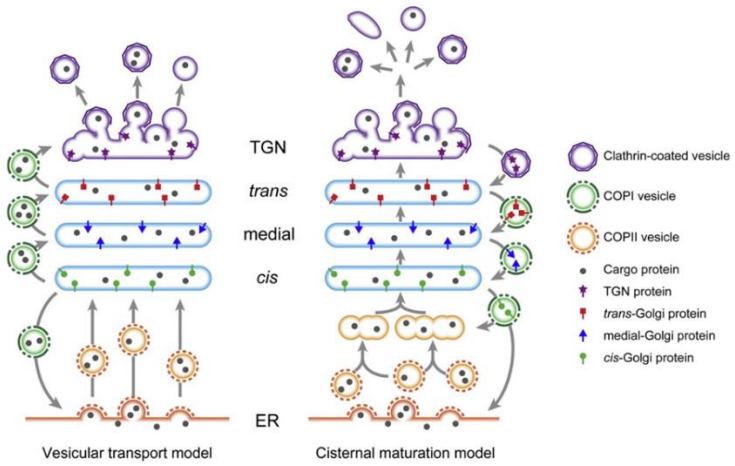

Figure 2. Two major models for intra-Golgi trafficking. (Left) The vesicular transport (stable compartments) model. In this model, the Golgi cisternae are stable and distinct sub-organelles with different resident proteins. Cargo proteins are transported from one cisterna to the next by anterograde COPI vesicles, whereas the Golgi proteins are excluded from them and remain in the cisternae. Cargo proteins reach the TGN and exit by clathrin-coated vesicles or other carriers. (Right) The cisternal maturation model. In this model, the Golgi cisternae themselves function as the cargo carriers. They are transient compartments that are newly formed by homotypic fusion of COPII vesicles, progress from cis to trans, and break down at the TGN stage. The Golgi proteins recycle back from later to earlier cisternae by retrograde COPI vesicles, and the nature of the cisternae gradually changes as they progress. Adapted from (Ito et al., 2014).

Pre-vacuolar Compartmens and Vacuole

The PVCs, also termed MVBs or LEs are single membrane-bound organelles considered to serve as intermediates in the transport of vacuolar proteins between the TGN and the vacuoles in the secretory pathway (Bethke & Jones, 2000; Lam et al., 2005; Tse et al., 2004). Besides that, PVCs also mediate the endocytic pathway to the vacuole serving as LEs (Lam, Ching, et al., 2007, Lam, Tse, Miao, et al., 2007, Lam, Tse, Robinson, Jiang, 2007, Lam et al., 2008; Robinson et al., 2007, 2008).

Vacuoles are the largest organelle in plant cells, occupying up to 80-90% of cell volume (Bassham, Brandizzi, et al., 2008; Eisenach et al., 2015; Marty, 1999) and they are involved in several essential functions, namely the storage of proteins, defence against pathogens and abiotic factors, as well as maintenance of cell homeostasis contributing to growth and development (Bassham, Brandizzi, et al., 2008; Martinoia et al., 2007; Marty, 1999). Besides, vacuoles are a site for storage of water, nutrients, hormones, ions, secondary metabolites, and proteins (Bassham et al., 2018), toxic cell residues, excess solutes and waste products (Bethke & Jones, 2000; Hatsugai et al.,

2004; Jiang et al., 2000; Martinoia et al., 2000), as well as participating in programmed cell death (Hara-Nishimura & Hatsugai, 2011).

In plant cells, there are two major types of vacuoles: the protein storage vacuoles (PSVs) and the lytic vacuoles (LVs). PSVs are responsible for the accumulation of vacuolar storage proteins, being found not only in storage tissues (cotyledons, endosperm, and tubers), but also in vegetative tissues of mature plants (bark, leaves, pods) (Müntz, 1998; Vitale & Hinz, 2005; Zouhar et al., 2010). To encompass these functions, PSVs have a higher pH and lower hydrolytic activity. Nevertheless, toxic proteins can also accumulate in PSVs, such as protease inhibitors and lectins (Jørgensen et al., 2011; Michael Lord & Spooner, 2011; Souza et al., 2011). In contrast, DSLVs have a lower pH and higher hydrolytic activity, as they mediate the degradation of macromolecules and other compounds (Frigerio & Hawes, 2008; Rogers, 2008) along with their role in senescence and programmed cell death (Bassham, Brandizzi, et al., 2008; Shimada et al., 2018). LVs are usually found in vegetative tissues (Shimada et al., 2018), are the equivalent of animal lysosomes or yeast vacuoles, and are used for storage of waste compounds (Jürgens, 2004). PSVs and LVs can sometimes coexist within the same cell, as reported in studies done in root tip cells of barley and pea seedlings (Olbrich et al., 2007; Paris et al., 1996). Curiously, another study done in Arabidopsis seeds reported that, during germination, the LV was not generated *de novo*, it was instead inserted in the PSV and derived from it (Bolte et al., 2011; Olbrich et al., 2007; Zheng & Staehelin, 2011).

The existence of two functionally different vacuoles with different contents alludes to the existence of distinct trafficking pathways for different cargoes. Moreover, LVs can be transformed into PSVs and *vice versa*, depending on the physiological conditions, to allow plants a higher degree of flexibility when facing a changing environment (Bolte et al., 2004; Herman & Larkins, 1999; Jürgens, 2004; Murphy et al., 2005; Pereira et al., 2014; Swanson & Jones, 1996; Vitale & Hinz, 2005).

1.2 soluble N-ethylmaleimide-sensitive-factor attachment protein receptors (SNAREs)

Protein trafficking within the secretory and endocytic pathways is a precise mechanism that is primarily mediated by vesicles, a mechanism present and crucial among eukaryotic cells (Sanderfoot et al., 1999). Vesicular transport involves the formation, translocation, tethering, and fusion of vesicles with the target compartment

(Cai et al., 2007). The specificity and subsequent fusion between the transport vesicle and the target organelle is determined by proteins such as specific vesicle soluble N-ethylmaleimide-sensitive-factor attachment protein receptors (SNAREs) (Jahn & Scheller, 2006) that were considered critical for membrane fusion (Söllner et al., 1993). These proteins are classified into Qa-, Qb-, Qc- and R-SNAREs in accordance with their central amino acids, and all share a hydrophobic domain (Jahn & Scheller, 2006). This system, conserved among eukaryotes (Jahn & Scheller, 2006; Pratelli et al., 2004; Surpin & Raikhel, 2004), is vital for the transport of newly synthesized proteins, recycling of pre-existent ones, as well as organelle formation (Jahn & Scheller, 2006). In the Arabidopsis genome, there are about 65 SNAREs, that are sub-grouped in several families (Saito & Ueda, 2009; Sanderfoot, 2007; Sanderfoot et al., 2000). These proteins are involved in various biological processes, including plant development, (Ohtomo et al., 2005), vacuolar transport and biogenesis (Ebine et al., 2008).

Vesicular fusion occurs through interactions between v-SNAREs (on the vesicles) and t-SNAREs (on the target compartment) to form a trans-SNARE complex (Söllner et al., 1993). The two membrane layers are brought in close proximity when v-SNAREs and t-SNAREs assemble into a tight trans-SNARE complex, which leads to the fusion of the two membranes and allows the release of vesicle contents to the lumen (Bassham & Blatt, 2008; McNew et al., 2000; Pompa et al., 2017; Saito & Ueda, 2009; Sanderfoot & Raikhel, 1999). After this, the trans-SNARE complex becomes a cis-SNARE complex. Trans-SNARE complexes are formed by three different Q-SNAREs and one R-SNARE (Bock et al., 2001) (Figure 3).

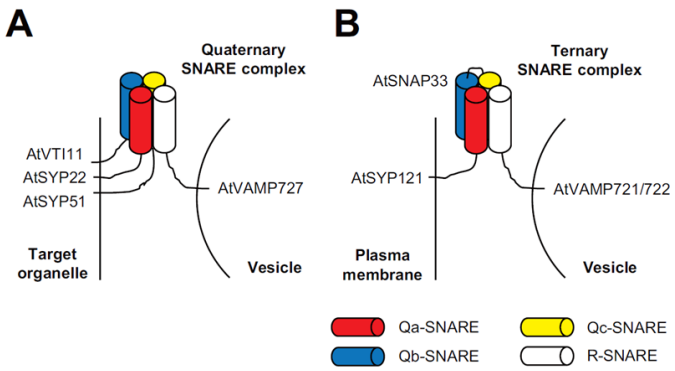

Figure 3. Two distinct types of SNARE complexes containing four αα-helices to drive vesicle fusion events. (A) Four different SNAREs (Qa+ Qb + Qc + R) form a quaternary SNARE complex for fusing a vesicle with an intracellular compartment, (B) three different ones (Qa+ Qbc + R) do a ternary SNARE complex for exocytosis (vesicle fusion with the PM). Known Arabidopsis SNARE complexes are; (A) AtSYP22-AtVTI11-AtSYP51-AtVAMP727 (Qa-Qb-Qc-R) quaternary SNARE complex, and (B) AtSYP121-AtSNAP33-AtVAMP721/722 (Qa-Qbc-R) ternary SNARE complex. Adapted from (Kwon et al., 2018) .

The SYP2 family of proteins has three genes, *SYP21/PEP12*, *SYP22/VAM3* and *SYP23/PLP*, which belong to the Qa-SNAREs group (Kim & Brandizzi, 2012; Sanderfoot, 2007; Sato et al., 1997; Yano et al., 2003). SYP21 localizes to the PVC (Conceição et al., 1997; Sanderfoot & Raikhel, 1999), while SYP22 localizes to the PVC and tonoplast (Ebine et al., 2008; Niihama et al., 2005; Sanderfoot, Kovaleva, et al., 2001; Yano et al., 2003). The role of SYP23, which lacks a transmembrane domain (TMD) and lies in the cytoplasm, is still uncertain. Moreover, the SYP2 family of proteins was shown to have redundant functions in several biological processes, such as vacuolar protein sorting. Single mutants were observed to be viable (Shirakawa et al., 2010), whereas *syp21/syp22* double mutants are known to be lethal, as SYP21 and SYP22 functions are interchangeable and redundant (El Kasmi et al., 2013; Shirakawa et al., 2010; Uemura et al., 2010; Zouhar et al., 2009). SYP22 forms a SNARE complex with VTI11 (Qb-SNARE), SYP5 (Qc-SNARE) and VAMP727 (R-SNARE), which was observed to be crucial for vacuolar traffic and vacuole morphogenesis (Ebine et al., 2008; Sanderfoot, Pilgrim, et al., 2001). The *syp22* mutant was shown to exhibit semi-dwarfism and late flowering (Ebine et al., 2012; Ohtomo et al., 2005; Shirakawa et al., 2009; Ueda et al., 2006). Regarding SYP23, it was demonstrated that it can also form a complex with VTI11 and SYP5, and overexpression of *SYP23* was observed to complement *syp22* mutant (Shirakawa et al., 2010). Thus, it has been hypothesized to function in vacuolar trafficking as SYP21 and SYP22. However, since it lacks the TMD, the mechanism of SYP23 function is poorly understood. It can either interact with a preformed SNARE complex, or it is recruited by other proteins to form the SNARE complex (Ohtomo et al., 2005). The *SYP2* single and double mutants were obtained by T-DNA insertion (Figure 4) (Ohtomo et al., 2005; Shirakawa et al., 2010).

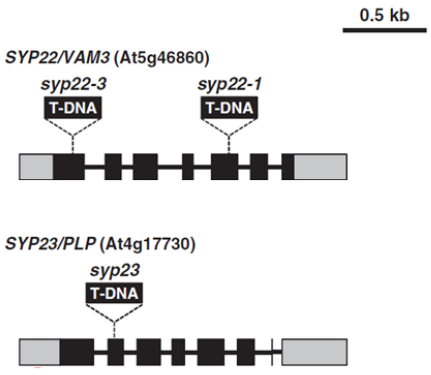

Figure 4. Exon–intron organization of the *SYP2* genes. T-DNA insertions are shown for *syp22-1* (SALK_060946), syp*22- 3* (SALK_075924) and *syp23* (SALK_073456). Closed boxes, exons; grey boxes, untranslated regions; solid lines, introns. Adapted from (Shirakawa et al., 2010).

1.3 Vacuolar trafficking

Vacuolar transport is characterized by the delivery of proteins to the plant vacuole (Cevher-Keskin, 2020; Ebine et al., 2014). When compared to mammalian or yeast systems, plants display unique and complex vacuolar trafficking pathways (Ebine et al., 2014). Due to the importance of plant vacuoles in maintaining cell homeostasis and the agronomic value of proteins stored in them, remarkable progress has been achieved in the last years, as new insights about plant vacuolar proteins, how they are sorted and the route they follow have been obtained (Marcos Lousa et al., 2012; Rojo & Denecke, 2008). Nevertheless, more recent studies have highlighted alternative mechanisms of vacuolar trafficking, that are considered unconventional, and have fuelled intense debate on the matter (Goring & Sansebastiano, 2018; Vieira et al., 2019). In the unconventional vacuolar route, some proteins reach the vacuole directly from the ER, bypassing the Golgi, probably through a recently described compartment called ERMEC (De Caroli et al., 2021).

Many proteins and other cargoes upon their synthesis follow a determined pathway until reaching their final destination. Protein-Protein interactions (PPIs) between the sorting receptors of the protein and the cargo proteins determine the route followed by it (Ahmed et al., 2000; Cereghino et al., 1995; Cooper & Stevens, 1996; DaSilva et al., 2005, 2006; Fuji et al., 2007; Humair et al., 2001; Jiang & Rogers, 1998; Kirsch et al., 1994; Paris et al., 1997; Shimada et al., 2003; Suen et al., 2010). Again, compared to mammal and yeast cells, studies about sorting motifs are scarce (Marcos Lousa et al., 2012). Overall, it is believed that proteins synthesized *de novo* leave the ER, go through the Golgi complex-TGN-PVC, and traffic to the vacuole, other compartments, or the cell surface, through the secretory pathway (Marcos Lousa et al., 2012; Rojo & Denecke, 2008).

Vacuolar sorting machinery

The traffic of vacuolar proteins to the different types of vacuoles is mediated by vesicles and encompasses the ER, the Golgi apparatus, the TGN and the endosomes/PVC. Vacuolar proteins reach vacuoles because they possess one or more Vacuolar Sorting Determinants (VSDs) that are recognized by sorting receptors (Lousa & Denecke, 2016; Luo et al., 2014; Peixoto et al., 2018). There are two families of sorting receptors: Vacuolar Sorting Receptors (VSRs) and receptor-homology-transmembrane-RING-H2 proteins (Jiang et al., 2000; Jiang & Rogers, 1998; Kirsch et al., 1994).

Vacuolar Sorting Determinants (VSDs) and Vacuolar Sorting Receptors (VSRs)

There are three different types of VSDs: the sequence-specific VSD (ssVSD), the C-terminal VSD (ctVSD), and the physical structure VSD (psVSD) (Matsuoka & Neuhaus, 1999; Vitale & Raikhel, 1999). ssVSDs are composed of conserved motifs in their sequence and are frequently located at the N-terminus of a protein, although they function independently of their molecular position (Koide et al., 1997, 1999; Neuhaus & Rogers, 1998), being described some located at the C-terminus and others internally (Maruyama et al., 2006). ssVSDs are mainly recognized by VSRs for sorting to the LV (Holwerda et al., 1992; Koide et al., 1997; Nakamura & Matsuoka, 1993; Sanmartín et al., 2007). In contrast, ctVSDs direct proteins to the PSV in most cases (Peixoto et al., 2016; Pereira et al., 2013), its sequence does not seem to be conserved, they are located at the C-terminal part of the protein, have hydrophobic amino acids (Frigerio et al., 2001) and C-terminal peptides are sufficient for vacuolar targeting, as it is the case of the C-terminal VSD of tobacco chitinase A (Bednarek & Raikhel, 1991; Neuhaus et al., 1991; Schroeder et al., 1993). psVSDs are mainly found in storage proteins, and molecules comprising these determinants are often dependent on the tertiary structure of proteins for proper formation of the final motif (Jolliffe et al., 2012; Neuhaus & Rogers, 1998; Zouhar et al., 2009).

During the trafficking of proteins towards the PSVs and LVs, there are numerous molecular factors involved, among which are the VSRs (Craddock et al., 2008; DaSilva et al., 2005, 2006; Fuji et al., 2007; Jolliffe et al., 2004; Shimada et al., 2003), which specifically recognize LV cargoes and PSV proteins among the other organellar proteins. In fact, they must bind to cargoes at the donor compartment and release them at the acceptor one. VSRs are transmembrane proteins highly conserved among plant species and contain a luminal domain, a TMD, and a C-terminal cytosolic tail. Their large luminal domain binds to proteins, while the cytosolic tail has signals required for receptor trafficking. They are involved in sorting to both lytic and storage vacuoles (Robinson & Neuhaus, 2016). A study showed that VSRs bind ligands at the ER and Golgi (Künzl et al., 2016). These data suggest that VSRs are involved in transport from the ER and/or Golgi to the TGN, while post-TGN trafficking to the vacuole is believed to be VSR-independent (Robinson & Neuhaus, 2016; Robinson & Pimpl, 2014). Nevertheless, further studies are required to understand the role of VSRs in vacuolar protein trafficking.

Pathways to the vacuoles - conventional and unconventional routes

Over the years, advances have been made in highlighting the molecular mechanisms behind vacuolar protein trafficking. Although some points of the trafficking mechanisms are common to both vacuoles (PSVs and LVs), there are some aspects that are specific to either trafficking to the LV or PSV. Moreover, those differences might be enhanced and challenged by the growing number of studies reporting unconventional routes to the vacuole. First, trafficking to the PSV will be described, followed by trafficking to the LV, always considering the classical and alternative routes.

Regarding the trafficking of proteins to the PSV, the route followed by the protein, being Golgi-dependent or Golgi-independent, is dictated by the cargo protein itself and the stage of plant development (Robinson et al., 2005; Rojo & Denecke, 2008). After being sorted at the Golgi, the trafficking of storage proteins into the PSV is mediated by DVs, small vesicles that carry intrinsic membrane proteins destined for the PSV (Vitale & Hinz, 2005). These vesicles were first discovered in common bean (Chrispeels, 1983), but more species like wheat, pea and Arabidopsis were reported to contain them too (Hinz et al., 1999, 2007; Kim et al., 1988). DVs formation is triggered by the accumulation of storage proteins at the cis-Golgi interface. Upon this, small vesicles are transferred to the TGN, ending with their release from the TGN (Hinz et al., 2007; Hwang, 2008). Surprisingly, DVs do not contain a protein coat, which allows them to fuse directly with the PSV or MVB (Hohl et al., 1996; Jiang et al., 2000, 2001; Robinson et al., 1998). MVBs, organelles that are common to all eukaryotes, are formed by multiple internal vesicles and take part in several post-Golgi processes of the biosynthetic trafficking pathway. After fusing to MVBs, proteins inside DVs are released and delivered to the PSV (Tse et al., 2004). Besides, instead of fusing with MVBs, DVs can also fuse directly with PSVs. The trafficking pathway to the PSV in a Golgi-dependent manner can be defined as the classic ER-Golgi-DVs-MVBs-PVC-PSV route (Figure 5). Despite receptor-mediated sorting might account for protein transport to the PSV, this transport mainly occurs through aggregation sorting (Molina et al., 2006). In what concerns receptor-mediated sorting, BP-80 homologues and RMR proteins are involved in trafficking to PSVs.

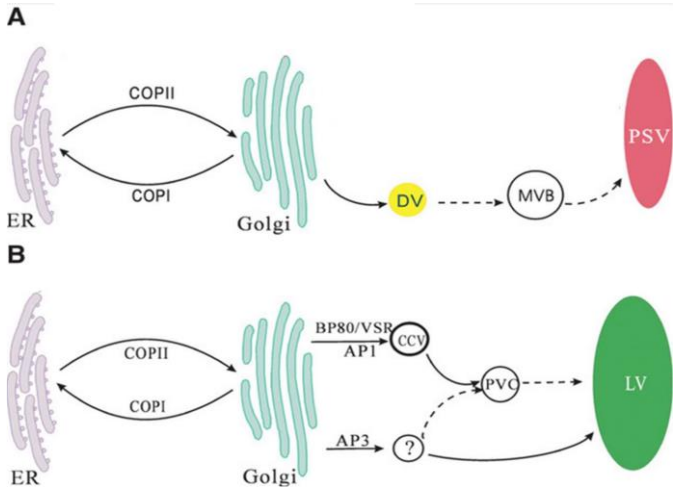

Figure 5. Conventional routes to the vacuoles. (A) Proteins targeted to the PSV begin their path in the cell at the ER and may follow a Golgi-dependent pathway. Through this pathway, proteins leave the ER via COPII vesicles to theGolgi, where they are aggregated and develop into the cargo of DVs, proceeding their journey to multivesicular bodies and finally fusing into the PSV. (B) Similar, LV resident proteins, after synthesis at the ER, are taken by COPII to the Golgi, where they are recognized BP80/VSR to become the cargo of CCV that are shipped to the PVC, before reaching the LV. Alternatively, proteins destined to the LV can follow a putative AP3-mediated pathway. Abbreviations: AP1, adaptor protein 1; AP3, adaptor protein 3; BP80, vacuolar sorting receptor; CCV, clathrin coated vesicle; COPI, coat protein complex I; COPII, coat protein complex II; DV, dense vesicles; ER, endoplasmic reticulum; MVB, multivesicular body; PSV, protein storage vacuole; PVC, pre-vacuolar compartment; LV, lytic vacuole; PV72/ RMR, vacuole sorting receptor; VSR, vacuolar sorting receptor. Adapted from (Xiang et al., 2013).

Many studies report the sorting of proteins to the PSV via DVs, such as legumin and sucrose-binding-protein homologue (Molina et al., 2006.; Wenzel et al., 2005). However, proteins can reach the PSV through an alternative/non-classical route from the ER, bypassing the Golgi (Figure 6). For instance, globulins which are the main storage proteins in pumpkins, were suggested to reach the PSV directly from the ER, in a transport mediated by precursor-accumulating compartments (PACs) (Hara-Nishimura et al.,1998). Being directly generated from the ER, PACs carry unglycosylated precursors of storage proteins, although they can also uptake glycosylated proteins derived from the Golgi as they progress towards the PSV (Hara-Nishimura et al., 1998; Jolliffe et al., 2005). They are known to mediate aggregation sorting and PACs content is incorporated in the lumen of the PSVs either by direct membrane fusion between the two (Shimada et al., 1994) or mediated by autophagy (Robinson et al., 1995.; Van der Wilden et al., 1980).

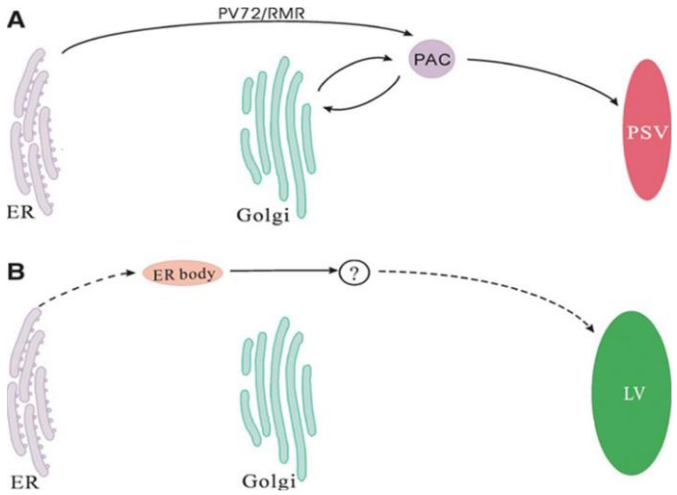

Figure 6. Unconventional routes to the vacuoles. (A) Storage proteins may arrive at the PSV in a Golgi-independent manner, as they leave the ER and are recognized by RMRs or VSRs (PV72 in the figure), leading to their package into precursor accumulating vesicles that take them to the PSV, without passing through the Golgi apparatus. (B) Similarly, LV resident proteins can reach this compartment in ER bodies, bypassing the Golgi. Abbreviations: ER, endoplasmic reticulum; LV, lytic vacuole; PAC, precursor-accumulating compartments; PSV, protein storage vacuole; PV72/ RMR, vacuole sorting receptor. Adapted from (Xiang et al., 2013).

In contrast to what has been described for sorting to the PSV, post-Golgi sorting of proteins to the LV/lysosome is mediated by CCVs rather than DVs, a process that seems to be conserved in eukaryotes. However, other studies have reported that the TGN can mature into PVCs/MVBs, that are involved in protein trafficking to the LVs, which suggest that LVs cargoes might be transported from the TGN to PVCs via multiple mechanisms. Transport through CCVs implies the recognition of specific sorting signals by receptors on the TGN membrane, that are further recruited into CCVs and transported into LV/lysosome (Robinson et al., 1998; Rouillé et al., 2000). In plant cells, the mechanisms of sorting and delivery to the LV are assumed to be similar to the ones in animal and yeast cells. Mannose 6-phosphate receptors (MPR) mediate the sorting of acid hydrolases to the lysosome in animal cells (Ghosh et al., 2003). This process is facilitated by Golgi localized, γ-adaptin ear-containing, ARF-binding proteins and by the AP1 complex interacting with MPRs tyrosine (YXXΦ) and dileucine (LL) motifs at the cytosolic tail. The recruitment of MPR-ligand complexes into CCVs occurs at the TGN (Doray et al., 2002; Ghosh et al., 2003). Nevertheless, there is a difference between plant and animal cells. Proteins targeted to the LVs, as example barley aleurain, interact with VSRs (Kirchhausen, 2000), which recognize ssVSDs in those proteins (Matsuoka & Neuhaus, 1999; Paris & Neuhaus, 2002). As a consequence, VSRs interact with AP1 (a complex known to mediate the formation of transport vesicles) through a tyrosine-based sorting motif, instead of a dileucine motif (Happel et al., 2004). The difference lies in this

fact. Cargo-VSR are assembled into CCVs that, in turn, are released from the TGN and fuse with the PVC, where they release their content (Hinz et al., 1999; Tse et al., 2004). Due to the low pH of the PVC, ligands detach from their receptor, which is then recycled back to the Golgi (Maxfield & McGraw, 2004; Raiborg et al., 2003; Seaman, 2005). Notably, an MPR-independent pathway to the LV has been reported in animal cells and a VPS10-independent pathway in yeast cells (Iwaki et al., 2006; Wolfenstetter et al., 2012). AP3 rather than AP1 seems to play a central role in this pathway. This protein recognizes both dileucine and tyrosine motifs in animal cells, while in yeast they only recognize dileucine signals (Bonifacino & Traub, 2003; Braulke & Bonifacino, 2009). More recent studies on sorting of tonoplast transporters in Arabidopsis mesophyll protoplasts revealed that plants perhaps have a similar route (Wolfenstetter et al., 2012). In addition, AP3 subunits might be involved in the biogenesis, morphology and function of the PVC and vacuoles in plants (Feraru et al., 2012; Niihama et al., 2009; Zwiewka et al., 2011).

Remarkably, proteins might be directly transported to the LV, bypassing the Golgi, a mechanism unique to plants and mediated by ER bodies (Hara-Nishimura et al., 2004). The plasticity exhibited by the plant ER to form these subcellular structures is one of the most outstanding differences that seems to differentiate plants from other eukaryotes (Matsushima et al., 2003). ER bodies are either accumulated at the ER or are conveyed to the LV. In plants, it was proposed that ER bodies bypass the Golgi and fuse directly with the LV (Hayashi et al., 2001; Herman & Schmidt, 2004). This non-canonical ER trafficking bypassing the Golgi to the lysosomes was previously reported in animal cells (Teckman & Perlmutter, 2000).

1.4. Plant Aspartic Proteinases

Aspartic proteinases (APs) are enzymes found in a wide variety of organisms such as plants, animals, parasites, fungi, and bacteria (Cruz et al., 2014; Davies, 1990; Dunn, 2002; Simões et al., 2011). Over the years, plant APs have been extensively characterized across many species (Athauda et al., 2004; Chen et al., 2015; Guo et al., 2013; Mazorra-Manzano et al., 2010; Mazorra-Manzano & Yada, 2008; Milisavljevic et al., 2008; Simões & Faro, 2004; Terauchi et al., 2004). APs are divided into 15 families and the plant ones belong to the A1 family (pepsin-like). These enzymes are active at acidic pH and contain two aspartic residues, which are responsible for their catalytic activity (Simões & Faro, 2004). Different APs are able to accumulate in different cellular compartments and depending on the cell type and developmental stage, the same

protein can either be secreted to the apoplast or directed to the vacuole (da Costa et al., 2010; Oliveira et al., 2010; Ramalho-Santos et al., 1998).

Cardosins

Cardosins are APs that were first isolated from the pistils of *Cynara cardunculus* (Ramalho-Santos et al., 1998; Vieira et al., 2001) and have been used in the manufacture of ewe cheese in Portugal for decades, due to its milk-clotting activity (Cordeiro, 1994). The two best-characterized cardosins are cardosin A and cardosin B (Pissarra et al., 2007; Ramalho-Santos et al., 1998; Veríssimo et al., 1996; Vieira et al., 2001). Although they show high sequence similarity, cardosin A and B can be found in different cellular compartments during plant development. In cardoon, cardosin A was demonstrated to accumulate in vacuoles (PSVs and LVs) (Oliveira et al., 2010; Pereira et al., 2008; Pissarra et al., 2007; Ramalho-Santos et al., 1997), whereas cardosin B was found outside the cell (Vieira et al. 2019). Their final cellular location is dependent on the plant developmental stage and cell needs. Besides, when expressed in other plants such as *Arabidopsis thaliana* or *Nicotiana tabacum*, cardosin A was accumulated in PSVs and LVs (Duarte et al., 2008; Pereira et al., 2013), while cardosin B was only found in LVs (da Costa et al., 2010). Altogether these features are quite intriguing and provide solid evidence for the use of cardosins as models for the study of APs vacuolar targeting and VSDs in plants. Cardosins (A and B) are synthesised as pre-proenzymes, with a presegment (PRE), followed by a prosegment (PRO), heavy and light chains and a Plant-Specific Insert (PSI). During maturation, the PRO sequence and the PSI are removed (Ramalho-Santos et al., 1997) (Figure 7).

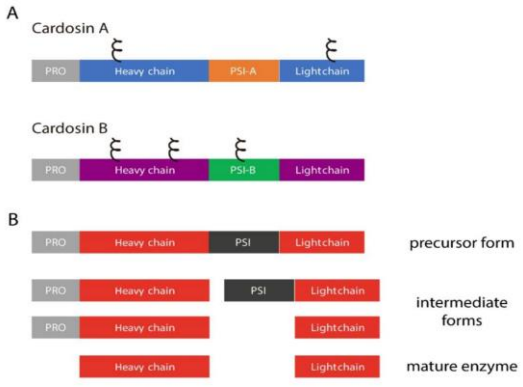

Figure 7. Domain organization of Cardosin A and B and the sequential processing steps to acquire the mature form. (A) In both cardosins, a presegment and a prosegment are observed, as well as the PSI separating the heavy (31 and 34 kDa, respectively) and light (15 and 14 kDa, respectively) chains of the mature form of the enzymes. The N-glycosylation sites are also illustrated (ξ). (B) Processing steps cardosins undergo along the endomembrane system to acquire their mature form, composed of heavy and light chains. Abbreviations: PRO, prosegment; PSI, plant specific insert domain. Retrieved from (Vieira et al., 2019).

1.5 Plant-Specific Insert

Some plant APs have a unique distinctive feature which is the presence of a protein domain of about 100 amino acids termed Plant-Specific Insert (Simões & Faro, 2004; Soares et al., 2019). This domain belongs to the saposin-like protein family (Mutlu & Susannah, 1999; Runeberg-roos et al., 1991). The function of the PSI still needs clarification, but some *in vivo* studies showeds that it was associated with the vacuolar targeting of APs (Egas et al., 2000; Pereira et al., 2013; Terauchi et al., 2006; Törmäkangas et al., 2001). Also, the PSI is frequently referred to as “an enzyme inside an enzyme” since, when isolated and *in vitro*, acts as a detergent, is able to induce membrane permeabilization and modulation and it also mediates membrane lipid interactions besides having a putative antimicrobial activity (Curto et al., 2014; De Moura et al., 2014; Egas et al., 2000; Frey et al., 2018; Muñoz et al., 2010, 2014; Terauchi et al., 2006). However, it is not clear if these roles, attributed to PSI *in vitro*, also occur *in vivo* after the PSI is cleaved from the proteinase precursor. A recent study (Frey et al., 2018) showed that a PSI expressed in Arabidopsis exhibited antimicrobial activity *in vivo*. Moreover, PSIs usually contain one putative N-glycosylation site (Almeida et al., 2012; da Costa et al., 2010; Domingos et al., 2000; Feijoo-Siota et al., 2018; Kervinen et al., 1999; Raimbault et al., 2013; Runeberg-roos et al., 1991), that is thought to confer stability to the proenzymes conformation and protect it from premature proteolytic processing inside the Golgi body (Costa et al., 1997; Frazão et al., 1999; Glathe et al., 1998; Payie et al., 2003).

A more recent study of four distinct plant APs highlighted that despite having highly conserved sequences and structural homology, the PSIs display different membrane interaction activities (Bryksa et al., 2017). Furthermore, the ability to interact with membranes is crucial to most of the proposed activities for the PSI. It has been hypothesized that PSIs roles are related to its ability to interact with phospholipid membranes in a pH-dependent manner (Bryksa et al., 2011; De Moura et al., 2014; Vaccaro et al., 1999), which also depends on the lipid composition (Egas et al., 2000). Interestingly, potato (*Solanum tuberosum*) PSI (StAP PSI) exhibits pH-dependent activities, and a previous study reported the pH-triggered dimerization of PSI (Guevara et al., 1999, 2001), and proposed that dimeric PSI is the active form responsible for membrane fusion (Bryksa et al., 2011). Also, PSIs structure may change from closed to open conformation (Bryksa et al., 2011; De Moura et al., 2014). In fact, potato PSI was observed to change from monomer to dimer, closed to open, with decreasing pH (Bryksa et al., 2017; Muñoz et al., 2011, 2014), and the dimeric association was stronger at acid pH (De Moura et al., 2014). Along the endomembrane system, there is a decrease in pH

and it was shown that the percentage of dimeric PSI was increased by lowering the pH, in a nearly linear fashion (Figure 8) (Zhao et al., 2020).

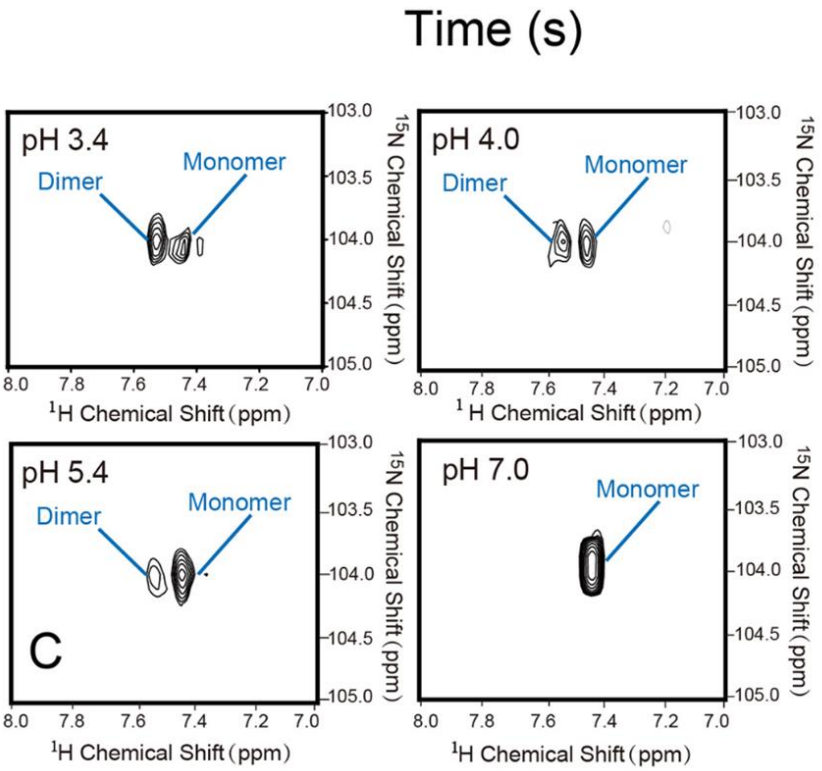

Figure 8. pH-dependent monomer-dimer equilibrium of PSI in solution. ^{1}H-15^{N} HSQC showing an expanded region for G40 corresponding to monomeric and dimeric species to demonstrate the pH-dependent monomer-dimer equilibrium. The percentage of dimeric PSI was obtained as a function of pH values. Adapted from (Zhao et al., 2020).

PSI-mediated routes

Cardosin A and cardosin B PSIs are able to redirect secreted proteins to the vacuole through different routes (Pereira et al., 2013). Cardosin A PSI (PSI A) can do a Golgi bypass, mediating an unconventional route to the vacuole, whereas cardosin B PSI (PSI B) follows a classic ER - Golgi - Vacuole route to this organelle. It has been shown that differences in the glycosylation state between both PSIs are determinant for this, as cardosin A PSI is not glycosylated, contrary to cardosin B (Vieira et al., 2019) (Figure 8). Despite all the information available, there are still uncertainties regarding the mechanisms behind these non-conventional sorting domains functions. Hence, it is pivotal to study vacuolar proteins that can do a Golgi bypass to unveil the mechanisms behind these unconventional routes.

As an increasing number of proteins are reported to traffic through unconventional routes that are not described in the classical textbooks, focus has been given to studying the role of PSIs from cardoon in vacuolar protein trafficking. A study by

Pereira and coworkers (2013) revealed that the PSI domain of cardosin A and B are capable of redirecting secreted proteins to the vacuole through different routes.

Cardosin A is characterized by having two domains acting as VSDs: the ctVSD, a typical VSD and, the PSI, which does not fit in any VSD category reported so far. These domains mediate a different trafficking pathway to the vacuole (Pereira et al., 2013). While PSI A mediates a direct ER-to-Vacuole route, (Vieira et al., 2019) the C-terminal peptide dictates a COPII-dependent ER-to-Golgi route towards the vacuole. Due to the existence of two sorting motifs in cardosin A, cells might have greater flexibility, as their activation might be dependent on the developmental stage and environmental conditions (Pereira et al., 2008, 2013). Regarding cardosin B, it also contains two vacuolar sorting signals, the C-terminal and the PSI, but, in this case, they both mediate a classical trafficking route to the vacuole. Moreover, the ctVSD present in cardosin A is dominant over the PSI signalling in the sorting process, in fully expanded leaves. However, when it was removed, PSI A would take over the sorting, being the unique player involved in directing APs to the vacuole. Likewise, when the ctVSD was removed from cardosin B, PSI B was sufficient and required to direct the AP to the vacuole (Vieira et al., 2019). Based on these findings, understanding what is behind such different sorting pathways is crucial, even though cardosins have a high degree of similarity. It also questions if the described VSDs are the only ones accountable for the sorting process, and even if those VSDs are efficient (Nishizawa et al., 2006).

Even though PSI A and PSI B mediate the trafficking of proteins to the vacuole, they do it differently. The PSI B-mediated sorting from the ER to the Golgi is accomplished via COPII vesicles, whereas the sorting mediated by PSI A is COPII-independent. In a study where co-expression with the dominant negative mutant $SarI^{H74L}$ was made, a mutant that blocks COPII-mediated transport, proteins were still able to reach the vacuole via PSI A-mediated sorting. However, in the same conditions, PSI B-mediated sorting was blocked (Vieira et al., 2019). These results support the Golgi-bypass mediated by the PSI A, although the mechanisms still need clarification. In an attempt to further understand the differences between PSI A and PSI B mediated sorting, the sequences of these domains were analysed, and differences in the glycosylation status of both PSIs were revealed, as a N-glycosylation site appeared in PSI B, but not in PSI A (Figure 8). These differences may explain the distinct trafficking pathways of PSIs. Supporting this statement, it was observed that when coexpressed with $SarI^{H74L}$, the glycosylated version of PSI A retained the protein in the ER, whereas non-

glycosylated PSI B was able to overcome the Golgi-bypass blockage and reached the vacuole.

The PSIs of barley (*Hordeum vulgare*) AP and soybean (*Glycine max*) soyAP1 are also glycosylated like PSI B and were shown to mediate vesicular trafficking via COPII-dependent pathways (Marti et al., 2010; Pereira et al., 2013; Törmäkangas et al., 2001; Vieira et al., 2019) . In contrast, soyAP2 PSI is not glycosylated and it mediates a COPII-independent transport (Vieira et al., 2019). The role glycosylation plays in this mediated transport is still unclear. Curiously, it is not uncommon for APs to have more than one system of vacuolar transport. In barley, PSI-removed phytepsin was exported through general bulk flow (Törmäkangas et al., 2001) ,while cardosin A is known to have a second and dominant VSD that participates in COPII-dependent trafficking (Pereira et al., 2013), as already described. The redundant trafficking domains exhibited by some PSIs along with the ability to direct proteins to the vacuole by conventional and non-conventional routes may be a clue on plant adaptation mechanism in response to specific conditions.

1.6 Aims

Over the years, the mechanisms behind protein sorting in plant cells have been thoroughly studied, leading to a solid knowledge of this matter. Most studies have focused on protein conventional sorting routes following the typical ER - Golgi - Vacuole pathway, but little is known about proteins that follow unconventional vacuolar routes, bypassing the Golgi, as it is the case of cardosin A PSI. The global aim of the study is to characterize the vacuolar transport mediated by PSI A and PSI B from cardoon APs, to further increase our knowledge of the mechanisms behind protein unconventional sorting routes. Therefore, we approached the subject using two different strategies.

Proteins following the unconventional pathway to the vacuole are capable of bypassing the Golgi, going directly from the ER to the vacuole. Thus, our first aim is to explore the localization of cardosins PSI A and PSI B in Arabidopsis mutants with impaired vacuolar trafficking. These plants were used for an ultrastructural characterization and co-expression with PSI A and PSI B was employed to evaluate how the sorting of these determinants is affected.

PSIs change their conformation from monomeric to dimeric and closed to open with a decrease in pH, and this impacts PSI functions. Thus, considering that PSI A and PSI B have different sorting routes to the vacuole and that the pH decreases along the

endomembrane system, our second aim is to test cardosins PSIs interactions in different pH conditions. It involved a Yeast Two-Hybrid assay, followed by the purification of the PSIs, carrying different tags to perform a pull-down or Co-immunoprecipitation (Co-IP) assay (dependent on the tag) at different pH conditions, to analyse PSIs interactions and how the pH affects its dimerization.

Therefore, we expect to contribute to the study of vacuolar proteins that can do a Golgi bypass to help unveil the mechanisms behind these unconventional routes. Besides that, and by comparing the PSIs interactions, we expect to deepen our knowledge of the characterization of PSIs sorting pathways and their structure-function relationship.

2. Materials and methods

2.1. Plant material and growth conditions

Four *Arabidopsis thaliana* knock-out lines (Table 1), ecotype Columbia-0 (Col-0), described as having vacuolar trafficking defects were selected for the present study, which were donated by Dr. Ikuko Hara-Nishimura and Dr. Haruko Ueda (Laboratory of Plant Cell Biology, Faculty of Science and Engineering, Konan University, Japan). 70% ethanol (v/v) was used to surface sterilize wild-type (WT) and mutant seeds for 5 minutes with gentle rotation and the seeds were left to dry onto filter paper inside the flow hood. Then, they were sown onto plates containing half-strength Murashige & Skoog (MS) medium (Duchefa, UK) supplemented with 1.5% (w/v) sucrose (Duchefa, UK) and 0.8% (w/v) agar (Duchefa, UK), pH 5.7. Plates were sealed with Micropore™ Surgical tape, and the seeds were stratified for 48 hours at 4°C. After this time, they were transferred to an indoor growth facility with 50-60% relative humidity and long-day conditions of 16 hours light at 22°C/ 8 hours darkness at 18°C (light intensity = 180 µmole m -2 s-1). For subsequent growth, after 15-20 days, seedlings were transferred onto pots with fertilized substrate (SIROPLANT, Portugal), they were covered for 7-10 days with plastic wrap for acclimatization and maintained under the same conditions. Images of plants with 15-day-old after sowing (DAS) were acquired with a SMZ168 Stereo Zoom Microscope (Motic, Barcelona, Spain) and images were captured using a Moticam 2500 (Motic, Barcelona Spain) camera and the Motic Imag3es Plus 2.0 (Motic) software.

Table 1. List of the *Arabidopsis thaliana* lines used.

NASC ID	Name	Obtained from
N68716	*syp22-3 or vam3-3*	Ueda et al. (2006)
N68719	*syp22-1 syp23 or vam3-1 plp*	Shirakawa et al. (2010)
N68720	*syp22-3 syp23 or vam3-3 plp*	Shirakawa et al. (2010)
N68718	*syp23 or plp*	Ohtomo et al. (2005)

Development assays

To evaluate the mutants development, an assay based on seven stages of the plant development processes was carried out according to Boyes et al. (2001) comparing *syp22-3*, *syp22-1 syp23*, *syp22-3 syp23* and *syp23* plants to WT. Seeds were germinated in solid MS medium, as already described, and were transferred to soil in the seedling stage (15 DAS). The time of appearance of different developmental points was recorded by checking on the plants two times per day for further analysis: cotyledons

fully opened; two, three and four rosette leaves; first flower buds visible; first flower open and presence of first siliques.

Furthermore, to assess if the mutations retrieved any delay in root growth, seeds from WT and the mutants were germinated as described in section 2.1 on square plates and left in a vertical position under the same conditions, as mentioned above. After 15 DAS, the primary root length was measured using ImageJ®/Fiji software.

2.2. Transmission Electron Microscopy

Leaves from *A. thaliana* seedlings (15 DAS) with defects in vacuolar trafficking and WT were grown as described in section 2.1. Leaf portions of approximately 1-2 mm were obtained and fixated in 1.25% (v/v), sodium 1,4-piperazine-diethane sulfonic acid (Na-PIPES) pH 7.2 with 2.5% (v/v) glutaraldehyde (Sigma-Aldrich, USA) for 1 hour at room temperature (RT). Then, the samples were washed with 1.25 % (v/v) Na-PIPES, pH 7.2 tree times for 10 minutes each and post-fixated in 4 % (v/v) osmium tetroxide (OsO4) (Agar Scientific, UK) prepared in 1.25% (v/v) Na-PIPES pH 7.2, for 1 hour at RT. The samples were washed again as before and dehydrated at RT in an ethanol graded series as follows: 10 % (v/v) for 10 minutes; 20 % (v/v), 30 % (v/v) and 50 % (v/v) for 15 minutes; and 70 % (v/v) and 100 % (v/v) for 20 minutes. After the last incubation step, the ethanol was replaced by propylene oxide 2 times for 15 minutes. Subsequently, 25 mL of Epoxi resin were prepared by mixing 12 mL of Agar 100 resin (Agar Scientific, UK) with 13 mL of Methyl Nadic Anhydrin (MNA) (Agar Scientific, UK) at RT for 20 minutes with agitation. Following that time, 0.5 mL of DMP-30 (Agar Scientific, UK) were added to the mixture and left in agitation for another 20 minutes. The biological material was then embedded in 10% Epoxy resin, and diluted in propylene oxide, for 15 minutes. A drop of resin was added every 10 minutes until a final proportion of 50% resin: 50% Propylene Oxide was reached. The samples were incubated overnight (ON). The following day, they were embedded in 100% resin for 24 hours. The tissues were then transferred to oriented moulds covered in Epoxy resin and polymerized at 60 °C for 24 hours. Ultrathin sections (60-80nm) were obtained using a diamond knife (Diatome) on an Ultracut UC6 (Leica, UK) ultramicrotome. The tissue sections were placed onto 400 mesh copper grids and post-stained for 5 minutes with Uranyless EM Strain (Uranyless©) and with Reynolds Lead citrate 3% (Uranyless©) for another 5 minutes. Between each stain, grids were washed in distilled water by emerging the grids several times. In the end, the samples were washed again as before and left to dry on filter paper. The stained sections were examined on a Jeol JEM 1400 transmission electron

microscope (JEOL, Ltd., Akishima, Japan). Images were recorded with an Orius® SC200D camera (Gatan, Pleasanton, CA, USA) and image analysis and processing were done using ImageJ®/Fiji software.

2.3 Vacuum infiltration for transient transformation of *Arabidopsis thaliana* seedlings

Seedlings from mutant Arabidopsis plants alongside the WT were transformed using an Agrobacterium-mediated infiltration technique by vacuum (Bernat-Silvestre et al., 2021) for transient expression. The constructs used were already available at the laboratory and were the following: SP-PSI-A-mCherry and SP-PSI-B-mCherry (Pereira et al., 2013).

Seedlings' growth conditions

Seeds from WT and *A. thaliana* mutants were sown as described in section 2.1. They were allowed to grow for 7 days, after stratification, point at which it was possible to observe expanded cotyledons in the resultant seedlings.

Agrobacterium tumefaciens culture preparation

Tree days before the plants transformation, 10 mL of Luria Broth (LB) Base Miller (15 g/L) medium (Duchefa, UK) supplemented with kanamycin (50 µg/mL), gentamicin (50 µg/mL) and rifampicin (50 µg/mL) were inoculated with one aliquot of a frozen glycerol stock of *Agrobacterium tumefaciens* harbouring the clone of interest. The cultures were incubated at 28 °C ON with shaking at 200 rpm, until the OD_{600} reached 2.2, approximately. Bacteria cells were harvested by centrifugation at 6000 x g for 15 minutes. After that, the medium was removed and the bacterial pellet was resuspended in 2 mL of liquid MS medium [2.2 g/L MS and 1.5% (w/v) sucrose, pH 5.7]. The OD_{600} was measured in a 1:20 dilution, by diluting 50 µL of the bacterial pellet suspension with 950 µL of infiltration buffer [liquid MS medium, 0.005% (v/v) Tween-20 (Sigma-Aldrich), 200 µM acetoseryngone]. After measuring the OD_{600}, the remaining bacterial suspension was diluted with infiltration buffer to an OD_{600} of 2, to improve the transfection efficiency. The Agrobacterium was kept in the infiltration buffer for 30-45 minutes at RT. After that time, in a clean 6-well plate, 7-day-old Arabidopsis mutants and WT seedlings were soaked with 4 mL of the Agrobacterium suspension. The plates were then placed into the vacuum desiccator and vacuum was applied 3 times with the duration of one minute each, with one minute pause, with increasing pressure. The Agrobacterium solution was

then removed from the plates and the seedlings were washed 3 times with liquid MS medium to avoid any contamination, after which they were kept in the growth chamber for 1 hour covered in aluminium foil. The foil was then removed, and the plates were kept for 3 days in the growth chamber under the same conditions as described in section 2.1, before image acquisition with a Confocal Laser Scanning Microscope (CLSM) (Leica SP5).

2.4 Constructs generation

During this work several constructions were prepared for some of the techniques employed (Table 2): **1)** For the pull-down assays, pGEX-6p-1-GST-PSIA_Y95A/L99A; **2)** For the 2in1 rBiFC assay, pDONR221-P1P4-SP-PSI A and pDONR221-P1P4-SP-PSI B. Besides, constructs used for Co-IP and pull-down assays were already available at the laboratory and are as follows: pET21a-FLAG-PSIA-6xHis, pET21a-FLAG-PSIB-6xHis, pGEX6p-1-GST-PSIA-6xHis, pGEX-6p-1-GST-PSIB-6xHis (Sampaio, 2020) (Table 2).

Table 2. List of constructs used.

Insert	Vector	Construct
PSI A_Y95A/L99A	pGEX-6p-1	pGEX-6p-1-GST-PSI A_Y95A/L99A-6xHis
PSI A	pDONR221-P1P4	pDONR221-P1P4-SP-PSI A
PSI B	pDONR221-P1P4	pDONR221-P1P4-SP-PSI B
PSI A	pDONR221-P3P2	pDONR221-P3P2-SP-PSI A
PSI B	pDONR221-P3P2	pDONR221-P3P2-SP-PSI B
PSI A	pET21a	pET21a-FLAG-PSIA-6xHis
PSI A	pGEX-6p-1	pGEX-6p-1-GST-PSIA-6xHis
PSI B	pET21a	pET21a-FLAG-PSIB-6xHis
PSI B	pGEX-6p-1	pGEX-6p-1-GST-PSIB-6xHis

Plasmid pGEX-6p-1 (Supplementary figure 36) and cDNAs (Table 3) were already available at the laboratory and maintained in *Escherichia coli DH5α* glycerol stocks. Gateway vectors (pDONR221-P1P4 (Supplementary figure 37) and pBiFCt-2in1-CC (Supplementary figure 38) were kindly provided by Dr. Di Sansebastiano (Universitá del Salento, Italy). Plasmids were extracted from *E. coli* using the Illustra plasmidPrep Mini Spin Kit (Cytiva, UK), according to the manufacturer's instruction, with exception that the final elution volume was 20 µL.

Table 3. List of cDNAs used.

cDNAs used	Obtained from
pVKH18En6-SP-PSICardA-mCherry	Pereira et al. (2013)
pVKH18En6-SP-PSICardB-mCherry	Pereira et al. (2013)
pCRBlunt- PSI A_Y95A/L99A	unpublished

DNA amplification

All constructs used in this study were generated by Polymerase Chain Reaction (PCR) using specific primers. PSI A_Y95A/L99A was amplified using primer pairs: 5'-end specific primer, 5'- AAAAAAGGATCCGTCATGAACCAGCAATGCAA, 3'-end specific primer, 5'-CGCAAGCTTGTCGACACAGGATAAGTGTTCACACG. The primers contain adapters for the chosen restriction enzymes: a SaII restriction site in the N-terminal portion of the insert and a HindIII restriction site in the C-terminal. For 2in1 rBiFC assay, through Gateway cloning, the PSI A sequence was amplified using the following primers: 5'-end gene-specific primer, 5'-GGGGACAAGTTTGTACAAAAAAGCAGGCTA TGAAGACTAATCTTTTTCTCT, 3'-end gene-specific primer, 5'-GGGGACAACTTTGT ATAGAAAAGTTGGGTGGGATAAGTGTTCACACAACTCGT. The PSI B sequence was amplified using the following primers: 5'-end gene-specific primer, 5'-GGGGACAAGTTTGTACAAAAAAGCAGGCTATGAAGACTAATCTTTTTCTCT, 3'-end gene specific primer, 5'-GGGGACAACTTTGTATAGAA AAGTTGGGTGTTCTGCAC TTGAAGTGGGTA. All included gateway attB sequences in both N-terminal and C-terminal regions to enable this cloning technique.

For amplification, NZYProof 2× Green Master Mix (NZYTech, Portugal) was used, and the PCR reaction mix and PCR programs are described in Table 4 and Table 5, respectively. The PCR products were analysed by electrophoresis in 1 % (w,v) agarose gel in 0.25x TAE [40 mM Tris-HCl, 1mM EDTA, pH8.3)] with 0.005 % (v/v) GreenSafe Premium (NZYTech, Portugal). GeneRuler DNA Ladder Mix (Thermo Fisher Scientific™, USA) and NZYDNA LadderIII (NZYTech, Portugal) were used as a molecular weight markers. The electrophoretic separation was made in a horizontal electrophoresis system (Horizon 58, Life Technologies) at 100 V for 25-35 min. Then, the amplified DNA fragments were purified using illustraTM GFXTM PCR DNA and Gel Band Purification kit (Cytiva, UK) in line with the manufacturer's procedure and quantified using 1 µL of DNA in a DS-11 Spectrophotometer/Fluorometer (DeNovix,USA).

Table 4. Component mix for PCR reactions using NZYProof 2× Green Master Mix (NZYTech, Portugal).

Components	Concentration	Volume
H_2O	-	9 µL
NZYProof 2× Green Master Mix	1x	12.5 µL
Forward Primer	0.5 µM	1.25 µL
Reverse Primer	0.5 µM	1.25 µL
DNA	5 ng	1 µL
Final volume	-	25 µL

Table 5. Program for PCR reactions using NZYProof 2× Green Master Mix (NZYTech, Portugal).

	Steps	Temperature	Time
Initial denaturation		95 °C	3 minutes
35x	Denaturation	95 °C	30 seconds
	Annealing	61 °C */58 °C**	30 seconds
	Extension	72 °C	60s/kb
Final extension		72 °C	10 minutes
Hold		4 °C	∞

*for PSI A_Y95A/L99A, ** for PSIs

Cloning

Enzymatic Restriction Cloning

The DNA fragment PSI A_Y95A/L99A was cloned into pGEX-6p-1 using the HindIII and SalI restriction sites. 1 ng of DNA or 20 µL of PCR product, 2 µL of Anza 10X Red Buffer, 1 µL of each restriction enzyme [Anza™ 16 HindIII and Anza™ 14 SalI (Invitrogen by Thermo Scientific), USA] and H_2O up to 20 µL were combined. The reactions were left incubating for 20 minutes at 37 °C followed by a cleanup using illustraTM GFXTM PCR DNA and Gel Band Purification kit (Cytiva, UK) according to the manufacturer's instructions. The products of each digestion reaction were resolved via agarose gel electrophoresis as mentioned in *DNA amplification* in section 2.4. The purified DNA fragments were then quantified in a DS-11 Spectrophotometer/Fluorometer (DeNovix, USA). After that, the digested DNA fragments were ligated with T4 DNA Ligase (Thermo Fisher Scientific™, USA), in line with the manufacturer's guidelines. 50 ng of vector DNA (pGEX-6p-1), 20 ng insert DNA (PSI A_Y95A/L99A), 1 µL 10x T4 DNA Ligase buffer, 1 µL T4 DNA ligase and H_2O up to 10 µL were combined. The reactions

were left incubating for 1 hour at RT followed by cell transformation, as described in *Bacteria heat-shock transformation* in section 2.4, with all the ligation reaction. This reaction consisted of 50 ng of vector and the amount of insert was calculated using the formula ng insert = ng plasmid x number of base pairs x 5 / number of base pairs of the plasmid.

Gateway Cloning

Invitrogen™ Multisite Gateway Recombination Technology was performed to obtain the constructs for 2in1 rBiFC assays which included the PSI A and PSI B. Constructs pDONOR221-P3P2-SP-PSI A and pDONOR221-P3P2-SP-PSI B were already available at the laboratory (Sampaio, 2020). Both PSI cDNAs (already amplified – *DNA amplification* in section 2.4.) were cloned into a donor vector through a BP recombination reaction [Gateway™ BP Clonase™ II Enzyme mix (Invitrogen™, USA)] according to the manufacturer's instructions. In a 1.5 mL microcentrifuge tube, 150 of ng of attB-PCR product PSI A or PSI B and 150 ng of donor vector pDONOR221-P1P4 were combined. BP Clonase™ II Enzyme mix was thawed on ice for 2 minutes, followed by vortexing the mix briefly twice, 2 seconds each time. Then, 1 µL of the mix was added to the previous combined samples, and the reactions were incubated for 2 hours at RT. After that time, 1 µL of Proteinase-K (Invitrogen™, USA) was added to terminate the reaction, and samples were incubated at 37 °C for 10 minutes. Following this, half of the BP reaction was used to transform *E. coli* cells as described in *Bacteria heat-shock transformation* in section 2.4. After confirmation, the BP constructs were used to transfer the PSI A/B and the PSI A/B interactor into the destiny vector pBiFCt-2in1-CC vector by an LR recombination reaction [Gateway™ LR Clonase™ II Enzyme mix (Invitrogen™)] according to the manufacturer's instructions. In a 1.5 mL microcentrifuge tube, 150 of ng of each entry clone and 150 ng of destination vector pBiFCt-2in1-CC were combined. LR Clonase™ II Enzyme mix was thawed on ice for 2 minutes, followed by vortexing the mix briefly twice, 2 seconds each time. Then, 1 µL of the mix was added to the previous combined samples, and the reactions were incubated for 1 hour at RT. After that time, 1 µL of Proteinase-K (Invitrogen™, USA) was added to terminate the reaction, and samples were incubated at 37 °C for 10 minutes. Following this, half of the LR reaction was used to transform *E. coli* cells as described in B*acteria heat-shock transformation* in section 2.4. Noteworthy, inserts for pBiFCt-2in1-CC had their stop codon removed to express the C-terminal Portion of YFP (cYFP). A schematic of the technique is represented in Figure 9. All combinations between PSI-PSI are represented in Table 6.

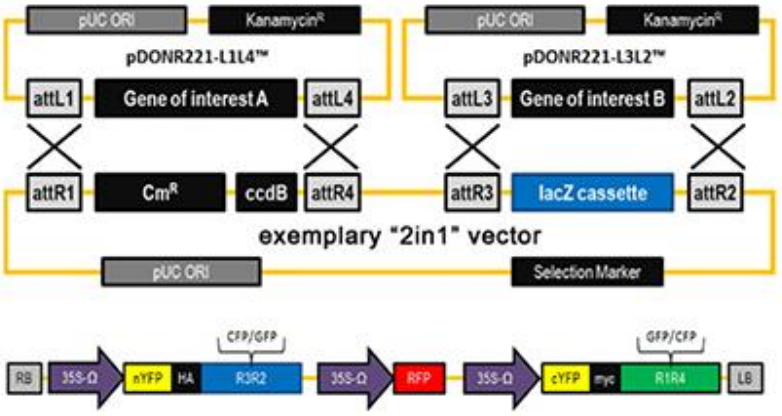

Figure 7. Model procedure to obtain a 2in1 rBiFC vector. Through Gateway cloning, inserts cloned into pDONR221-L1L4 and pDONR221-L3L2 recombine with attR1 and attR4 and with attR3 and attR2 sequences of the pDEST vector. By recombining, CmR, ccdB lethal gene and lacZ cassette are removed and the inserts placed in their region. Abbreviations: CmR, chloramphenicol acetyltransferase resistance gene, ccdB, gyrase inhibitor gene; pUC ORI, origin of replication for *Agrobacterium tumefaciens* and *Escherichia coli*; Adapted from (Grefen & Blatt, 2012).

Table 6. Gateway cloning combinations performed for 2in1 rBiFC constructs.

pDONOR constructs	pDEST constructs
pDONR221-P3P2-SP-PSI A	pBiFCt-2in1-CC (PSI A / PSI A)
pDONR221-P3P2-SP-PSI B	pBiFCt-2in1-CC (PSI A / PSI B)
pDONR221-P1P4-SP-PSI A	pBiFCt-2in1-CC (PSI B / PSI B)
pDONR221-P1P4-SP-PSI B	

Preparation of chemical competent cells

E. coli (*E. coli DH5α* and *E. coli BL21*) were grown in plates with LB medium supplemented with 1.5 % (w/v) agar ON at 37 °C. Then, a single colony was inoculated in 25 mL of liquid LB medium and left growing at 37 °C ON, with shaking at 200 rpm. The starter cultures were inoculated in 225 mL of liquid LB medium supplemented with $MgCl_2$ (1M) and $MgSO_4$ (1M) and allowed to grow at 37 °C for 2 hours at 200 rpm, until OD_{600} reached 0.7. The cultures were then moved to ice for 10 minutes and the cells were harvested by centrifugation at 3000 x g for 5 minutes. The supernatant was decanted, and the pellet resuspended in RF1 [100 mM RbCl, 10 mM $CaCl_2$, 15 % (v/v) glycerol, pH 5.8, autoclaved; 50 mM MnCl2 and 35 mM Kac] and left on ice for 15 minutes. The centrifugation step was repeated as before and the supernatant was removed. Cells were then resuspended in 16 mL RF2 [10 mM RbCl, 75 mM $CaCl_2$, 10 mM MOPS and 15 % (v/v) glycerol, pH 8.0, autoclaved], and aliquoted into 100 µL and stored at -80 ºC.

Bacteria heat-shock transformation

One µL of expression constructs pET-21a-FLAG-PSIA-6xHis, pET-21a-FLAG-PSIB-6xHis, pGEX-6p-1-GST-PSIA-6xHis, pGEX-6p-1-GST-PSIB-6xHis and pGEX-6p-1-GST- PSI A_Y95A/L99A were used to transform *E. coli BL21 (DE3)*. 2 µL of BP and LR reactions and total ligation volume of pGEX-6p-1-GST- PSI A_Y95A/L99A were used to transform *E. coli DH5α*. In all cases, the corresponding DNA volume was added to 100 µL of competent cells and kept on ice for 30 minutes. The cells were then submitted to a heat shock at 42 °C for 40 seconds followed by another 2 minutes on ice. 1 mL of liquid LB medium was added for cell recovery followed by an incubation of 1 hour at 37 °C with shaking at 200 rpm. The cells were centrifuged at 3600 x g for 4 minutes, 1 mL of the supernatant was removed, and the bacteria pellet was resuspended in the remaining 100 µL. The transformed cells were spread on 1.5 % (w/v) LB agar with the corresponding antibiotics and supplements (Table 7) and left incubating at 37 ºC ON.

Table 7. Bacteria used to replicate and express each construct and their respective antibiotic and concentration.

Bacteria	Construct	Antibiotic	Supplements to medium
E.coli BL21(DE3)	pET-21a-FLAG-PSIA-6xHis	Ampicillin 100 µg/mL	None
	pET-21a-FLAG-PSIB-6xHis		
	pGEX-6p-1-GST-PSIA-6xHis		
	pGEX-6p-1-GST-PSIB-6xHis		
	pGEX-6p-1-GST-PSIA_Y95A/L99A		
	pDONR221-P1P4-SP-PSI A	Kanamycin (50 µg/mL)	
	pDONR221-P1P4-SP-PSI B		
E. coli DH5α	pBiFCt-2in1-CC (PSI A / PSI A)	Spectinomycin (100 µg/mL) IPTG (0.1 mM)	X-Gal (40 µg/mL)
	pBiFCt-2in1-CC (PSI A / PSI B)		
	pBiFCt-2in1-CC (PSI B / PSI B)		

Bacteria screening

Screening for positive clones

The screening for positive clones after the transformation of *E. coli* cells was performed by enzymatic digestion. Several colonies of each transformation were inoculated in 5 mL of liquid LB medium, supplemented with the appropriate antibiotic (Table 7) and left to grow ON at 37 °C, shaking at 200 rpm. The following day, bacterial plasmid DNA was extracted from the liquid cultures using the Illustra plasmidPrep Mini Spin Kit (Cytiva, UK), according to the manufacturer's instruction, with the exception the final elution volume was 20 µL. Plasmid DNA was quantified using DS-11 Spectrophotometer/Fluorometer (DeNovix, USA). The positive clones were screened by enzymatic restriction using Anza Thermo Fisher Scientic™ enzymes in line with the manufacturer's procedures. EcoRI and Eco32I were used for the pBiFC plasmids, while XhoI and BamHI for the other construct (pGEX-6p-1-GST-PSIA_Y95A/L99A). Separation of obtained DNA fragments was done through electrophoresis on a 1% agarose gel in a horizontal electrophoresis system (Horizon 58, Life Technologies) at 100 V for 25-35 min, in 1xTAE. The clones showing the expected size bands after electrophoresis were sent for sequencing (Eurofins, Germany). With that purpose, regarding the pGEX-6p-1-GST-PSIA_Y95A/L99A construct, a tube was prepared containing 500 ng of DNA, 5 µM primer PSIA fwd (Table 8) and H_2O up to final volume 10 µL. For the 2in1 rBiFC assay, both pDONR constructs and pBiFC plasmids were also sent for sequencing by combining 500 ng of DNA, 5 µM primer M13 rev (Table 8) and H_2O up to final volume 10 µL. Sequencing data was analysed using SnapGene software (www.snapgene.com). The bacterial colonies of interest were stored in 25 % (v/v) glycerol at -80 ºC.

Table 8. List of primers for sequencing.

Primer name	Sequence
PSIA fwd	5'- CAGGAAACAGCTATGAC-3'
M13 rev	5'- AAAAAAGGATCCGTCATGAACCAGCAATGCAA-3'

2.5 Large scale protein production and purification

For the large-scale production, to induce expression of the protein, 10 colonies of *E. coli BL21* were left growing in 20 mL of LB medium supplemented with the appropriate antibiotic (Table7) ON at 37 °C, with shaking at 200 rpm. The following day,

the starter culture was transferred to an Erlenmeyer containing 1 L of LB medium supplemented with the appropriate antibiotic (Table 7) and the culture was maintained for 4 hours at 30 °C with shaking at 200 rpm. Then, the temperature was lowered to 23 °C and the culture incubated for one more hour. At this point, 1 mL of culture was centrifuged for 30 seconds at 1400 x g and the bacterial pellet was resuspended in 200 µL of 1x SDS-Page Sample Loading Buffer (NZYTech, Portugal) - uninduced fraction. 5 µM of isopropyl β-D-1-thiogalactopyranoside (IPTG) was added to the culture, and induction was carried out ON at 23 °C, shaking at 200 rpm. After, 330 µL of culture was centrifuged for 30 seconds at 1400 x g and the pellet was resuspended in 200 µL of 1x SDS-Page Sample Loading Buffer - uninduced fraction. The remaining culture was centrifuged at 4000 x g for 15 minutes at 4 °C. The pellet was resuspended in 10 mL of Lysis buffer [50 mM Tris-HCl pH 8, 200 mM NaCl, 10 mM Imidazole, 1 mM DTT, 0.1 % (v/v) Tween-20], and 125 µL of Protease Inhibitor Cocktail for General Use (Sigma-Aldrich, USA) and lysozyme (1 mg/mL) were added. The lysate was incubated on ice for 15 minutes. After that time, the cells were sonicated two times for 30 seconds, using three different outputs (10,15 and 20) (XL-2000 - QSONICA), with 1 minute pause between them. After sonication, 5 µL of lysate was added to 45 µL of 1x SDS-Page Sample Loading Buffer – lysate fraction. Subsequently, lysates were cleared for 45 minutes at 35000 x g at 4 °C. During that time, 750 µL of HisPur™ Ni-NTA Superflow Agarose beads (Thermo Fisher Scientific™, USA) were washed 2 times, 5 minutes each, with 15 mL of ice-cold lysis buffer. Between the washes, beads were centrifuged at 700 x g for 2 minutes. After centrifugation, the cleared lysate (supernatant) was recovered and 4 µL of the supernatant was added to 45 µL of 1x SDS-Page Sample Loading Buffer – soluble fraction. Then, the cleared lysate was used in a batch purification protocol by addition to the pre-washed beads, and the mixtures were left incubating for 1 hour in a Tube Revolver/Rotator (Thermo Fisher Scientific™, USA) at 4 °C. The mixture was centrifuged at 700 x g for 3 minutes, and 5 µL of the supernatant was added to 45 µL of 1x SDS-Page Sample Loading Buffer – flow through fraction. The remaining supernatant was removed and 750 µL of lysis buffer was added to the resin. 10 µL of the resin was added to 500 µL of lysis buffer, centrifuged at 700 x g for 3 minutes, the buffer removed, and 45 µL of 1x SDS-PAGE sample buffer was added – bound to resin fraction. Afterwards, the resin was washed 2 times, 5 minutes each, with 10 mL of ice-cold wash buffer [25 mM Tris-HCL, pH 8, 200 mM NaCl, 25 mM imidazole], and between the washes a centrifugation step was made as before. After the last wash, 750 µL of ice-cold wash buffer was added to the resin and 10 µL of this mixture were centrifuge, the supernatant was removed and 500 µL of 1x SDS-PAGE sample buffer was added –

washed resin fraction. The proteins were eluted with 1 mL of elution buffer [50 mM Tris-HCl pH 8, 150 mM NaCl, 250 mM imidazole] that was added to the resin and incubated for 5 minutes in an overhead rotator. This step was repeated 5 times to obtain five elution fractions (elution fractions 1 to 5). Between each incubation, a brief centrifugation step at 7440 x g for 15 seconds was performed and the supernatant (elution fraction) was collected into an Eppendorf tube. After each centrifugation, 5 µL of elution fraction was added to 45 µL of 1x SDS-PAGE sample buffer- elution fractions 1 to 5. At the end, 1 mL of elution buffer was added to the resin and 5 µL of the eluted resin was added to 45 µL of 1x SDS-PAGE sample buffer – resin after elution fraction. The several fractions were analysed by sodium dodecyl sulphate-polyacrylamide gel electrophoresis (SDS-PAGE) as described in section 2.7. Gels were stained with BlueSafe (NZYTech, Portugal), according to the manufacturer's instructions. Throughout the entire procedure, both solutions and containers were kept refrigerated.

2.6 Protein-protein interactions

Yeast Two-Hybrid

Yeast cells transformed with bait and prey plasmids were already available at the laboratory (Supplementary figure 39). One colony of each strain for mating (Table 9) was left growing in 1 mL of Yeast Peptone Dextrose Adenine (YPDA) medium [10g/L yeast extract (Sigma-Aldrich, USA), 20 g/L tryptone (Sigma-Aldrich, USA), 40 % (w/v) glucose filter sterilized, 0.2 % (w/v) adenine hemisulfate filter sterilized] ON at RT, with shaking at 200 rpm. 50 µL of the mated yeasts were plated onto double dropout medium SM-Leu-Trp [6.7 g/L Yeast Nitrogen Base without Aminoacids (Sigma-Aldrich, USA), 20 g/L agar, 0.6 g/L DO Supplement -Leu-Trp-His-Ade (Clontech, USA), 0.2 g/L Adenine Hemisulfate (Sigma-Aldrich, USA), 0.2 g/L L-Histidine (Sigma-Aldrich, USA)] plates. After 3 to 5 days of incubation at 30 °C (VWR® INCU-Line®IL 23R), a single colony was streaked on SM-Leu-Trp-His [6.7g/L Yeast Nitrogen Base without Aminoacids, 20g/L agar, 0.6 g/L DO Supplement -Leu-Trp-His-Ade, 0.2 g/L Adenine Hemisulfate] and SM-Leu-Trp-His+3AT [6.7g/L Yeast Nitrogen Base without Aminoacids, 20g/l agar, 0.6 g/L DO Supplement -Leu-Trp-His-Ade, 0.2 g/L Adenine Hemisulfate, 0.84 g/L 3-amino-1,2,4-triazole (3AT) (Sigma-Aldrich, USA)] plates, which were incubated at 30 °C for 10 days. For the final plates, mated yeast cells were resuspended in 100 µL of sterile PBS. Then, a sequential 10-fold dilution series (1:10) was made for each mating. 20 µL of each solution were placed into SM-Leu-Trp, SM-Leu-Trp-His and SM-Leu-Trp-His+3AT plates

to form a drop. The plates were kept at 30 °C for 7 days. Plates images were acquired using ChemiDoc™ MP Imaging system (Bio-Rad, USA).

Table 9. List of experimental matings.

Mating ID	Strain 1 - AH109	Strain 2 - Y187
M1	p53_pGBKT7	antigen_pGADT7
M2	p53_pGBKT7	pGADT7
M3	pGBKT7	antigen_pGADT7
M4	PSIA_pGBKT7	PSIA_pGADT7
M5	PSIA_pGBKT7	pGADT7
M6	pGBKT7	PSIA_pGADT7
M7	PSIB_pGBKT7	PSIB_pGADT7
M8	PSIB_pGBKT7	pGADT7
M9	pGBKT7	PSIB_pGADT7
M10	PSIA_pGBKT7	PSIB_pGADT7
M11	PSIB_pGBKT7	PSIA_pGADT7

Co-immunoprecipitation assay

The Co-IP assays were performed to assess protein-protein interactions *in vitro* between purified PSI proteins. For this purpose, 2 µg of FLAG-PSI A/B-6xHis, 0.5 µL of DYKDDDDK Tag Monoclonal Antibody mouse (Agrisera, Sweeden) and 100 µL of binding buffer [20 mM Tris-HCl, 150 mM NaCl, 0.05 % (v/v) Tween-20] were incubated for 1 hour at RT on a rotator. The putative interactions were tested at two different pH values: 3.5 and 4.5. During the incubation step, 20 µL of Pierce™ protein G (Thermo Fisher Scientific, USA) agarose resin was washed 2 times, 5 minutes each, with 500 µL of binding buffer with slow rotation at 4 ºC. Between the washes, the beads were centrifuged at 700 x g for 5 minutes. Two controls were made: one to assess the binding of the FLAG-PSI A/B purified proteins to the beads (positive control), and the other to ensure that the putative interactor wasn't binding to the beads (negative control). The positive controls were made by combining 2 µg of FLAG-PSI A/B-6xHis with 0.5 µL antibody, 100 µL of binding buffer and 20 µL of beads, whereas the negative controls were made by combining 2 µg of GST-PSI A/B-6xHis with 0.5 µL antibody, 100 µL of binding buffer and 20 µL of beads. 20 µL of prewashed beads and 6 µg of GST-PSI A/B-6xHis were added to the mixture, and the reactions were incubated for another hour at RT, with slow rotation. Post-incubation, the beads were centrifuged at 700 x g for 3 minutes at 4 °C, followed by a washing step 2 times, 5 minutes at 4 °C, with slow rotation. Between the washes, the samples were centrifuged as described before. The supernatant was removed, and the beads were complexed with 20 µL of 1xSDS-Page sample loading buffer (NZYTech, Portugal), heated at 95 °C for 5 minutes and

centrifuged at maximum speed for 4 minutes. Denaturated proteins and inputs were then separated in a 15 % polyacrylamide gel as described in section 2.7.

Pull-down assay

In vitro pull-down assays were performed using purified PSI proteins. 30 µL of Pierce™ Glutathione Agarose (Thermo Fisher Scientific, USA) beads were washed three times, 5 minutes each, with 1 mL of pull-down buffer [50 mM Hepes, 50 mM NaCl, 0.1 % Triton X-100, 5 mM DTT]. Three pH values were tested, pH 5.0, 6.8 and 7.4. Since, binding of GST-tagged proteins is not efficient at pH less than 6.5, 25 µL of ChromoTek DYKDDDDK Fab-Trap™ Agarose (Chromotech, Germany) beads were used to test the interactions at pH 5.0. Between the washes, the beads were centrifuged at 500 x g for 5 minutes. After the last wash, a 50 % slurry of the beads was made with pull-down buffer: the supernatant was discarded and 15 µL of pull-down buffer was added to the beads. 6 µg of GST-PSI A/B-6xHis were incubated with 2 µg of FLAG-PSI A/B-6xHis, and the final volume was brought up to 100 µL with pull-down buffer. The reactions were incubated for 1 hour at 4 °C on an overhead rotator. Two controls were made: one to assess the binding of the GST-tagged proteins to the beads (positive control), and the other to ensure that the putative interactor wasn't binding to the beads (negative control). The positive controls were made by combining 30 µL of beads with 6 µg of GST-PSI A/B-6xHis and binding buffer up to 100 µL final volume, whereas the negative controls were made by combining 2 µg of FLAG-PSI A/B-6xHis with 30 µL of beads and binding buffer up to 100 µL final volume. Beads were washed two times 15 seconds with 500 µL of pull-down buffer and centrifuged at 500 x g for 15 seconds. After the last wash, 20 µL of 1xSDS-Page sample loading buffer (NZYTech, Portugal) was added, heated at 95 °C for 5 minutes and centrifuged at maximum speed for 4 minutes. Inputs and pull-down samples were then separated in a 15 % polyacrylamide gel as described in section 2.7 and stained with Silver Staining. During the entire procedure, samples were kept on ice.

2.7 Polyacrylamide gel electrophoresis (SDS-PAGE)

Purified proteins, Co-IP and pull-down samples were separated on a 15% acrylamide gel under denaturing and reducing conditions (β-mercaptoethanol). The electrophoresis apparatus (Bio-Rad, USA) was mounted according to manufacturer's instructions and a 15 % acrylamide running gel prepared [1.7 mL distilled deionized water, 1.9 mL of polyacrylamide (40 % acrylamide/bisacrilamide solution - Bio-Rad), 1.35 mL 1.5 M Tris pH 8.8, 50 µL 10 % (w/v) SDS, 50µL 10 % (w/v) APS and 2 µL of TEMED

(N, N, N', N'-Tetramethylethylenediamine - Sigma)]. Following the addition of the mixture into the space between the glass and the plate, isopropanol was added on top of the running gel to enable polymerization and level the gel surface. After polymerization, isopropanol was removed by rinsing the running gel surface with distilled and deionized water, and a 4 % acrylamide stacking gel was made [2.472 mL distilled deionized water, 375 L of polyacrylamide (40)]. oRad), 130 mL of 0.5 M Tris pH 6.8, 10 mL of 10 % (w/v) SDS, 10 mL of 10 % (w/v) APS, and 3 mL of TEMED]. The gel was then added onto the top of the polymerized running gel and a comb was placed. After polymerization, the comb was removed, and the wells were washed with water.

Protein samples were prepared by adding 1xSDS-Page sample loading buffer (NZYTech, Portugal) to protein extracts. The samples were incubated at 95 °C for 5 minutes and centrifuged for 4 minutes at maximum speed immediately before application. Electrophoresis was conducted at 100-150 V in SDS-PAGE running buffer [165 mM Trizma base, 128 mM glycine and 1 % (w/v) SDS] until the blue color from the SDS-PAGE sample buffer ran out of the gel.

Coomassie and Silver staining

Band visualization from the Co-IP and protein purification samples was done using Coomassie staining technique by incubating the polyacrylamide gel with 25 mL BlueSafe (NZYTech, Portugal) ON, following the manufacturer's instructions.

Samples of the pull-down assays were stained with Silver Stain Plus Kit (Bio-Rad, USA), according to the manufacturer's instructions. Immediately after running the gel as described above, it was rinsed with distilled and deionized water to remove any remaining SDS-PAGE running buffer. Then, the gel was submersed in fixative [40 % methanol, 10 % acetic acid (v/v)] for 30 minutes. After that time, the solution was removed and replaced by oxidizer [90 mL of H_20, 10 mL of Oxidizer Concentrate (Bio-Rad, USA)] for 5 minutes. The gel was then washed for 15 minutes with large volumes of water and the wash was changed 7 times during the first 5 minutes. After that, the gel was incubated for 20 minutes in Silver reagent [90 mL of H_20, 10 mL of Silver Reagent Concentrate (Bio-Rad, USA)] followed by a quick water rinse. Developer [32 g Developer (Bio-Rad, USA) per 1 L of H_20] was then added to the gel until a brown precipitate appeared. Upon this, the solution was removed, and fresh developer was added. This step was repeated, and the gel remained in developer until the bands reached the desired intensity. The reaction was ended with stop solution [5 % acetic acid (v/v)] and after 15 minutes gel images were acquired. During the entire procedure, gels were completely immersed in the solutions, and glass recipients washed with distilled and

deionized water were used as well as gloves to avoid contact with the gel. Besides, all incubations were done under constant agitation.

Western Blot

To confirm the specificity of the bands detected in the Silver staining, samples were transferred to a membrane for western blot analysis. Transfer to a PVDF membrane (Protran nitrocellulose Hybridization Transfer Membrane, 0.2 mM - Schleicher and Schuell) was performed using a semidry transfer system (Trans-Blot Turbo, Bio-Rad, USA), according to manufacturer's instructions. The membrane was then briefly washed with TBS-T [50 mM Tris, 200 mM NaCl, 0.1 % (v/v) Tween 20]. Non-specific binding was blocked with TBS-T and 5 % non-fat dry milk (w/v) for one hour at room temperature. Primary antibody (DYKDDDDK Tag Monoclonal Antibody, Thermo Fisher Scientific™, USA) was diluted 1:1000 in blocking buffer and the membrane was incubated with this dilution overnight at 4 °C, with shaking. Afterwards, the membrane was washed with TBS-T (fifteen minutes plus three times five minutes) and incubated for one hour at room temperature with a secondary antibody (Goat Anti-Mouse IgG (H + L)-HRP Conjugate, Bio-rad, USA), diluted 1:5000 in blocking buffer. The membrane was washed again as before and one final time with TBS-T for five minutes. The bands were revealed using the Clarity™ Western ECL Substrate (Bio-Rad, USA) according to manufacturer's instructions and chemiluminescence visualized in a ChemiDoc™ MP Imaging System (Bio-Rad, USA) running ImageLab (Bio-Rad, USA).

2.8 Cell imaging: Confocal Laser Scanning Microscopy Analysis

A. thaliana seedlings infiltrated by vacuum (section 2.3) expressing the constructs of our interest were imaged using CLSM Leica SP5 (Leica, Germany). The constructs were as follows: fusions of PSI A and PSI B with *m-Cherry*. Prior to the imaging, cotyledons from *A. thaliana* were isolated and placed on a slide with a drop of sterile water and covered by a cover slip. *mCherry* emission was detected between 580-630 nm, using 561nm excitation. The images obtained were of the leaf lower epidermis and were analysed with ImageJ 1.53 image processing software.

2.9 Data processing and statistical analysis

SDS-PAGE gel images were analysed with ImageJ 1.53 image processing software (Schneider et al., 2012) and western blots using the ImageLab software version 4.1 (Bio-Rad, USA). Graphical representations were all constructed using GraphPad

Prism 8.0.1 software (GraphPad Software, USA). All experiments were repeated at least three times, as it is indicated in the figures legends. The data was analysed with the student's t-test for significance (development assay). The statistical significance was elucidated as $P \geq 0.05$, not significant (ns), $P < 0.05$(*).

3. Results

3.1 Characterization of *Arabidopsis thaliana syp2* mutants

Phenotypic and developmental analysis

The mutants used in this study were already characterized at the phenotypical level, and syp22 was found to have a primary function in plant growth and development (Ohtomo et al., 2005; Shirakawa et al., 2010; Ueda et al., 2006). However, and because only two time points of plant growth were compared, we conducted a morphological and developmental assay. All plants were grown under the same conditions, after sustaining 72 hours of seed inhibition (see section 2.1).

A morphological comparison between the mutants and WT plants (Figure 10) showed that *syp22-3* mutant plants were slightly shorter compared to WT. No visible defects were detected in *syp23* plants. However, plants from the double mutants *syp22-1 syp23* and *syp22-3 syp23* exhibited the most pronounced morphological defects among the selected lines. Both presented to be smaller and have fewer and wavy leaves when compared to WT or *syp22-3* and *syp23* single mutants.

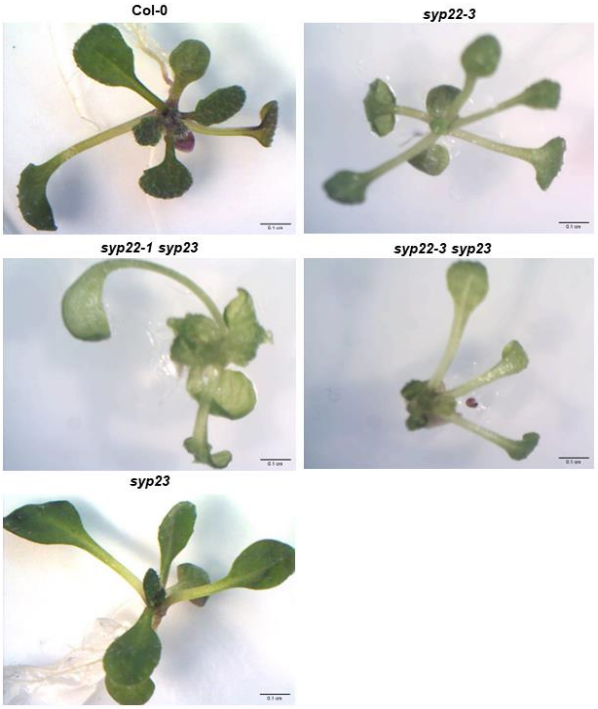

Figure 8. *Arabidopsis thaliana syp2* mutant seedlings (Col-0), at 15 days after sowing (DAS). The mutant name is indicated above the corresponding seedling. Seeds were sown and germinated on half-strength Murashige and Skoog medium supplemented with 1.5% (w/v) sucrose and 0.8% (w/v) agar and kept in a growth chamber under long-day conditions. Scale bar, 0.1cm. Results are representative of at least 20 plants. Images acquired with Moticam 2500.

After, we tested the effect of mutations on root length. When compared to WT plants, *syp22-3*, *syp22-1 syp23* and *syp22-3 syp23* plants showed statistically significant differences in primary root length, with an overall decrease in primary root growth. In single mutant *syp22-3,* the primary root length was further reduced when compared to the double mutants, whereas *syp23* plants were not affected in primary root length (Figure 11).

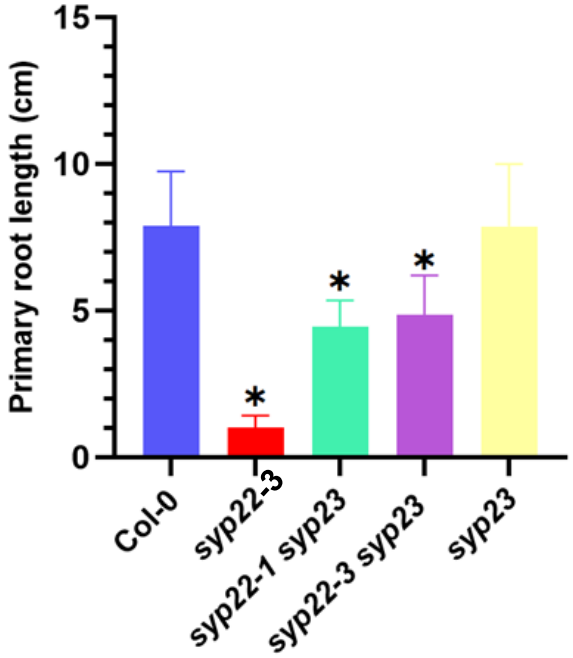

Figure 9. *Arabidopsis thaliana syp2* mutants (Col-0) primary root length measurement. Seeds were germinated on half-strength Murashige and Skoog medium supplemented with 1.5% (w/v) sucrose and 0.8% (w/v) agar and kept in a growth chamber under long-day conditions for 15 days after sowing (DAS). Data and error bars represent mean ± SD (n=15). * Indicates significant differences according to student's t-test between Col-0 and *syp2* mutant lines (*p < 0.05).

Considering the differences observed among the lines, a growth-stage-based phenotypic analysis (Boyes et al., 2001) was performed and seven stages of *syp2* mutants' growth were compared to WT plants (Figure 12, green bars). The *syp23* single mutant (Figure 12, red bars) did not show a delay during its development, as indicated by similar growth stage times, compared to WT plants. Nevertheless, the single mutant *syp22-3* (Figure 12, blue bars) and the double mutants *syp22-1 syp23* (Figure 12, yellow bars) and *syp22-3 syp23* (Figure 12, purple bars) presented a pronounced delay in growth relative to WT. We also observed that *syp22-3* (Figure 12, blue bars), among all the mutants and WT, presented the slowest growth, as it is the last to present cotyledons fully opened, and this delay was maintained in the following stages, until the presence of

the first siliques. Among the double mutants, differences seem to be similar between the two, when compared to WT. However, the emergence of the first flower buds was more delayed in double mutants, than in single mutant *syp22-3* (Figure 12, blue bars).

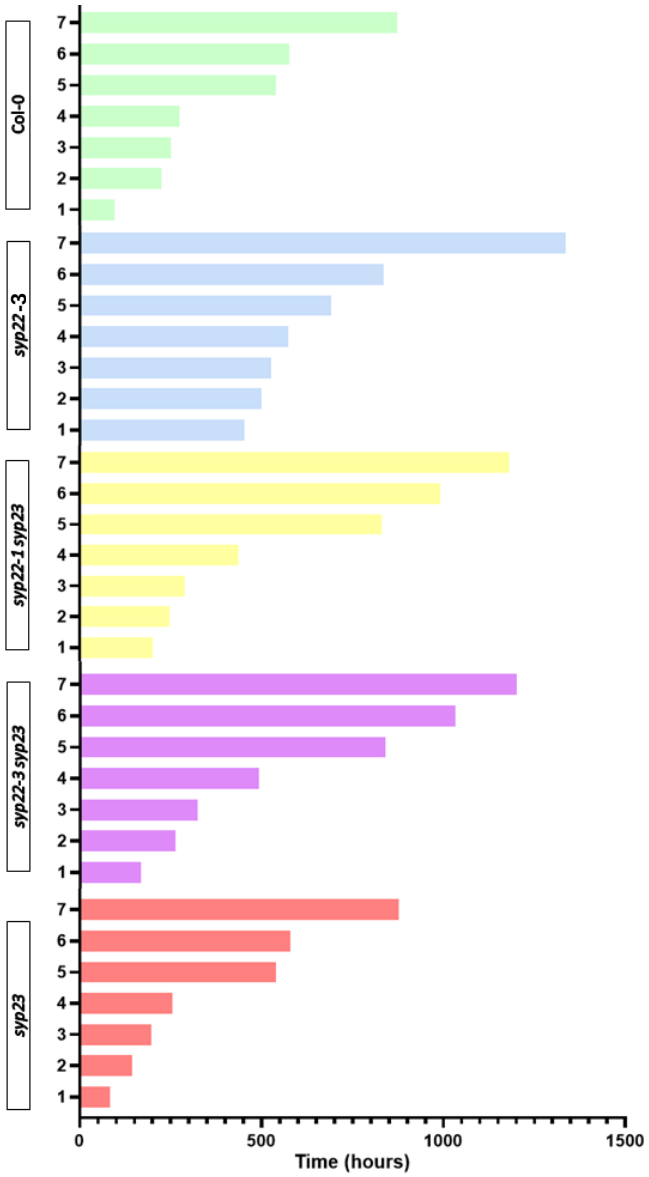

Figure 10. Developmental stages of *Arabidopsis thaliana syp2* mutants (Col-0). Seeds were germinated and grown on half-strength Murashige and Skoog medium supplemented with 1.5% (w/v) sucrose and 0.8 % (w/v) agar, after a stratification of 3 days at 4 °C. 15 days after sowing (DAS), seedlings were transferred into pots with fertilized substrate and kept in a growth chamber under long-day conditions. Selected growth time points were measured in hours. Results are representative of at least three independent assays.1: Cotyledons fully opened; 2 -Two rosette leaves; 3: Three rosette leaves; 4: Four rosette leaves; 5: First flower buds visible; 6: First flowers open; 7: Presence of first siliques.

Ultrastructural characterization of syp2 lines

After the morphological characterization of the mutant lines, the ultrastructure of the cells was assessed through TEM, as described in section 2.2, to evaluate whether the mutations affect or not the organelles structure, in particular those from the

endomembrane system. Ultrathin sections of 15-day-old seedlings' leaves of WT (Figure 13) and *syp22-3*, *syp22-1 syp23* and *syp23* (Figure 14-16) plants were observed. During the timeline of this work, it was not possible to obtain images for the *syp22-3 syp23* mutant.

The WT leaves (Figure 13) presented the natural organization and structures found in plant cells, namely cell wall and chloroplasts. These are well organized, and chloroplasts show normal thylakoid formation, as we can observe the organization in grana stacks and stroma lamellae, as well as starch granules in the stroma. Besides, inside the chloroplasts, little plastoglobuli inclusions can be observed (Figure 13A and 13B). The cell wall and the cytoplasmatic membrane are well preserved, and scattered through the cytoplasm are organelles, such as mitochondria (Figure 13B, yellow arrow) and Golgi apparatus (Figure 13D, yellow arrow). Some vesicles (Figure 13D, yellow arrow) were also observed, usually in the vicinity of Golgi and ER, and a large vacuole, occupying most of the cell space.

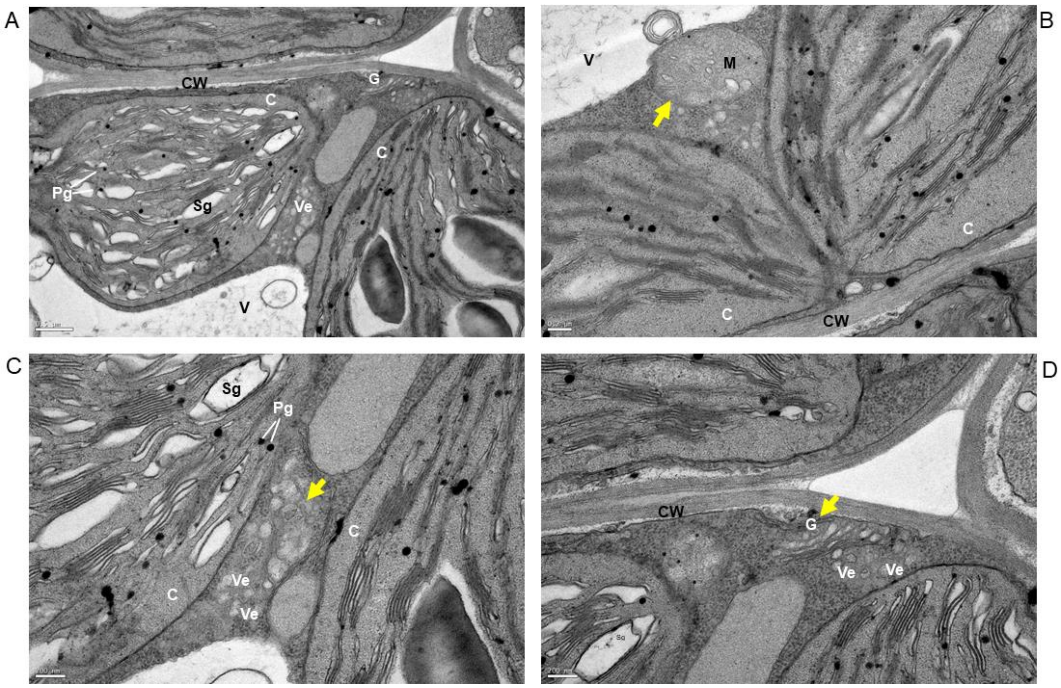

Figure 11. Transmission electron micrographs of 15-day-old leaf cells from *Arabidopsis thaliana* wild-type (Col-0) A) to D). Scale bars, indicated on left bottom corner of each image. Images were analysed and processed using ImageJ software. Abbreviations: C: Chloroplast; Cw: Cell-wall; G: Golgi apparatus; M: mitochondria; Pg: Plastoglobuli; Sg: Starch granules; V: vacuole; Ve: Vesicle.

In the *syp22-3* mutant (Figure 14), contrary to what was observed in WT cells, no starch granules were found inside chloroplasts, but there are still some plastoglobuli. Nevertheless, chloroplasts presented the usual crescent shape, with developed

thylakoids. One intriguing feature of this mutant is the density of the cytoplasm, which is very compact and clustered. Moreover, the vacuole lumen is not as translucent as in the WT, with more content accumulated inside. Also, a dark precipitate can be seen along the tonoplast, facing the lumen of the vacuole (Figure 14A and 14C, orange arrows).

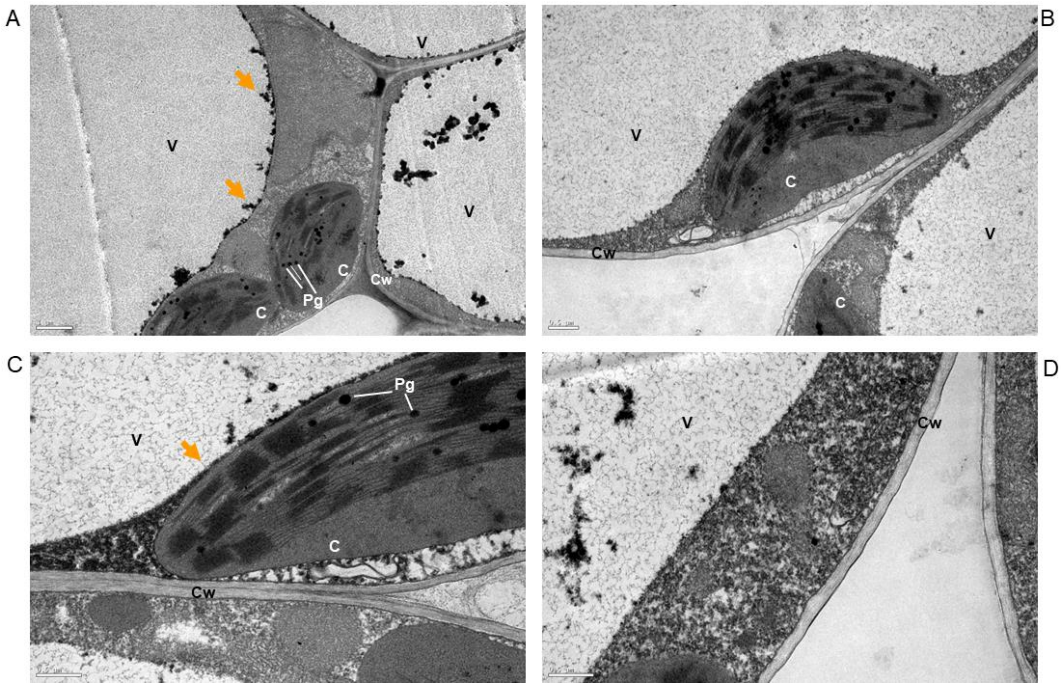

Figure 12. Transmission electron micrographs of 15-days-old leaf cells from *Arabidopsis thaliana syp22-3* mutant (Col-0) A) to D). Scale bars, indicated on left bottom corner of each image. Images were analysed and processed using ImageJ software. Abbreviations: C: Chloroplast; Cw: Cell-wall; Pg: Plastoglobuli; V: vacuole.

In the *syp22-1 syp23* mutant (Figure 15), chloroplasts lacked internal membrane structures, such as stromal thylakoids or stacked grana thylakoids. The starch granules were smaller compared to the ones found in WT cells (Figure 15A). As observed for the *syp22-3* mutant, the density of both cytoplasm and vacuole is higher than in WT cells. Moreover, several vesicles were observed in the cytoplasm (Figure 15B and 15C, yellow arrows).

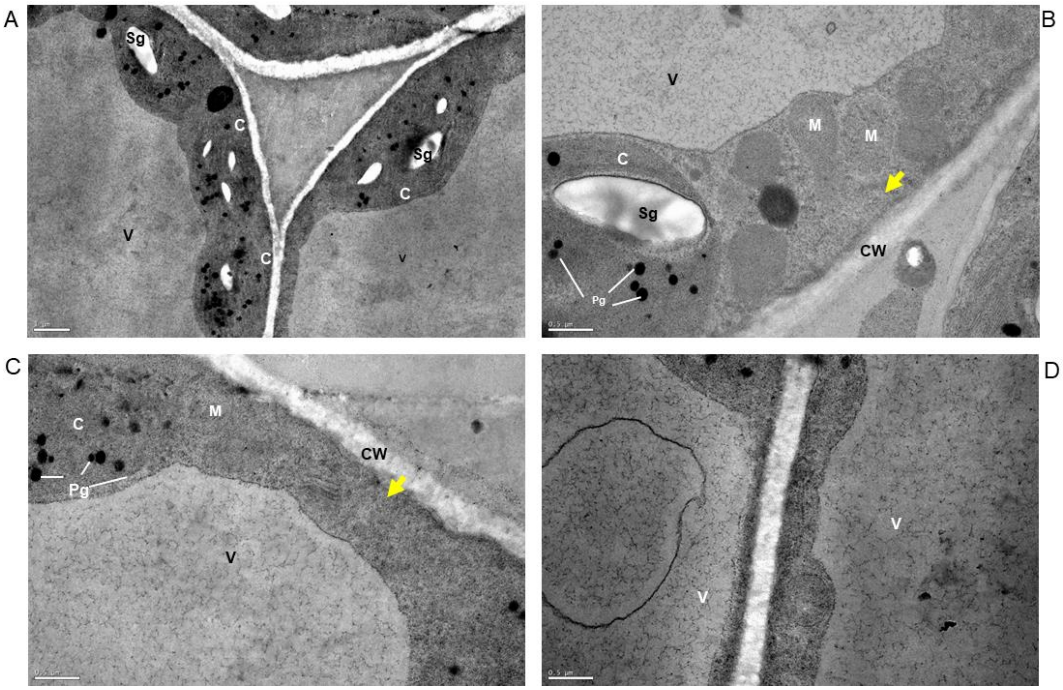

Figure 13. Transmission electron micrographs of 15-days-old leaf cells from *Arabidopsis thaliana syp22-1 syp23* mutant (Col-0) A) to D). Scale bars, indicated on left bottom corner of each image. Images were analysed and processed using ImageJ software. Abbreviations: C: Chloroplast; Cw: Cell-wall; M: mitochondria; Pg: Plastoglobuli Sg: Starch granules; V: vacuole.

Finally, in the *syp23* mutant (Figure 16), one of the major differences when comparing with WT line was the huge well-defined starch granules observed in the chloroplasts (Figure 16A), despite chloroplasts presented a normal morphology. Interestingly, a plasmodesmata can be observed. The Golgi apparatus presented enlarged cisternae (Figure 16B, yellow arrows), and numerous mitochondria and vesicles (Figure 16C, yellow arrow) may be observed in the cytoplasm along with PVC/MVB/LE vesicles (Figure 16D, yellow arrow). Similarly to what was observed in the other mutants, the vacuole is filled with content (Figure 16).

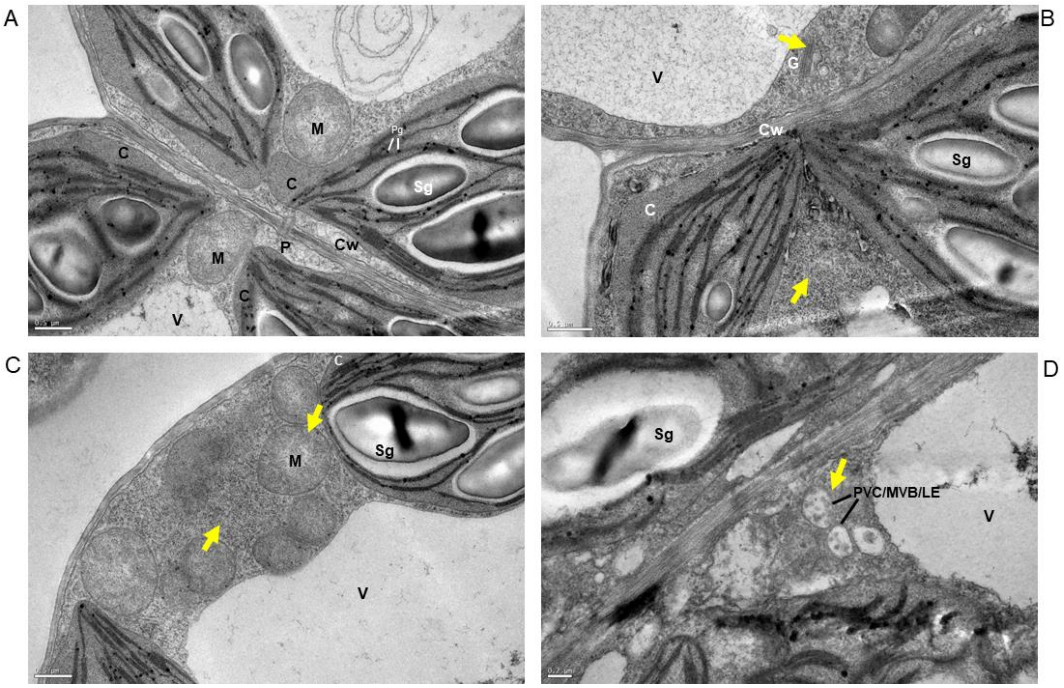

Figure 14. Transmission electron micrographs of 15-day-old leaf cells from *Arabidopsis thaliana syp23* mutant (Col-0) A) to D). Scale bars, indicated on left bottom corner of each image. Images were analysed and processed using ImageJ software. Abbreviations: C: Chloroplast; Cw: Cell-wall; M: mitochondria; P: Plasmodesmata; Pg: Plastoglobuli; PVC/MVB/LE: Pre-vacuolar compartment/ Multivesicular body/ Late endosome; Sg: Starch granules; V: vacuole.

3.2 Expression of PSIs in vacuolar trafficking defective plants

The heterologous expression of PSIs fused with mCherry allowed us to assess the localization of PSI A and PSI B in the vacuolar defective lines. The constructs used have a signal peptide (SP) isolated from tobacco chitinase A.

PSI A was only found in the vacuolar compartments in the WT line (Figure 17A). However, in *syp22-3* this domain besides being observed in the vacuole, was also found in multiple spherical structures within the lumen of this organelle (Figure 17C, white arrows). One intriguing feature was the pattern observed in the vacuole lumen, where two distinct zones can be distinguished (Figure 17C). In the double mutants, PSI A was not observed in the vacuole, and more differences relative to the WT were observed. In *syp22-1 syp23*, PSI A was detected in the ER, and in the membrane of spherical structures within the vacuole lumen (Figure 18C, white arrows). Similarly, in the *syp22-3 syp23* line, PSI A appeared in the ER (Figure 18E).

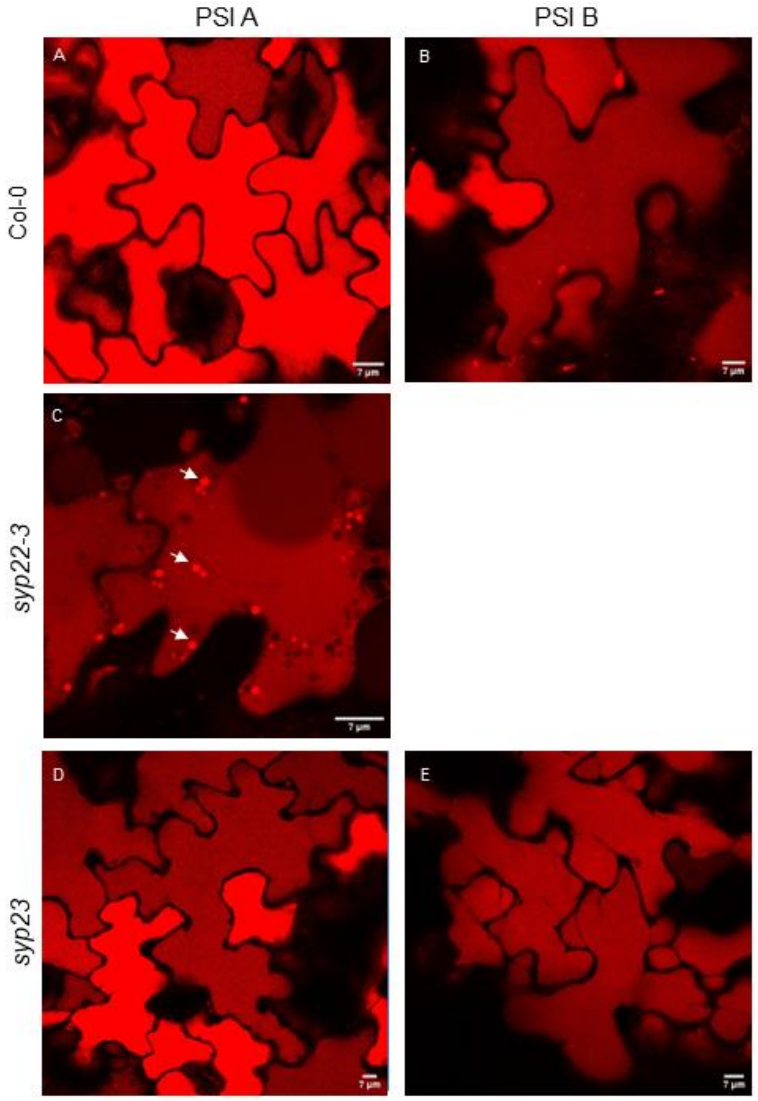

Figure 15. Subcellular localization of Cardosin PSI A and PSI B fused with mCherry in cotyledon leaves of *Arabidopsis thaliana* wild-type and *syp22-3* and *syp23* mutant plants. (A) Expression of PSI A-mCherry in wild-type, found in the vacuole; (B) Expression of PSI B-mCherry in wild-type, found in the vacuole; (C) Expression of PSI A-mCherry in *syp22-3*, found in the vacuole; (D) Expression of PSI A-mCherry in *syp23,* found in the vacuole; (E) Expression of PSI B-mCherry in *syp23*, found in the vacuole. Note the evident vacuolar accumulation in the Arabidopsis lines (wild-type, *syp22-3* and *syp23*). White arrows indicate other subcellular accumulation sites. All images were acquired 3 days post-infiltration and were analysed and processed using ImageJ/Fiji software. Scale bar: 7 µm.

Regarding PSI B localization, in WT it was mostly found in the vacuole, and at the cell periphery (Figure 17B). In the *syp22-1 syp23* mutant plants, PSI B was observed in the ER (Figure 18D). The same is observed for *syp22-3 syp23* (Figure 18F). In *syp23*, PSI B was only observed in the vacuolar compartments (Figure 17E). Transformation of *syp22-3* line with PSI B was not successful and for that reason the correspondent images are not presented.

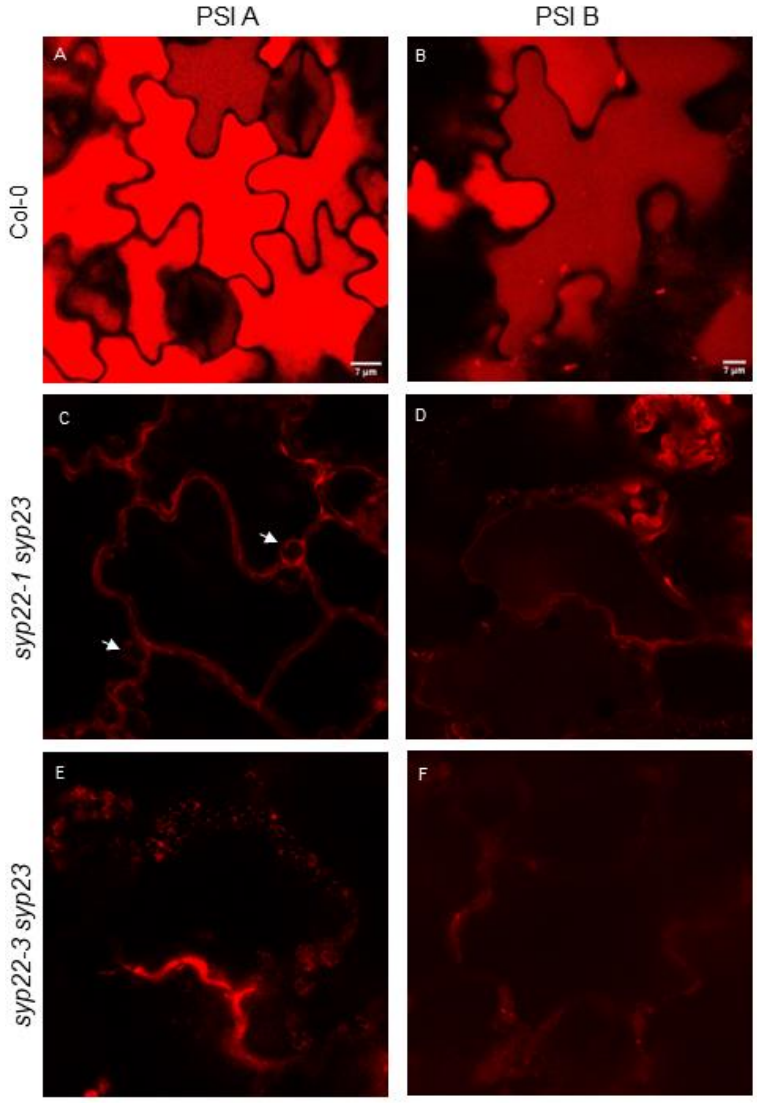

Figure 16. Subcellular localization of Cardosin PSI A and PSI B fused with mCherry in cotyledon leaves of *Arabidopsis thaliana* wild-type, *syp22-1 syp23* and *syp22-3 syp23* mutant plants. (A) Expression of PSI A-mCherry in wild-type, found in the vacuole; (B) Expression of PSI B-mCherry in wild-type, found in the vacuole; (C) Expression of PSI A-mCherry in *syp22-1 syp23*, found in early endomembrane compartments; (D) Expression of PSI B-mCherry in *syp22-1 syp23,* found in early endomembrane compartments; (E) Expression of PSI A-mCherry in *syp22-3 syp23,* found in early endomembrane compartments; (F) Expression of PSI B-mCherry in *syp22-3 syp23*, found in early endomembrane compartments. Note the evident vacuolar accumulation in the Arabidopsis wild type. White arrows indicate other subcellular accumulation sites. All images were acquired 3 days post-infiltration and were analysed and processed using ImageJ/Fiji software. Scale bar: 7 µm.

3.3 In-vitro search for PSI-PSI interactions

PSI purification from bacteria

Cloning

As we were interested in assessing if a motif in cardosin PSI A (Frazão et al., 1999) was somehow involved in its interaction capability, we started by obtaining the construct GST-PSI A_Y95A/L99A. First, we amplified PSI A_Y95A/L99A, with a PCR reaction, followed by analysis of the fragments obtained by electrophoresis in an agarose gel. With specific enzymes, PSI A_Y95A/L99A was fused to pGEX-6p-1 plasmid, that already had a GST-tag. After enzymatic assembly, colonies from the bacterial transformation were screened by enzymatic digestion to verify the presence of PSI A_Y95A/L99A in pGEX-6p-1. The digestion fragments (312 bp and 4984 bp) had the expected sizes (Figure 19, lane 4). Finally, the GST-PSI A_Y95A/L99A construct was confirmed by DNA sequencing (Figure 20). One positive clone was selected and used to transform BL21 cells.

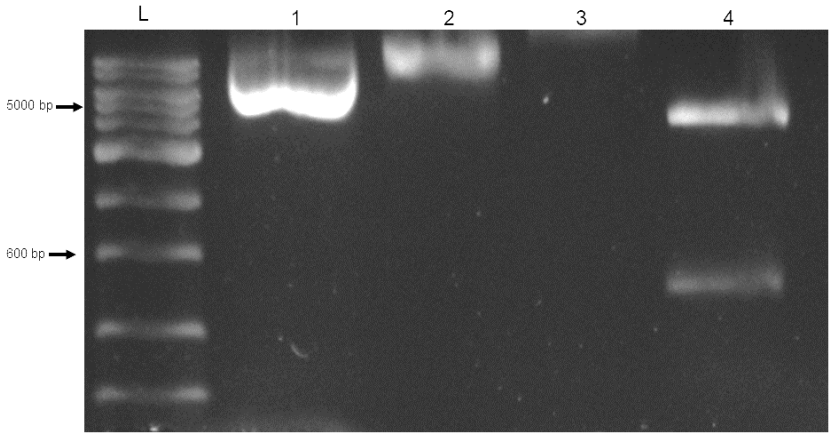

Figure 17. Restriction digestion analysis of pGEX-6p-1-GST-PSI A_Y95A/L99A with XhoI and BamHI enzymes. pGEX-6p-1-GST-PSI A_Y95A/L99A was cut with Anza XhoI and Anza BamHI (Invitrogen by Thermo Scientific, USA). The resulting DNA fragments had the expected sizes (312 bp and 4984 bp). L: DNA ladder (GeneRuler DNA Ladder Mix (Thermo Scientific)); 1, 2, 3, 4: digestion of distinct miniprep of pGEX-6p-1-GST-PSI A_Y95A/L99A.

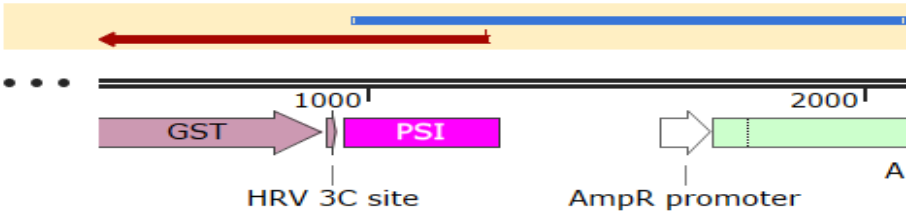

Figure 18. Alignment of the sequencing results of pGEX-6p-1-GST-PSIA. The sequencing results were aligned with the respective expected of pGEX-6p-1-GST-PSIA_Y95A/L99A sequence. The sequence alignment was performed resorting to SnapGene software (www.snapgene.com). Red and blue portions in the yellow box represent sequence match and alignment, whereas white portions represent no alignment.

Large scale purification

The purified PSIs - GST-PSI (A/B)-6xHis and FLAG-PSI (A/B)-6xHis - were obtained by batch purification from bacterial lysates with HisPur Ni-NTA Superflow Agarose, as described in section 2.5. The presence of the PSIs on the several fractions was evaluated by Coomassie blue stained SDS-PAGE gels (Figure 21-24). The expected band sizes are ~40 kDa for GST-tagged PSIs and ~15kDa for FLAG-tagged PSIs.

Regarding the purification of GST-tagged PSI A and PSI B, the protein of the expected size was observed in all the lanes, although the protein yield is variable among all (Figures 21 and 22). The analysis of the gel pertaining to GST-PSI A purification (Figure 21) showed that there was a difference between the non-induced (NI) and induced (I) fractions (Figure 21, lanes NI and I), with the appearance of a stronger band around 35 kDa. This band was also present in the bacterial lysate (Figure 21, lane L), but did not seem to be present in the soluble fraction (SF) and flow through fraction (FT) (Figure 21, lanes SF and FT). However, it appeared again in the bound to resin fraction (BR) and washed resin fraction (WR), confirming that GST- PSI A was successfully bound to the resin (BR) (Figure 21, lanes WR and BR). Furthermore, the band was also observed in the elutions (Figure 21, lanes E1-E5) as well as in the resin after elution (RE) fractions (Figure 21, lane RE).

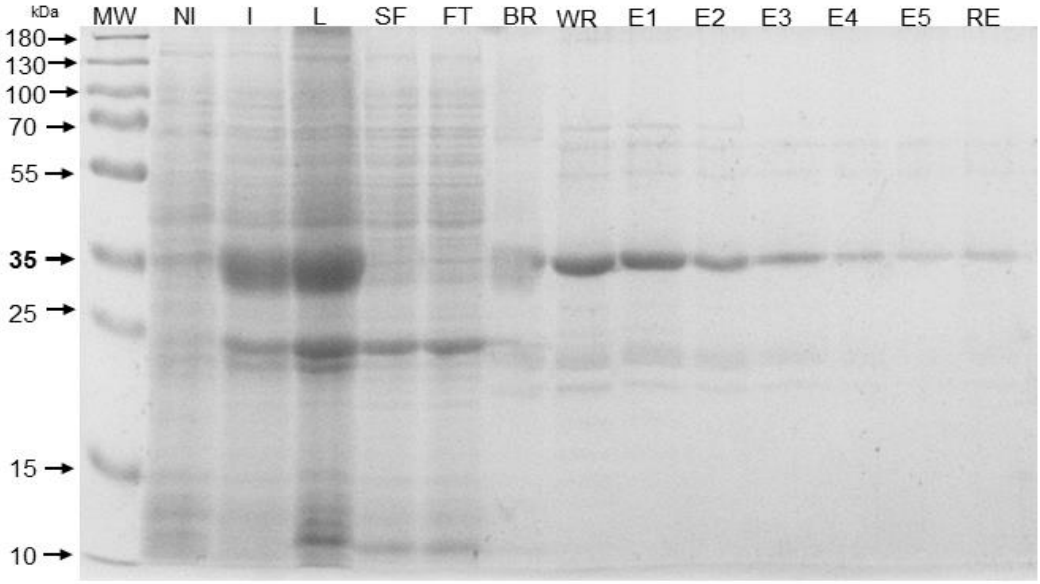

Figure 19. SDS-PAGE analysis of GST-PSI A-6xHis purification. Coomassie blue-stained 15 % SDS-PAGE gel of purified fractions obtained during His-tagged GST-PSI A purification. MW: Molecular weight (PageRuler™ Prestained Protein Ladder, Thermo Scientific); NI: non-induced fraction; I: induced fraction; L: lysate fraction; SF: soluble fraction; FT: flow through fraction; BR: bound to resin fraction; WR: washed resin fraction; E1-E5: elution fractions; RE- resin after elution fraction. kDa: kilodaltons.

Regarding GST-PSI B purification, a similar band pattern was observed, however, some variations were found. A slight difference between the non-induced and induced fractions was observed (Figure 22, lanes NI and I), although not as evident as in the case of GST-PSI A purification. Also, by comparing the intensity of the elution fraction bands (Figure 21 and 22, lanes E1-E5), GST-PSI B seemed to have more protein content, judging by the band intensity. These results confirmed the success of GST-PSI (A/B) purification process. Furthermore, no apparent signals of protein degradation were detected.

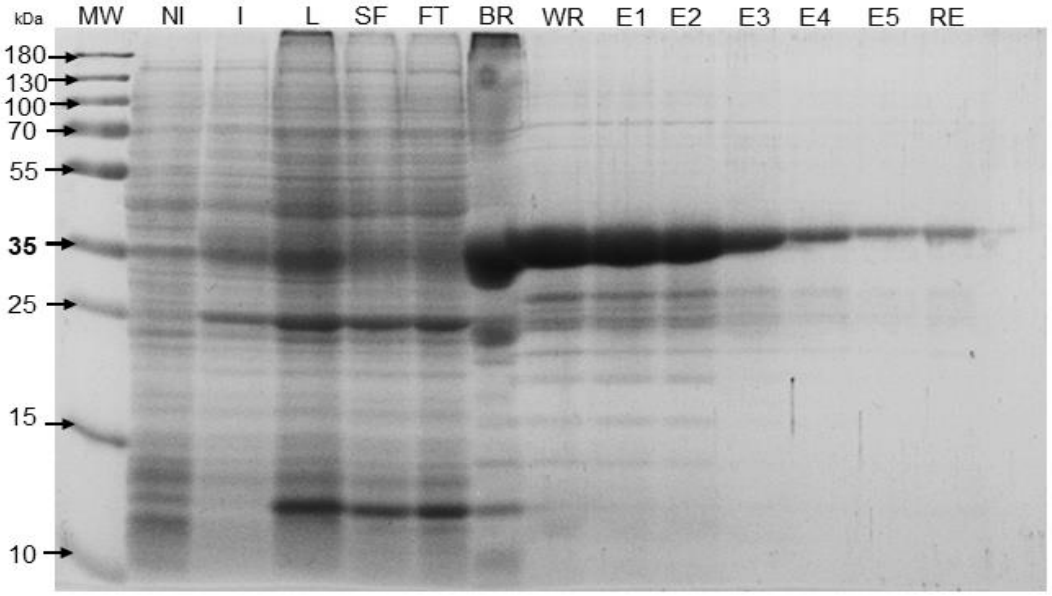

Figure 20. SDS-PAGE analysis of GST-PSI B-6xHis purification. Coomassie blue-stained 15 % SDS-PAGE gel of purified fractions obtained during His-tagged GST-PSI B purification. MW: Molecular weight (PageRuler™ Prestained Protein Ladder, Thermo Scientific); NI: non-induced fraction; I: induced fraction; L: lysate fraction; SF: soluble fraction; FT: flow through fraction; BR: bound to resin fraction; WR: washed resin fraction; E1-E5: elution fractions; RE: resin after elution fraction. kDa: kilodaltons.

Regarding the purification of FLAG-tagged PSI (A/B), the analysis of the gels revealed that the protein of interest was not observed in all the lanes. In the analysis of FLAG-PSI A gel (Figure 23) no differences were found between the non-induced and induced fraction. A band around 15 kDa was observed in the bacterial lysate, soluble fraction, and flow through fraction (Figure 23, lanes L, SF and FT). However, it was absent in the bound to resin fraction, and it appeared again in the washed resin fraction (Figure 23, lanes BR and WR). Nevertheless, the band was also observed in elution 1 and was not found in the remaining elutions (Figure 23, lanes E1-E5). For FLAG-PSI B, the purification gel analysis revealed some differences relative to the ones mentioned above for FLAG-PSI A purification. As so, the induced fraction (Figure 24, lanes NI and I) showed a band of approximately 15 kDa that was not visible in the non-induced fraction. This band was then observed in the soluble fraction, flow-through fraction, bound-to-resin fraction, and washed resin fraction (Figure 24, lanes SF, FT, BR and WR). This demonstrates that FLAG-PSI B was successfully bound to the resin. The five elution lanes all contained the band corresponding to PSI B (Figure 24, lanes E1-E5). Similarly, by comparing the intensity of the elution fraction bands (Figure 23 and 24, lanes E1-E5), FLAG-PSI B seemed to have more protein content, judging by the band intensity. These results show we were successful in purifying FLAG-PSI (A/B) and again no evident signals of degradation were detected.

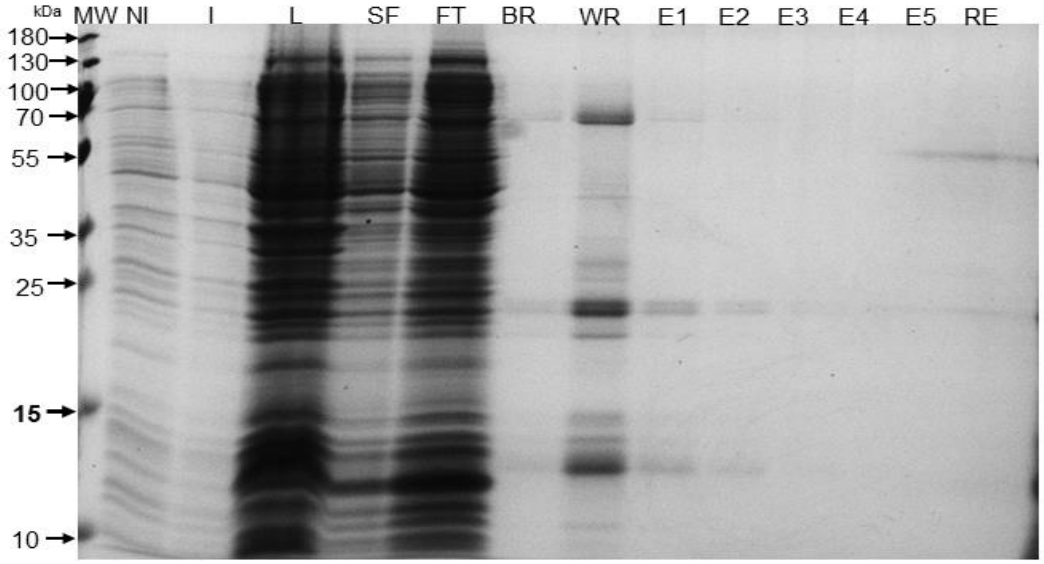

Figure 21. SDS-PAGE analysis of FLAG-PSI A-6xHis purification. Coomassie blue-stained 15 % SDS-PAGE gel of purified fractions obtained during His-tagged FLAG-PSI A purification. MW: Molecular weight (PageRuler™ Prestained Protein Ladder, Thermo Scientific); NI: non-induced fraction; I: induced fraction; L: lysate fraction; SF: soluble fraction; FT: flow through fraction; BR: bound to resin fraction; WR: washed resin fraction; E1-E5: elution fractions; RE: resin after elution fraction. kDa: kilodaltons.

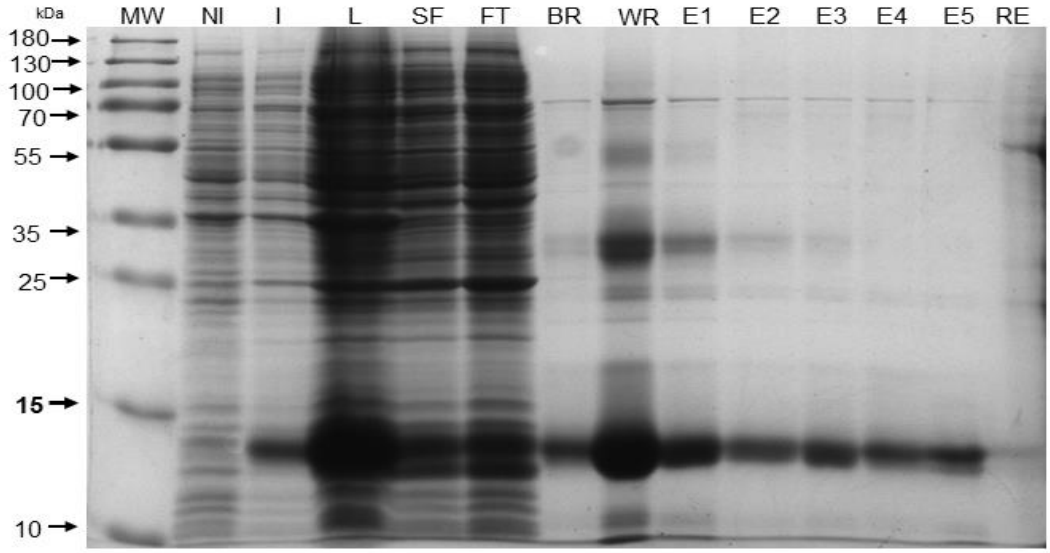

Figure 22. SDS-PAGE analysis of FLAG-PSI B-6xHis purification. Coomassie blue-stained 15 % SDS-PAGE gel of purified fractions obtained during His-tagged FLAG-PSI B purification. MW: Molecular weight (PageRuler™ Prestained Protein Ladder, Thermo Scientific); NI: non-induced fraction; I: induced fraction; L: lysate fraction; SF: soluble fraction; FT: flow through fraction; BR: bound to resin fraction; WR: washed resin fraction; E1-E5: elution fractions; RE: resin after elution fraction. kDa: kilodaltons.

Finally, Figure 25 illustrates the gel corresponding to GST-PSI A_Y95A/L99A purification. Although several bands appeared in the non-induced, induced, lysate, soluble and flow through fractions, there was no band around 35 kDa in those lanes

(Figure 25, lanes NI, I, L, SF and FT). In the bound to resin and washed resin fractions, a band around 35 kDa was present (Figure 25, lanes BR and WR). These results showed that PSI A_Y95A/L99A was bound to the resin. All the elution fraction lanes showed GST-PSI A_Y95A/L99A. However, the sequential elution fractions seemed to have decreasing amounts of protein, judging by the band intensity (Figure 25, lanes E1-E5). Lastly, some GST-PSI A_Y95A/L99A was still bound to the resin at the end of the purification as a band can be observed in resin after elution lane, although in a much lower amount when compared to the washed resin lane (Figure 25, lane RE).

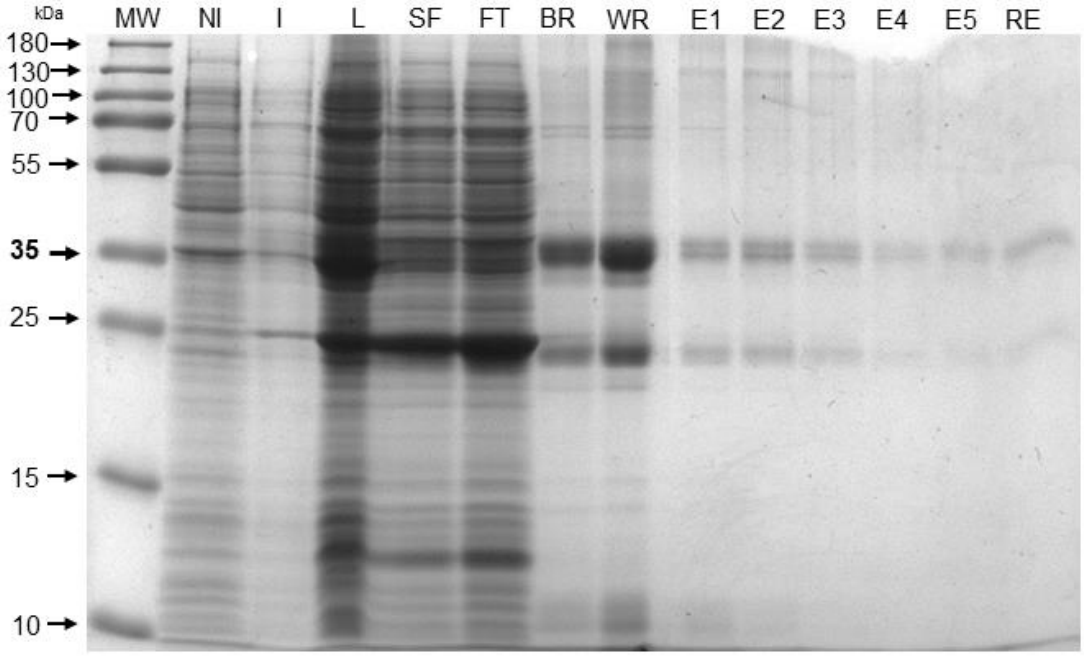

Figure 23. SDS-PAGE analysis of GST-PSI A_Y95A/L99A-6xHis purification. Coomassie blue-stained 15 % SDS-PAGE gel of purified fractions obtained during His-tagged GST-PSI A purification. MW: Molecular weight (PageRuler™ Prestained Protein Ladder, Thermo Scientific); NI: non-induced fraction; I: induced fraction; L: lysate fraction; SF: soluble fraction; FT: flow through fraction; BR: bound to resin fraction; WR: washed resin fraction; E1-E5: elution fractions; RE: resin after elution fraction. kDa: kilodaltons.

For all PSIs [GST-PSI (A/B), FLAG-PSI (A/B), PSI A_Y95A/L99A], the concentration of elution 1 (E1) was determined in a microvolume spectrophotometer, using the Extinction Molar Coefficient and Molecular weight values, calculated in ExPASy ProtParam webtool (web.expasy.org/cgi-bin/protparam/protparam). The concentration values pertaining to elution 1 from FLAG-PSI A confirm that protein was successfully purified, and band differences were due to an error while loading the gel (Table 10).

Table 10. Parameters and concentration of elution 1 resultant from PSI A and PSI B purification.

Elution 1	Instability Index	Extinction Coefficient (M^{-1} cm^{-1}, at 280 nm)	Molecular Weight (Da)	Concentration (mg/mL)
(GST) PSI A	44.01	51965	40538.71	0.63
(GST) PSI B	36.04	44975	40457.55	3.18
(FLAG) PSI A	44.01	10345	15093.91	0.54
(FLAG) PSI B	36.04	3355	15012.75	4.25
PSI A_Y95A/L99A	44.01	51965	40538.71	1.00

In-vitro PSI interactions

Pull-down assay

As a first approach to test the PSI-PSI interactions *in-vitro* we performed a pull-down assay using glutathione-agarose beads according to *Pull-down assay* in section 2.6. Two different pH conditions, pH 7.4 and 6.8, were chosen based on the fact that binding of GST-tagged proteins is not efficient at pH less than 6.5 or greater than 8. PSIs fused to GST tags were used as bait to capture putative interactors. In this assay, the expected band sizes are ~40 kDa for GST-tagged PSIs and ~15kDa for FLAG-tagged PSIs.

At pH 7.4, the PSI A and PSI B GST-tagged and FLAG-tagged correct size bands were present in the input lanes (Figure 26A, lanes 1-3; 8-10). In the pull-down reaction lanes correspondent to the reaction controls (Figure 26A, lanes 4, 5, 11, 12), we observed that GST-tagged proteins were successfully bound to glutathione-agarose-beads and there was no nonspecific binding of FLAG-tagged proteins to the beads. Furthermore, in the pull-down reactions to test PSI A-PSI A, PSI A-PSI B and PSI B-PSI B interactions, bands corresponding to PSI A and PSI B fused to GST were observed in all lanes (Figure 26A, lanes 6, 7, 13, 14). Alongside this, in lane 6, to test the interaction of GST-PSI A with FLAG-PSI A (PSI A-PSI A), a band corresponding to FLAG-PSI A was noticed (Figure 26A, lane 6, yellow arrows). This result suggests that at pH 7.4, FLAG-PSI A is pulled by GST-PSI A.

After assessing PSI-PSI interactions at pH 7.4, we performed the same assay at pH 6.8, to assess if the interactions were pH dependent. The input lanes showed the correct sized bands for both GST PSI (A/B) and FLAG (PSI A/B) (Figure 26B, lanes 1-3; 8-10). In the pull-down reaction lanes (Figure 26B, lanes 4,5,11 and 12) correspondent

to the reaction controls, we observed that GST-tagged proteins were successfully bound to glutathione-agarose-beads and there was no nonspecific binding of FLAG-tagged proteins to the beads. Furthermore, in the pull-down reactions to test PSI A-PSI A, PSI A-PSI B and PSI B-PSI B interactions, bands corresponding to PSI A and PSI B fused to GST were observed in almost all lanes, except in lane 14 (Figure 26B, lanes 6,7 and 13, yellow arrows). However, no bands corresponding to FLAG-PSI (A/B) were detected.

To confirm the bands corresponding to the interactions with FLAG-PSIs, observed in the pull-downs, the same samples were subjected to a western blot using an anti-FLAG antibody. At pH 7.4, the input bands corresponding to FLAG-PSI A and FLAG-PSI B are observed (Figure 27A, lanes 2, 3, 9, 10). The interaction between GST-PSI A and FLAG-PSI A observed in Figure 26A, lane 6, was confirmed by the presence of a soft band corresponding to FLAG-PSI A in the western blot (Figure 27A, lane 6, blue arrow). Likewise, at pH 6.8, the input bands corresponding to FLAG-PSI A and FLAG-PSI B are also observed (Figure 27B, lanes 2, 3, 9, 10). A soft band corresponding to FLAG-PSI B was found in the western blot (Figure 27B, lane 7, blue arrow). This shows that at pH 6.8, PSI A interacts with PSI B.

Curiously, in the input lanes of all SDS-PAGE gels, some non-specific bands were observed besides the specific expected bands for purified PSIs. This is indicative of PSIs forming aggregates or associated with other proteins (Figure 21 to 27).

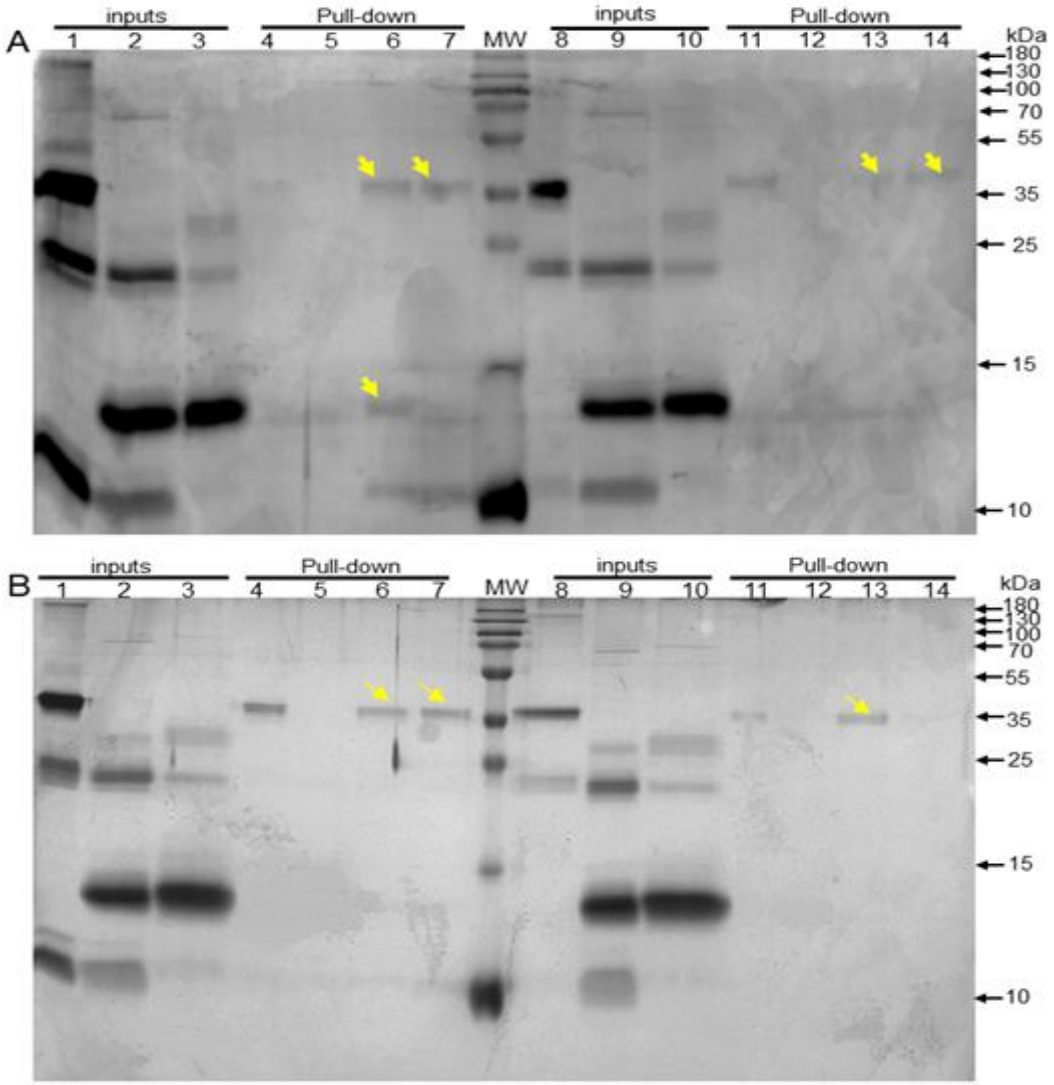

Figure 24. SDS-PAGE analysis of PSI-PSI interactions by pull-down assay at pH 7.4 (A) and 6.8 (B). Inputs and pull-down reactions were analysed on a 15% acrylamide gel under denaturing and reducing conditions (β-mercaptoethanol). Each pull-down lane was loaded with 15 µl pull-down reaction, and input lanes were loaded with 1/3 of the amount of purified protein added to each reaction. As controls, GST-PSI (A/B) and FLAG-tagged PSI (A/B) were assayed as binding to the beads (Pierce Glutathione agarose beads.). After binding to the beads, the GST-tagged PSI were released by elution with 1x SDS-Sample Buffer.The SDS-PAGE gels were stained with Silver staining kit (Bio-Rad). 1: input GST-PSI A; 2: input FLAG-PSI A; 3 input FLAG-PSI B; 4: GST-PSI A + beads; 5: FLAG-PSI A + beads; 6: GST-PSI A+FLAG-PSI A+ beads; 7: GST-PSI A+FLAG-PSI B+ beads; MW: Molecular Weight (PageRuler™ Prestained Protein Ladder, Thermo Scientific); 8: input GST-PSI B; 9: input FLAG-PSI A;10: input FLAG-PSI B;11: GST-PSI B + beads;12: FLAG-PSI B + beads;13: GST- PSI B + FLAG PSI A + beads; 14: GST- PSI B + FLAG PSI B + beads. kDa: kilodaltons.

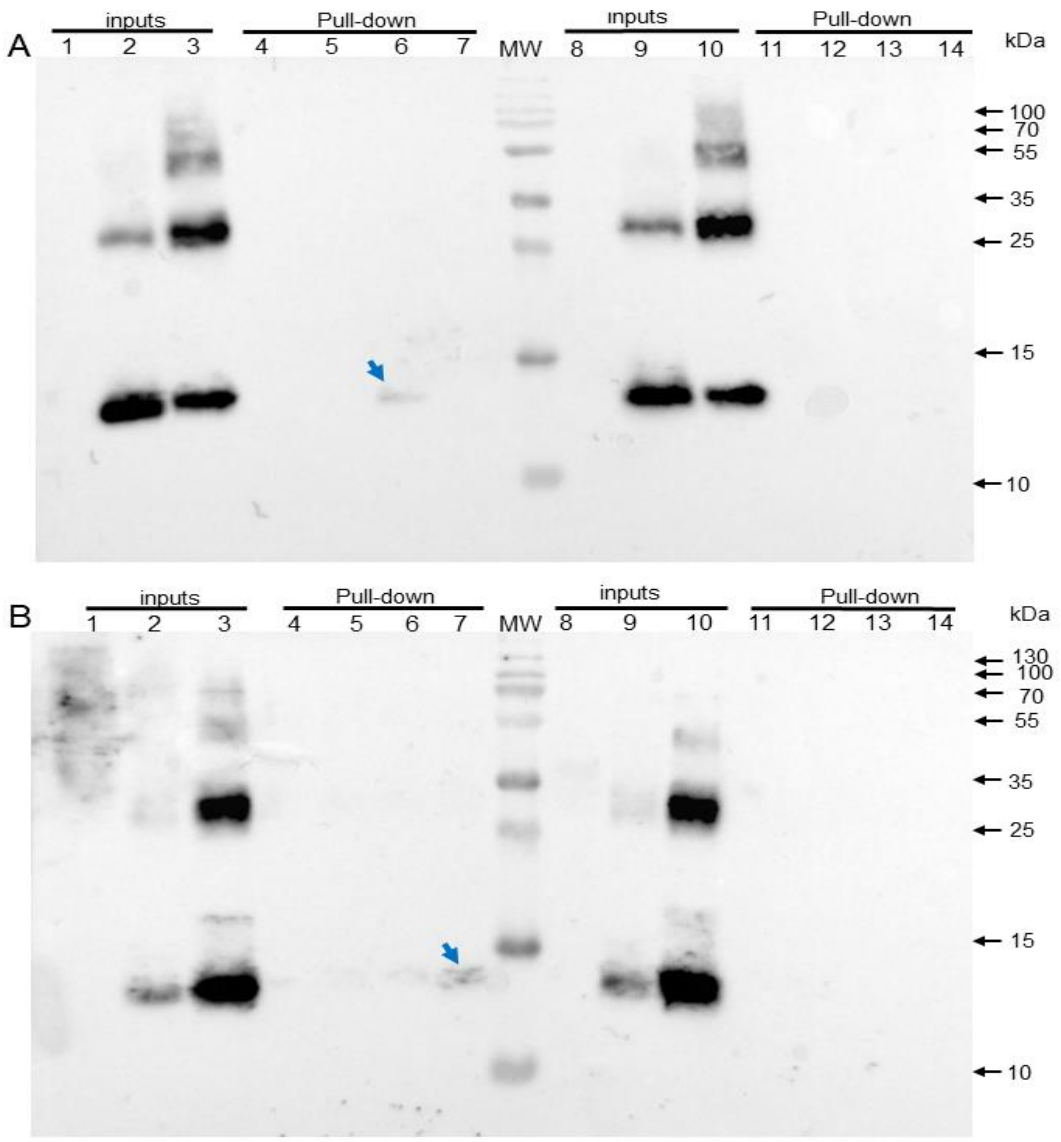

Figure 25. Western Blot analysis to evaluate the presence of FLAG-tagged PSIs at pH 7.4 (A) and 6.8 (B). Inputs and pull-down reactions were loaded on 15% SDS-PAGE under denaturing and reducing conditions (β-mercaptoethanol), 5 µL/lane, and then transferred to PVDF membranes. The presence of FLAG-tagged PSIs was detected with a mouse anti-FLAG tag antibody (clone FG4R) followed by a goat anti-mouse IgG HRP-coupled antibody.1: input GST-PSI A. 2: input Flag-PSI A; 3 input FLAG-PSI B; 4: GST-PSI A + beads; 5: FLAG-PSI A + beads; 6: GST-PSI A+FLAG-PSI A+ beads; 7: GST-PSI A+FLAG-PSI B+ beads; MW: Molecular (Weight PageRuler™ Prestained Protein Ladder, Thermo Scientific); 8: input GST-PSI B; 9: input Flag-PSI A; 10: input Flag-PSI B; 11: GST-PSI B + beads; 12: FLAG-PSI B + beads;13: GST- PSI B + FLAG PSI A + beads;14: GST- PSI B + FLAG PSI B + beads. Chemiluminescence was detected after 5 seconds of exposure time.

Co-immunoprecipitation

To further test the PSI-PSI interactions at acidic pH (< 6.5), Co-IP assays using Pierce Protein G agarose beads were performed, as described in *Co-immunoprecipitation assay* in section 2.6. Protein G is known to bind to IgG. Therefore, we used a mouse anti-FLAG antibody to bind to the beads that, in turn, through the

antibody were bound to the FLAG-tagged PSI. We expected to observe a band at ~40 kDa corresponding to GST-tagged PSIs and a band at ~15kDa for FLAG-tagged PSIs.

At pH 4.5, the correct size bands for FLAG-PSI (A/B) and GST-PSI (A/B) are present in the input lanes (Figure 28A, lanes 1- 4). Regarding the Co-IP reaction lanes (Figure 28A, lanes 5-14), no bands were detected. Looking into the positive controls (Figure 28A, lanes 5 and 10), where the binding of FLAG-tagged PSI to the beads was assessed, no bands were observed, indicating that or the FLAG-PSI-antibody complex is not forming, or the antibody used is not binding to the beads.

Likewise, at pH 3.5, the correct-sized bands of inputs also appeared (Figure 28B, lanes 1-4), but no bands were found in the pull-down reaction lanes correspondent to the reaction controls (Figure 28B, lanes 5 and 10), so the FLAG-tagged proteins were not bound to the beads.

Moreover, and since no expected bands were observed in the positive control lanes, the beads used may not be suitable to test PSI-PSI interactions at the chosen pH values. This may be due to inefficient binding of the antibody to the beads that, consequently, would not allow the binding of FLAG-tagged PSI to the beads. Given this, we cannot exclude that at acidic pH (<5) no PSI-PSI interactions occur.

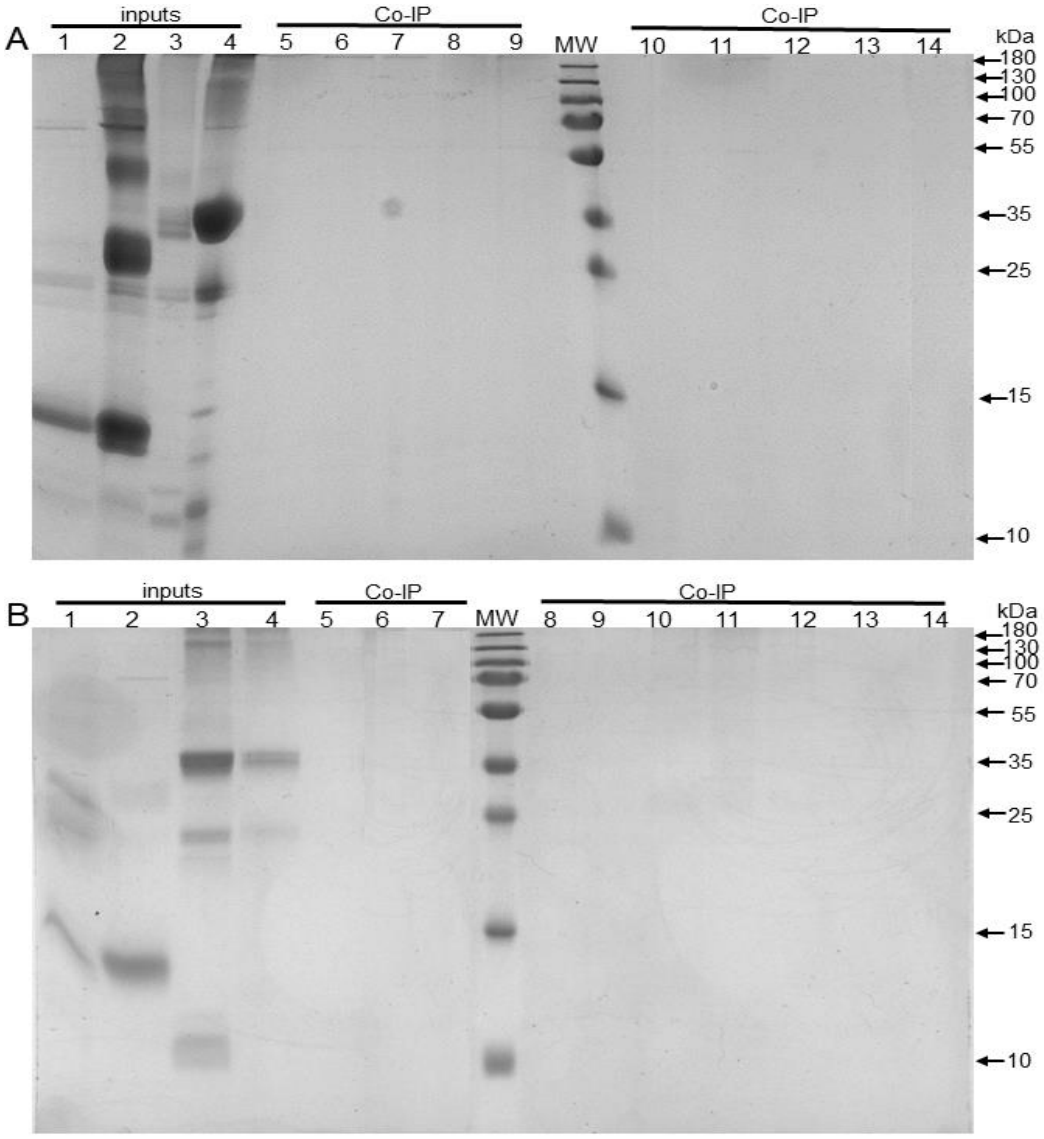

Figure 26. SDS-PAGE analysis of PSI-PSI interactions by co-immunoprecipitation at pH 4.5 (A) and 3.5 (B). Inputs and pull-down reactions were analysed on a 15% acrylamide gel under denaturing and reducing conditions (β-mercaptoethanol). Each Co-IP lane was loaded with 10 µl of Co-IP reaction, and input lanes were loaded with 1/3 of the amount of purified protein added to each reaction. The SDS-PAGE gels were stained with Coomassie Blue for 20 minutes. As controls, FLAG-PSI (A/B) combined with anti-FLAG antibody and GST-PSI (A/B) combined with the same antibody were assayed for binding to the beads (Pierce Protein G agarose beads). After binding to the beads, the FLAG-tagged PSI were released by elution with 1x SDS-Sample Buffer.1: input FLAG-PSI A; 2: input FLAG-PSI B; 3: input GST-PSI A. 4: input GST-PSI B; 5: FLAG-PSI A + antibody+ beads; 6: GST-PSI A +antibody+ beads; 7: GST-PSI B + antibody+ beads; 8: FLAG-PSI A + antibody + beads + GST-PSI A; 9: FLAG-PSI A+ antibody+ beads+ GST-PSI B; MW: Molecular Weight (PageRuler™ Prestained Protein Ladder, Thermo Scientific); 10: FLAG-PSI B + antibody + beads; 11: GST-PSI A+ antibody + beads; 12: GST-PSI B + antibody + beads; 13: FLAG-PSIB+ antibody + beads+ GST-PSI A; 14: FLAG-PSI B+ antibody+ beads+ GST-PSI B. kDa: kilodaltons.

Pull-down assay at acidic pH

As we aimed to further characterize the PSI-PSI interactions at acidic pH (<6.5), and since the Co-IPs did not allow us to do so, we performed a pull-down assay using different beads from the ones mentioned in *Pull-down assay* in section 3.3. Therefore, Fab-Trap agarose beads were used to test interactions with DYKDDDDK-tagged fusion proteins (FLAG-tagged proteins). In this assay, interactions were tested at pH 5.0 (Figure 29), and the expected band sizes are ~40 kDa for GST-tagged PSIs or ~15 kDa for FLAG tagged PSIs.

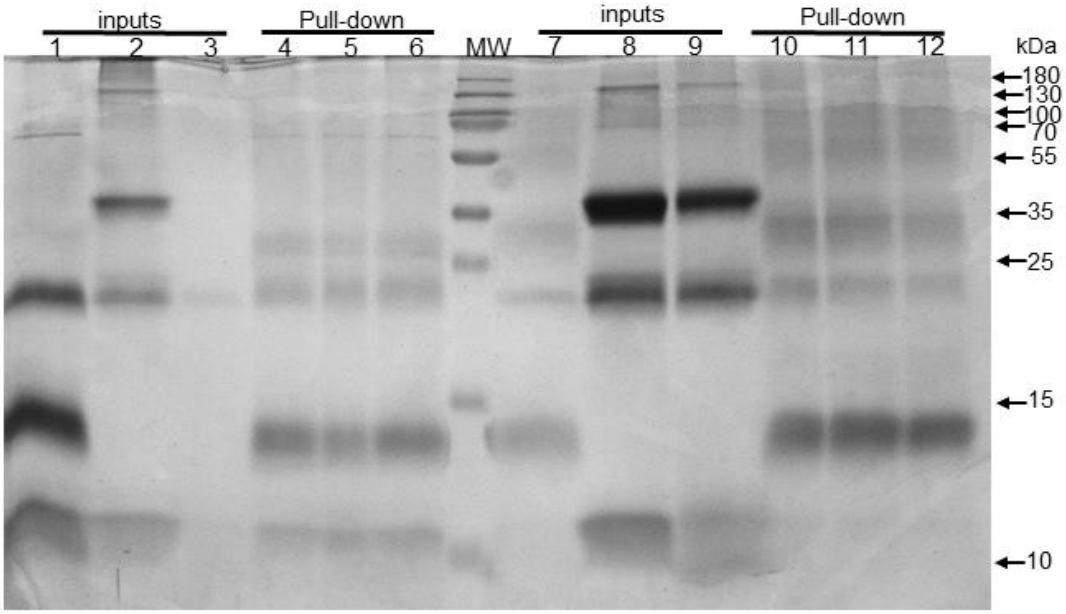

Figure 27. SDS-PAGE analysis of PSI-PSI interactions by pull-down assay at pH 5.0. Inputs and pull-down reactions were analysed on a 15% acrylamide gel under denaturing and reducing conditions (β-mercaptoethanol). Each pull-down lane was loaded with 15 µL of pull-down reaction, and input lanes were loaded with 1/3 of the amount of purified protein added to each reaction. As controls, FLAG-PSI (A/B) and GST-PSI (A/B) were assayed for binding to the beads (ChromoTek DYKDDDDK Fab-Trap™ Agarose beads). After binding to the beads, the FLAG-tagged PSI were released by elution with 1x SDS-Sample Buffer. The SDS-PAGE gels were stained with Silver Staining kit (Bio-Rad). 1: input FLAG-PSI A; 2: input GST-PSI A; 3 input GST-PSI B; 4: FLAG-PSI A + beads; 5: FLAG-PSI A+GST-PSI A+ beads; 6: FLAG-PSI A+GST-PSI B+ beads; MW: Molecular Weight (PageRuler™ Prestained Protein Ladder, Thermo Scientific); 7: input FLAG-PSI B; 8: input GST-PSI A; 9: input GST-PSI B;10: FLAG-PSI B + beads;11: FLAG- PSI B + GST- PSI A + beads; 12- FLAG-PSI B+ GST-PSI B+ beads

In the input lanes, the correct sized band for FLAG-PSI A (Figure 29, lane 1) and FLAG-PSI B (Figure 29, lane 7) were present, along with the correct bands for GST-PSI (A/B) (Figure 29, lanes 2, 3, 8, 9). However, the input band of GST-PSI B on lane 3 was not present, probably due to a technical problem. Regarding the pull-down itself, in the lanes referent to the reaction controls (Figure 29, lanes 4 and 10), FLAG-tagged proteins were successfully bound to Fab-Trap beads. However, a band corresponding to GST-

PSI A was not found in the interaction lanes (Figure 29, lanes 5 and 11), nor GST-PSI B (Figure 29, lanes 6 and 12), suggesting that PSIs do not interact at pH 5.0. Again, as in the SDS-PAGE analysis of pull-down reactions in the input lanes, some non-specific bands were observed.

Pull-down assay with PSI A_Y95A/L99A

The motifs or regions within the PSI domain through which PSIs interact are still unidentified. Therefore, and in an attempt to further characterize this domain, we purified PSI A with a mutation in the C-terminal region of PSI A that due to its amino acids characteristics may be involved in PPIs (Frazão et al., 1999) . For this purpose, a pull-down assay at pH 7.4 and 6.8 was performed, similarly to the ones already presented and where PSI-PSI interactions were observed. Regarding pH 7.4, in the input lanes (Figure 30A, lanes 1-3), GST- PSI A_Y95A/L99A and FLAG-PSI (A/B) expected bands were present. Furthermore, in the control pull-down lanes, a band of the correct size for GST- PSI A_Y95A/L99A was observed, confirming that it was effectively bound to the glutathione-agarose beads (Figure 30A, lane 4). No bands corresponding to FLAG-PSI A or FLAG-PSI B were present in the respective control lanes (Figure 30A, lanes 5 and 6). Moreover, in the pull-down interaction lanes, the GST- PSI A_Y95A/L99A band was present (Figure 30A, lanes 7 and 8) whereas no bands were detected corresponding to FLAG-tagged PSIs (Figure 30A, lanes 7 and 8). At pH 6.8 (Figure 30B), the bands observed were the same as described above for pH 7.4, with a slight difference. In the pull-down lanes, GST- PSI A_Y95A/L99A bands were not detected (Figure 30B, lanes 7 and 8).

To confirm these observations, we performed a western blot of the pull-down reactions with an anti-FLAG antibody. At both pH 7.4 and 6.8, the input bands corresponding to FLAG-PSI A and FLAG-PSI B are observed (Figure 31A and 31B, lanes 2 and 3), but no bands were seen in the lanes from the pull-down reactions, which confirms the Silver staining results (Figure 30). As so, these results suggest that at pH 7.4 and pH 6.8, the mutation in the PSI A sequence inhibits the interaction with itself and with PSI B, respectively.

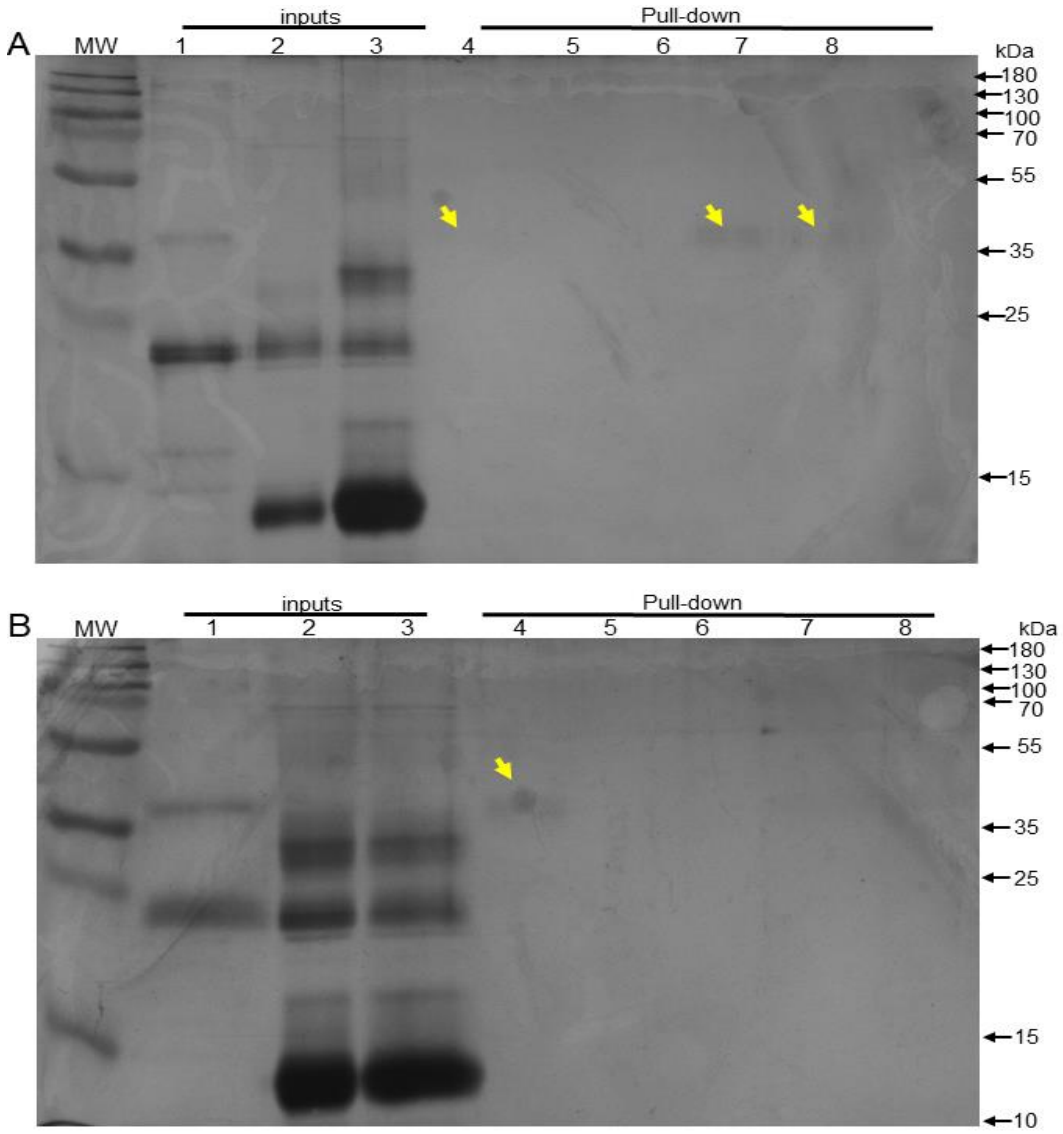

Figure 28. SDS-PAGE analysis of PSI-PSI interactions by pull-down assay at pH 7.4 (A) and 6.8 (B). Inputs and pull-down reactions were analysed on a 15% acrylamide gel under denaturing and reducing conditions (β-mercaptoethanol). Each pull-down lane was loaded with 15 µL of pull-down reaction, and input lanes were loaded with 1/3 of the amount of purified protein added to each reaction. As controls, GST- PSI A_Y95A/L99A and FLAG-PSI (A/B) were assayed for binding to the beads (Glutathione Agarose beads). After binding to the beads, the GST-tagged PSI were released by elution with 1x SDS-Sample Buffer. The SDS-PAGE gels were stained with Silver Staining kit (Bio-Rad). 1: input GST-PSI A_Y95A/L99A; 2: input FLAG-PSI A; 3 input FLAG-PSI B; 4: GST- PSI A_Y95A/L99A + beads; 5: FLAG-PSI A + beads; 6: FLAG-PSI B + beads; 7: GST- PSI A_Y95A/L99A + FLAG-PSI A + beads. 8: GST PSI A_Y95A/L99A + FLAG-PSI B+ beads. kDa: kilodaltons.

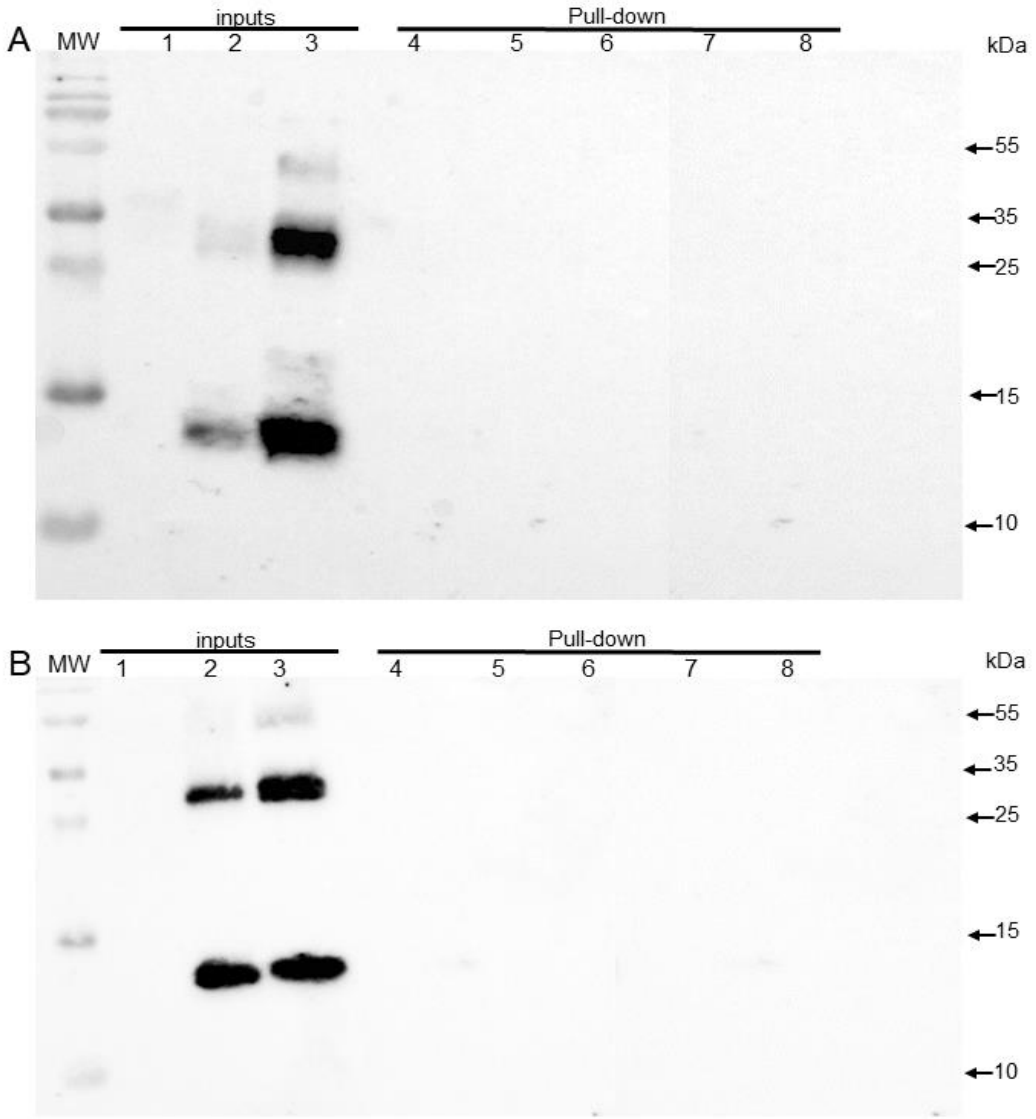

Figure 29. Western Blot analysis to evaluate the presence of FLAG-tagged PSIs at pH 7.4 (A) and 6.8 (B). Inputs and pull-down reactions were loaded on 15% SDS-PAGE under denaturing and reducing conditions (β-mercaptoethanol), 5 µL/lane, and then transferred to PVDF membranes. The presence of FLAG-tagged PSIs was detected with a mouse anti-FLAG tag antibody (clone FG4R) followed by a goat anti-mouse IgG HRP-coupled antibody. MW: Molecular Weight (PageRuler™ Prestained Protein Ladder, Thermo Scientific); 1: input GST- PSI A_Y95A/L99A; 2: input FLAG-PSI A; 3 input FLAG-PSI B; 4: GST- PSI A_Y95A/L99A + beads; 5: FLAG-PSI A + beads; 6: FLAG-PSI B + beads; 7: GST- PSI A_Y95A/L99A + FLAG-PSI A + beads. 8: GST PSI A_Y95A/L99A + FLAG-PSI B+ beads. Chemiluminescence was detected after 5 seconds of exposure time.

In vivo confirmation of PSI-PSI interactions

Y2H

Yeast-two hybrid (Y2H) is an *in vivo* method that tests protein-protein interactions in living yeast cells. In the context of this study, the Y2H analysis for the interactions between PSI A-PSI A, PSI A-PSI B and PSI B-PSI B are shown in Figure 32. Yeast strains with bait and prey vectors were already available at the laboratory.

Three different plates differing in their composition were used as described in *Yeast Two-Hybrid* in section 2.6. The plates used all lacked leucine and tryptophan to select for the presence of both bait and prey plasmids. Double-dropout plates lacking histidine (SM-Leu-Trp-His) were used to test for reporter gene activation and, growth on these plates suggests bait and prey plasmids interaction. 3-AT was added to reduce autoactivation and prevent false positives. Positive and negative growth controls were made. Comparison of the experimental interactions with the controls were used to assess interactions. If a control grows on media containing 3-AT, this means the construct is problematic for the Y2H analysis. The analysis of the plates revealed that positive control grew (Figure 32BA, BB and BC, lane 1), but the negative controls also in all three different types of plates (Figure 32BA, BB and BC, lanes 2,3,5,6,8 and 9), even when 3-AT was present in the media. This indicates that prey plasmids could autonomously activate the reporter gene in the absence of prey protein. Therefore, these cells are not suitable for screening of PSI-PSI interactions. No conclusions can be obtained from these results since cells grew at the same rate on the negative controls.

A

Lane	Bait vector	Prey plasmid	Purpose
1	p53_pGBKT7	antigen_pGADT7	Positive interaction control
2	p53_pGBKT7	pGADT7	Negative interaction control
3	pGBKT7	antigen_pGADT7	Negative interaction control
4	PSIA_pGBKT7	PSIA_pGADT7	Test of interaction PSI A-PSI A
5	PSIA_pGBKT7	pGADT7	Negative interaction control
6	pGBKT7	PSIA_pGADT7	Negative interaction control
7	PSIB_pGBKT7	PSIB_pGADT7	Test of interaction PSI B-PSI B
8	PSIB_pGBKT7	pGADT7	Negative interaction control
9	pGBKT7	PSIB_pGADT7	Negative interaction control
10	PSIA_pGBKT7	PSIB_pGADT7	Test of interaction PSI A-PSI B
11	PSIB_pGBKT7	PSIA_pGADT7	Test of interaction PSI B-PSI A

B

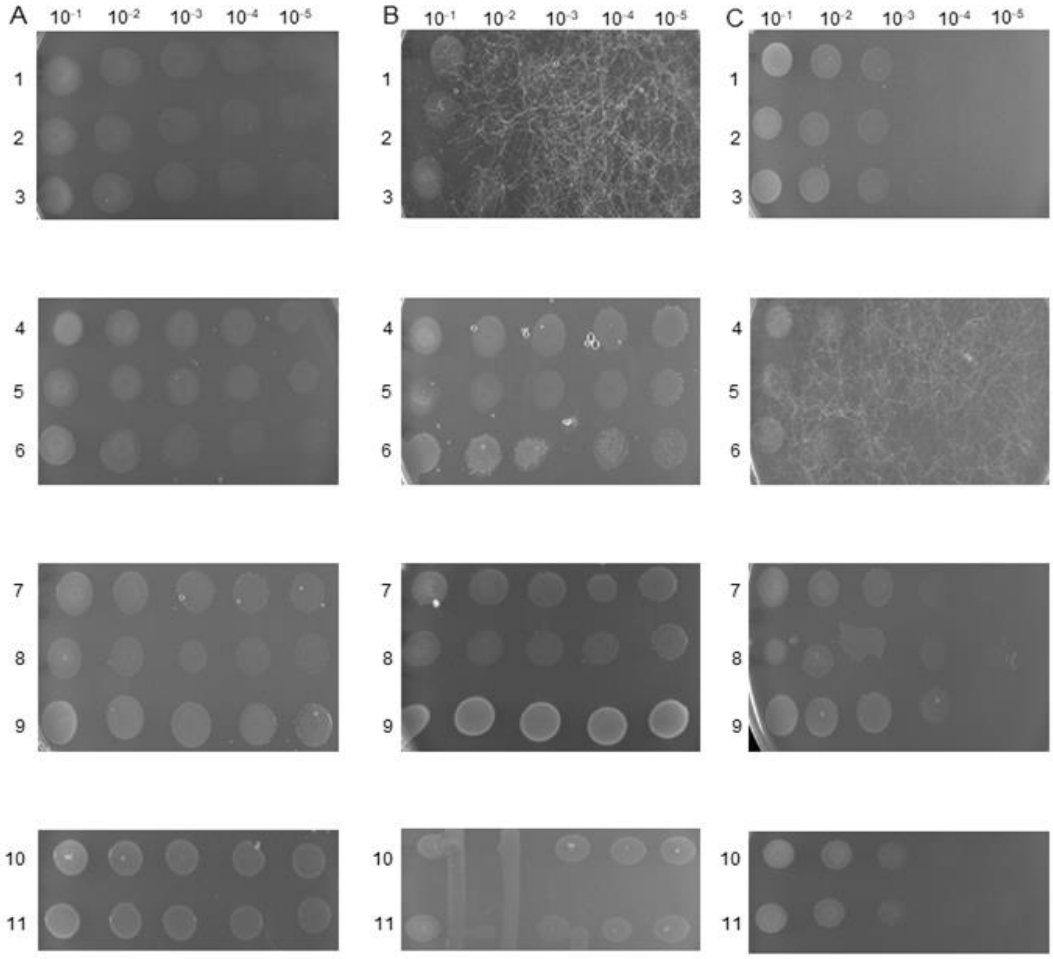

Figure 30. Y2H analysis of PSI-PSI interactions. The content and the purpose of each interaction illustrated in (B) is described in (A). The figure shows yeast growth on selective plates. (BA) Control plate (SM-Leu-Trp). (BB) Interaction test plate (SM-Leu-Trp-His). (BC) Plate to reduce autoactivation (SM-Leu-Trp-His+3AT). Cells were plated in serial dilutions and cultivated for 7 days at 30 °C. The control interactions were spotted in lane 1, 2, 3, 5, 6, 8 and 9, while experimental interactions were applied in lane 4,7,10 and 11. Images were acquired using ImageLab (Bio-Rad, USA).

2in1 rBiFC

Cloning

In the context of this study and considering that *in vitro* results are not *per se* sufficient to confirm protein-protein interactions, a 2in1 rBiFC assay using the PSIs was performed.

To verify the presence of PSI A and PSI B in pDONOR221-P1P4, a restriction digestion analysis using EcoRI and Eco32I was performed (Figure 33). The cloning of PSI A and PSI B into pDONOR221-P1P4 was confirmed by DNA sequencing (Figures 34 and 35). The final Gateway constructs were also obtained. The next step is to confirm these constructs by DNA sequencing.

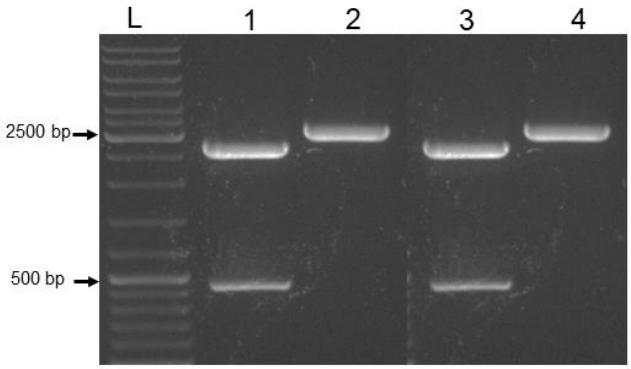

Figure 31. Restriction digestion analysis of pDONR221-P1P4 with EcoRI and Eco32I enzymes. pDONR-P1P4-SP-PSI A and pDONR-P1P4-SP-PSIB were cut with Anza EcoRI and Anza Eco32I (Invitrogen by Thermo Scientific, USA). The resulting DNA fragments had the expected sizes (450 bp and 2491 bp). L: DNA ladder (GeneRuler DNA Ladder Mix (Thermo); 1, and 2: digestion of distinct miniprep pDONR-P1P4-SP-PSI A; 3 and 4: digestion of distinct miniprep pDONR-P1P4-SP-PSI B.

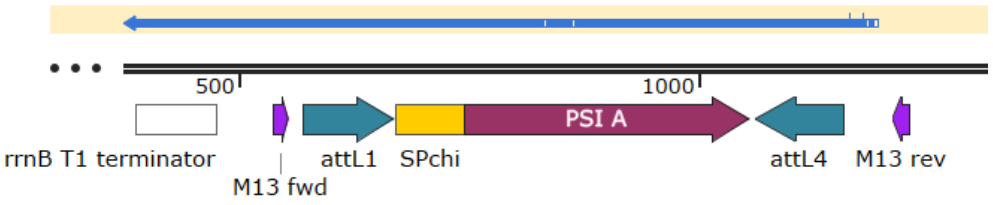

Figure 32. Alignment of the sequencing results of pDONOR221-P1P4-PSI A. The sequencing results with M13 rev primer were aligned with the respective expected pDONR221-P1P4-PSI A sequence. The sequence alignment was performed resorting to SnapGene software (www.snapgene.com). Blue portions in the yellow box represent sequence match and alignment, whereas white portions represent no alignment. PSI A: plant specific insert cardosin A; M13fwd: M13 sequencing sequence forward; M13 rev, M13 sequencing sequence reverse; SP, signal peptide chitinase.

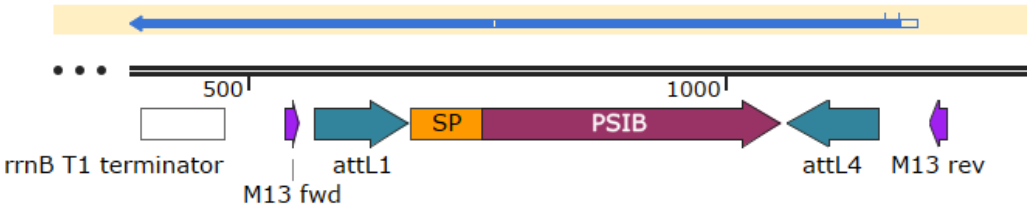

Figure 33. Alignment of the sequencing results of pDONOR221-P1P4-PSI B. The sequencing results with M13 rev primer were aligned with the respective expected pDONR221-P1P4-PSI B sequence. The sequence alignment was performed resorting to SnapGene software (www.snapgene.com). Blue portions in the yellow box represent sequence match and alignment, whereas white portions represent no alignment. PSI A: plant specific insert cardosin A; M13fwd: M13 sequencing sequence forward; M13 rev, M13 sequencing sequence reverse; SP, signal peptide chitinase.

4.Discussion

Over the years, focus has been given to the study of the mechanisms and regulation of plant vacuolar trafficking. However, novel unconventional routes to the vacuole are being unravelled, such as is the case of Chitinase A (Stigliano et al., 2013) and PSI from cardosin A (Pereira et al., 2013). The PSI is a domain found in some plant APs (Simões & Faro, 2004; Soares et al., 2019). *in vitro* experiments showed that isolated PSIs have biological activities such as lipid membrane interaction, antimicrobial activity, induction of membrane permeabilization and modulation (Egas et al., 2000; Muñoz et al., 2014). Furthermore, several reports from *in vivo* studies showed that the PSI domain is associated with anti-pathogen activity (Bryksa et al., 2011; Frey et al., 2018) and with the vacuolar targeting of APs (Egas et al., 2000; Pereira et al., 2013; Terauchi et al., 2006; Törmäkangas et al., 2001). The main goal of this study is to uncover the molecular mechanisms behind the unconventional sorting routes mediated by the PSI. As so, we decided to approach this from a genetic and proteomic view.

4.1 Characterization of vacuolar defective lines

As a first approach, we used Arabidopsis mutants that were reported to exhibit vacuolar trafficking defects, to determine how the lack of specific genes would affect the cell, and the localization of PSIs. To further characterize the mechanisms behind cardoon PSIs routes, we started by performing a morphological and developmental characterization of the selected homozygous lines: *syp22-3*, *syp22-1 syp23*, *syp22-3 syp23* and *syp23*, ecotype Col-0. It is important to mention that these mutants have already been characterized and used in studies with different goals (Ebine et al., 2008; Ohtomo et al., 2005; Shirakawa et al., 2009, 2010; Ueda et al., 2006). Also, it has been showed that the double mutant *syp21 syp22* is lethal (Shirakawa et al., 2010), illustrating well the importance of these genes.

Among the single mutants studied, *syp22*-3 showed semi-dwarfism. The double mutants, *syp22-1 syp23* and *syp22-3 syp23*, exhibited a similar morphology to *syp22-3*, besides having fewer and curly leaves. A mutation in *SYP23* in a *syp22* background seemed to enhance the growth defects. Reduced primary root growth was also observed for all the mutants (*syp22-3*, *syp22-1 syp23*, *syp22-3 syp23*), except for *syp23*, indicating a primary function of SYP22 in plant primary root growth. A developmental assay based on Boyes et al. (2001) revealed that *syp23* mutants had similar growth, compared to WT. On the contrary, a delay in growth was observed in the single mutant *syp22-3* and the

double mutants. The last line to flower was *syp22-3*, but *syp22-1 syp23* and *syp22-3 syp23* bolted later compared to the WT, and the other mutant lines analysed. Again, *SYP23* seemed to enhance the *syp22* phenotype. Surprisingly, our data shows that SYP23 ecotype Col-0 ($SYP23_{Col-0}$) is functional (Shirakawa et al., 2010), which was not expected given that it lacks the TMD, characteristic of the SYP2 family. To date, no protein lacking a TMD and localized to the cytosol has been reported to be functional. But two questions remain: what is the function of SYP23? And how does a SNARE lacking a TMD exerts its function on plants cells? A previous study by Ohtomo et al. (2005) reported that SYP23 of another ecotype, *Landsberg erecta* ($SYP23_{Ler}$), different from the one used in this study, complemented *syp22*. However, multiple copies of *SYP23Col-0* were needed to complement *syp22* (Shirakawa et al., 2010). It has been then proposed that *SYP22* and *SYP23* may have arisen from segmental genome duplication, meaning that both gene products have overlapping functions. Moreover, the Col-0 derived *SYP23* might have lost its function, or it retained part of the original function, or even has a new function (Ohtomo et al., 2005; Vision et al., 2000). Our findings seem to suggest that $SYP23_{Col-0}$ retained part of the original function, given when it is absent, no visible anomalies are observed but, when in a *syp22* background, the defects exhibited by *syp22-3* are enhanced by the lack of *SYP23*. These results suggest that the two *SYP2* genes, *SYP22* and *SYP23*, have redundant functions in plant growth, and their contribution to these processes is variable to several degrees. However, SYP22 has a primary function in plant growth and development (Shirakawa et al., 2010). In fact, functional redundancy has been reported for other SNARE proteins, such as SYP121/SYR1/PEN1 and SYP122, both required for plants development (Assaad et al., 2004). Nevertheless, a previous study seems to contradict our results, and reported that mutations in each gene of the SYP2 family were lethal (Sanderfoot, Pilgrim, et al., 2001). The discrepancies observed may be due to differences in the plant growth conditions used among the several studies. Due to the high number of SNAREs in the Arabidopsis genome when compared to animals or yeast, plants might have evolved multigene families to have more plasticity and a fast adaptation to an ever-changing environment. In fact, this redundancy was also partially observed in the VTI1 family of v-SNAREs (Surpin et al., 2003).

Additionally, Transmission Electron Microscopy was employed to further explore and characterize the ultrastructural modifications in the endomembrane system caused by mutations in the *SYP2* genes. In this work, it has been shown that *syp22-3* plants lacked starch granules inside chloroplasts and had a dense cytoplasm, that was tightly packed. Although the three SYP2 proteins were reported to have redundant functions,

SYP22 had a primary function in plant growth and development (Shirakawa et al., 2010). Therefore, *syp22* plants which exhibited semi-dwarfism, could be using their reserves to overcome the development issues due to the lack of *SYP22*. This effort also seems to be patent in the dense cytoplasm presented by the mutant, a characteristic that is common to cells under high metabolic activity. The double mutants chloroplasts lacked internal organization. This is consistent with the delayed growth presented by both *syp22-1 syp23* and *syp22-3 syp23* mutant plants, and with a previous report where the phenotype of those lines was described (Shirakawa et al., 2010). Moreover, the *syp23* line had huge starch granules and enlarged Golgi cisternae. SYP23 is thought to be recruited and anchored to the membrane by partially interacting with Qb-SNARE VTI11 and/or Qc-SNARE SYP5 on the membrane, forming a SNARE complex that probably is involved in TGN-to-PVC trafficking (Sanderfoot, Kovaleva, et al., 2001). The absence of *SYP23* does not seem to affect the level to which SYP5 accumulates. The swollen Golgi cisternae observed in the absence of *SYP23* can be related with the SNARE complex assembly being affected, impairing the traffic between the TGN and PVC, thus leading to an accumulation of proteins inside the Golgi cisternae. Moreover, and since *VTI12* is reported to substitute *VTI11* in its absence (Sanmartín et al., 2007; Surpin et al., 2003), the lack of *SYP23* and consequently *VTI11*, might lead to the overexpression of *VTI12*, thus augmenting the protein trafficking to the vacuole to be recycled/degraded, shown here by the content observed inside *syp23* vacuoles. Interestingly, a common characteristic was found among the lines, as the vacuoles appeared to have more content, when compared to WT. In the absence of *SYP2* genes, leaf cells might accumulate inside the vacuole proteins that lack the final signal for membrane fusion with it, and they are accumulated inside the vacuole for posterior recycling. This is consistent with the reports that SYP2 proteins have redundant functions in vacuolar protein sorting (Shirakawa et al., 2010).

During this work, we only characterized seedlings with 15-day-old. Another study would be needed to evaluate the ultrastructure in mature leaf cells and assess if the differences found in young leaves, persisted throughout the plant growth and development.

4.2 Definition of trafficking pathways in vacuolar defective plants

Despite sharing high homology regarding its sequence, PSI A and PSI B seem to be very different, regarding its function. Moreover, the ability shown by PSI A and PSI B to direct proteins to the vacuole made them to be considered unconventional sorting

determinants since they do not fit the classic VSD types (Pereira et al., 2013; Vieira et al., 2019). Therefore, and considering that PSIs from cardoon can sort proteins to the vacuole through different routes, PSIs are useful tools for vacuolar trafficking studies.

To further explore and characterise the PSI-mediated trafficking, we expressed PSI A and PSI B fused to mCherry in the mutant lines. PSI A was localized in the vacuole in WT and *syp23* plants. Although in *syp22-3*, PSI A was in the vacuole, a differential accumulation inside this organelle was observed, as well as inside round spherical structures that we hypothesize to be bulbs (Saito & Ueda, 2009; Ueda et al., 2006). In double mutants, *syp22-1 syp23* and *syp22-3 syp23*, PSI A was observed in the ER and in those structures named bulbs, inside the vacuole lumen. Our data regarding the vacuolar localization of PSI A in WT and *syp23* is consistent with what has been reported in heterologous systems (Duarte et al., 2008; Pereira et al., 2013). However, the deletion of both *SYP22* and *SYP23* genes seemed to retain PSI A in the ER. The pattern of PSI B localization on the same lines (WT, *syp22-3*, *syp22-1 syp23*, *syp22-3 syp23*, *syp23*) was similar to PSI A. It was reported that PSI B follows the conventional ER-Golgi-PVC route to the vacuole (Pereira et al., 2013). The SYP2 family of proteins as mentioned above was reported to mediate vacuolar traffic between the PVC and the vacuole (Ohtomo et al., 2005; Shirakawa et al., 2010; Ueda et al., 2006). Our data suggests that PSI A, in the absence of two *SYP2* genes, is unable to reach the vacuole. However, when only one of the genes is lacking both PSI A and PSI B are observed in the vacuole. For unknown reasons, this result is inconsistent with a previous report that each *SYP2* gene has redundant function in vacuolar protein sorting (Shirakawa et al., 2010), but in accordance with an older one (Sanderfoot, Pilgrim, et al., 2001). A recent study from our lab (unpublished data) reported that *in-vitro* PSI A interacts with SYP23, and it was proposed, since SYP23 lacks a TMD, that PSI A would interact with SYP23 in the budding and docking process, indicating that the absence of the TMD somehow might be related to non-classical sorting routes. Our data indicates that if PSI A thus in fact interacts with SYP23, this does not seem to be fundamental to the PSI sorting to the vacuole. Additionally, our results are a bit puzzling and further studies are needed to understand the function of SYP23, and how this may influence PSI trafficking. However, our study suggests that PSIs vacuolar sorting is disrupted by the SYP2 family of proteins, being the first report to show a more mechanistic description of PSIs-mediated trafficking, particularly the one related to unconventional routes. In fact, to date, no information was available regarding the involvement of the SYP2 family in unconventional trafficking routes. We must consider that the tissue observed were cotyledonary leaves, and their cells are viewed as a transient stage between both seed tissue and vegetative tissue. To

confirm these results, stable lines expressing the PSIs in the several mutants background should be obtained.

4.3 In vitro cardoons' PSI-PSI interactions

PSI expression and purification

Plasmids carrying PSIs were already available for use, with a His tag. Two constructs were made for each PSI carrying either a FLAG tag or a GST tag, which was an advantage for the interactions tests, as different affinity supports were used. First, we had to proceed with protein purification. PSI A_Y95A/L99A was also successfully purified. PSI B revealed a higher expression level when compared to PSI A, under the same conditions. The differences in expression levels may be due to various reasons. For instance, by looking at the Instability Index computed by ProtParam tool (ExPasy), we noted that PSI A sequence was regarded unstable, whereas PSI B protein was stable. This may cause degradation of the protein inside the cells or during the purification process. Additionally, some protein was still adhered to the resin at the end of the purification of both PSIs. Since imidazole is a strong competitor for the nickel residues present in the agarose resin, it would likely be necessary to increase the amount of imidazole in the elution buffer to solve this issue. Nevertheless, the purifications were successful, and the amounts of purified proteins were enough for the experiments planned.

PSI-PSI interactions

Little is known regarding the roles of PSI, both as part of the proenzyme or when isolated. Surprisingly, it was proposed that PSI dimers might exert distinct functions from their isolated counterparts (Cheung et al., 2020). Furthermore, it has been postulated that PSI functions are somehow related to their capability to interact with membranes, in a pH- and lipid-composition-dependent manner (Bryksa et al., 2011; De Moura et al., 2014; Vaccaro et al., 1999). Previous works using potato PSI showed that it changes from monomer to dimer with decreasing pH (Bryksa et al., 2017; Muñoz et al., 2011, 2014), and binding is stronger between the monomers at acidic pH (De Moura et al., 2014). It was also suggested that dimeric PSI is the active form responsible for membrane fusion activity (Bryksa et al., 2011), however, how the dimer and the pH-triggered activity relate remains elusive. The purpose of this part of the study based on findings regarding potato PSI was to uncover if cardosin PSIs also dimerize and if it is

pH-dependent. Therefore, two similar *in vitro* techniques were employed based on their pH limitations.

Our results regarding the pull-down assays showed that at pH 7.4, PSI A interacts with itself, as shown by the presence of the same band, one from GST-PSI A and the other from FLAG-PSI A, in the input lanes and in the pull-down lanes. This indicates that previous to the denaturation step, PSI A was forming an *in vitro* complex with itself. In contrast, PSI B pull-down lanes despite presenting the GST-PSI band, did not show the band corresponding to FLAG-PSI B. At pH 6.8, PSI A interacts with PSI B, as the same bands present in the input lanes of PSI A and PSI B are present in the pull-down lane. Similarly to what was mentioned above, this illustrated that previous to denaturation, PSI A was forming and *in vitro* complex with PSI B. No interactions were detected between PSI A-PSIA at pH 6.8, PSI A-PSI B at pH 7.4, nor PSI B-PSI B or PSI B-PSI A at pH 7.4 and 6.8. All these results were confirmed by western blotting. At first, it is an intriguing result since PSIs were reported to form dimers with decreasing pH, and we observed PSI-PSI dimers in near-neutral pH conditions. Besides, a subtle decrease in pH, from 7.4 to 6.8, also seemed to alter the interactions. While PSI A interacts with PSI A at pH 7.4, this is not observed at pH 6.8. PSI A only interacts with PSI B at pH 6.8.

As we wanted to further test PSI dimerization at acidic pH and since the glutathione agarose beads had an optimal pH binding between 6.5 and 8.0, we used DYKDDDDK Fab Trap Agarose beads that contain an anti-DYKDDDDK-tag Fab fragment, covalently bound to the beads. These beads allowed us to perform a pull-down at pH 5.0, and FLAG-fused PSI A and PSI B were used as “bait” protein, and as “prey” the putative binding partners, GST-tagged PSI A and PSI B. Although FLAG-PSIs were binding to the beads, our results showed no interaction between PSIs, as no band was detected in the pull-down lanes corresponding to GST-PSI A/B. We cannot exclude that at pH 5.0, cardosins PSIs do not dimerize, contrary to what was observed in studies with potato PSI (Bryksa et al., 2011; De Moura et al., 2014; Zhao et al., 2020).

Although our results do not directly show dimeric association at acidic pH, they suggest that cardosins PSI dimerization is pH-dependent. Similar results have been obtained for recombinant non-glycosylated cirsin from spear thistle (*Cirsium vulgare*) PSI, as it was observed as a dimer under nonreducing conditions at pH 7.5 (Bryksa et al., 2017; Curto et al., 2014). Moreover, in a comparative study between four distinct PSIs from barley, potato, Arabidopsis, and cardoon, the authors, through Trp fluorescence studies, reported a deviation to the proposed monomer-dimer equilibrium model attributed to potato PSI, as they found that cardosin PSI A at pH 7.4 appeared as

a dimer (Bryksa et al., 2017). Our findings seem to corroborate this result. Dimeric association at near-neutral conditions was also observed in animal proteins. A recent study using a SARS-CoV-2 protein, named M^{pro} protein, reported that it forms a dimer at pH 7.4, exhibiting pH-dependent activity and dimerization (Boonamnaj et al., 2022). This protein is functional as a dimer (Chen et al., 2006; Goyal & Goyal, 2020; Xia & Kang, 2011) and, has a tendency to dimer dissociation at acidic pH (Chou et al., 2004). Curiously, the M^{pro} is rich in acidic residues, like the C-terminal region of cardosin A PSI (Bryksa et al., 2017), suggesting a role for this region in PSI A dimerization.

A putative binding site has been described in cardosin A. It is a region with a Leucine (L) and Tyrosine (T) residues within the PSI A presenting hydrophobic side chains, characterized by being a cell attachment motif (D'Souza et al., 1991; Frazão et al., 1999). Considering the binding properties of this sequence, we cloned and purified the PSIA_Y95A/L99A. In the pull-down lanes, no bands corresponding to both GST-PSIA_Y95A/L99A and the putative interacting partners PSI A/PSI B (FLAG-tagged) were detected. Through western blotting, we confirmed these observations. Our results suggest a role of the C-terminal region of PSI A that due to its amino acids characteristics may be involved in PPIs and, thus in the ability of PSI A to dimerize, not only with itself at pH 7.4, but also with PSI B at pH 6.8. Moreover, PSI-terminal domains are highly conserved regions, and an 11-residue chain in the C-terminal part of the PSI was found to be conserved among potato, barley, cardoon, and Arabidopsis (Bryksa et al., 2017). This suggests that this region must exert important functions, as it is evolutionarily conserved.

Nonetheless, and considering that most studies involved potato PSI, insights gained by *in silico* studies revealed that PSIs from other species display inconsistent pH-dependency for dimerization (Bryksa et al., 2017; Curto et al., 2014). Also, despite the high sequence homology and primary structure similarities seen among PSIs, they might show different sequence-dependent mechanisms (Qi & Grabowski, 2001). Regarding PSI B, our data shows that at the tested pH, this domain was not able to dimerize. We hypothesized that this could be due to the absence of glycosylation. The protein sequence of both PSI A and B are very similar, and the major difference is the N-glycosylation site in PSI B sequence (Pereira et al., 2013; Vieira et al., 2019). This post-translational modification besides being responsible for the different routes taken by the PSI, might also account for the interactions/dimeric association differences we observed between both PSIs. In fact, this post-translational modification does not occur in the expression system we used to purify the PSIs. Given this, the results obtained for PSI B might not be accurate. Potato PSI, which has the ability to dimerize, has no putative

glycosylation site (Cheung et al., 2020), and we only observed dimeric association of PSI A (non-glycosylated), revealing that glycosylation might be important for PSI B dimeric association. This could also be a hint to the different routes followed by both PSIs, as dimeric association in the early part of the endomembrane system might enable PSI A to interact and drive membrane budding to be able to do a Golgi bypass by fusing to unknow organelles/ vesicles, and in this way follow a non-conventional route. Inversely, as PSI B follows the conventional ER-Golgi route, the ability to dimerize at more neutral pH might not be necessary, as pH decreases along the endomembrane system. Interaction between PSI A and B is also intriguing since these proteins follow distinct routes to lead proteins to the vacuole. As previously mentioned, the PSI domain is not present in all APs and the majority of PSIs contain a glycosylation motif, as is the case of cardosin B PSI, with only a few being reported as non-glycosylated (Simões & Faro, 2004). Two PSIs from the aspartic proteinases of soybean, soyAP1 and soyAP2, also reported to be involved in vacuolar sorting, share the same dichotomy as cardosins PSIs. While soyAP1 PSI is glycosylated, soyAP2 PSI is not glycosylated (Terauchi et al., 2004, 2006). Therefore, a similar study testing the interactions between soyAP PSIs would be interesting to help us understand the influence of glycosylation in PSI dimerization.

Taking into consideration the results obtained from the *in vitro* tests, cardosins PSIs, unlike potato PSI, do not seem to form dimers under acidic pH conditions. Nonetheless, the methods employed have their limitations. First, the affinity supports used have different binding conditions, with limited pH variations and, as we are interested in testing the dimer-pH relationship, this was one of the major constraints. Second, the proteins expressed in bacterial cells often lack key post-translational modifications that can play a part in protein interactions. Third, the buffer conditions employed may influence protein stability or even their correct folding, leading to difficulties in detection. Moreover, if cardosins PSIs dimer formation is transient, it will be harder to detect.

4.4 In vivo cardoons' PSI-PSI interactions

Almost all the PSIs reported functions were only observed *in vitro*, so there is the need to sustain these results with an *in vivo* study. Moreover, little is known about structure-function relationship of PSIs (Cheung et al., 2020). After assessing putative interactors using *in vitro* techniques, we decided to perform two different techniques, not only to confirm those interactions in living systems, but also to assess the cellular localization of those same interactions.

The Y2H is one of the oldest techniques used to identify interactions between two proteins in living yeast cells (Fields & Song, 1989). The strains used in this study have bait and prey plasmids harbouring the HIS3 reporter gene. Activation of the reporter gene is detected by growth on minimal media lacking the nutrients the enzymes provide (histidine). The HIS3 reporter is viewed as the most sensitive, but the least selective, as it is reported to be leaky in most strains (Gietz et al., 1997). The addition of 3-AT to the media, a histidine analogue, usually reduces background growth (Brückner et al., 2009). The HIS3 reporter gene was activated in all tested interactions (PSI A-PSI A, PSI A-PSI B, PSI B-PSI A and PSI B-PSI B), but also in the positive and negative controls. Even when 3-AT was added to the media, the same results were observed. Our data suggest the reporter gene is being autoactivated (Dreze et al., 2010). One approach to overcome this would be using another reporter gene, for example URA3. This gene is under the control of a promotor that is triggered by auto-activators and, upon addition of 5-fluoroorotic acid, it harms yeast cells containing auto-activators, as it was done in a study in which the authors report the removal of auto-activators in *Marchantia polymorpha* (Shivhare et al., 2021).

Alongside the Y2H we choose to conduct a 2in1 rBiFC assay, a bimolecular fluorescence-based technique with some changes. The 2in1 rBiFC system enables the co-expression of fusion proteins on the same plasmid. Both genes are cloned simultaneously on the same vector (fused to half YFP each) through Gateway recombinant technology, with a fluorescent marker (mRFP), that will be used for expression control and interaction quantification, using a ratiometric analysis (Grefen & Blatt, 2012). During this work, we successfully cloned the PSIs into the expression plasmid for 2in1 rBiFC, that will be used in the future to transform *Nicotiana tabacum* leaves and analyse and validate the interactions observed *in vitro.*

5. Conclusions

Although our knowledge about membrane trafficking has increased over the years, large gaps are still waiting to be filled. As novel unconventional routes started to be unravelled, like the one mediated by cardosin PSI A, researchers are now focused on characterizing these routes and finding their purpose. Cardosins PSIs have the ability to sort proteins to the vacuole through conventional (cardosin B PSI) and non-conventional (cardosin A PSI) routes (Vieira et al., 2019). Moreover, the correct sorting of proteins to the right compartment is an essential cellular function and, interestingly the PSI dimer was reported to induce membrane fusion, in a pH-dependent manner (Zhao et al., 2020).

Through a genetic approach we were able to gain new insights on the route followed by both cardosin A PSI and cardosin B PSI. The expression of both PSIs in *syp22 syp23* double mutants, two members of the SYP2 family of SNARES, revealed that alterations in PVC and/or vacuolar integrity inhibits PSIs trafficking to the vacuole, whether the protein follows a conventional or non-conventional route.

Moreover, *in vitro* PPIs studies showed that cardosins PSIs can form dimers under near-neutral pH conditions. From the pull-down assays performed, PSI A interacts with itself at pH 7.4, and with PSI B at pH 6.8. A motif in the C-terminal PSI A sequence was found responsible for its homo- and heterodimeric association. Interactions involving PSI B were not detected. Thus, the role of glycosylation in the dimerization of PSIs needs further investigation. The aforementioned results need to be sustained with in vivo interaction confirmation, using techniques such as 2in1 rBiFC or fluorescence lifetime imaging microscopy (FRET-FLIM), that enables direct visualisation of protein interactions in living cells.

Although the results obtained give promising insights on the molecular determinants that might account for differences in PSI-mediated routes, this is a preliminary study towards cardosins PSIs dimerization and uncovering the mechanisms behind their function as vacuolar sorting domains. Furthermore, the 2in1 rBiFC assays are of major importance to sustain all the data obtained with the *in vitro* study performed and are yet to be finished since the constructs are not confirmed yet.

We can conclude that PSIs interact with themselves but also with other proteins along the endomembrane system. However, how dimerization contributes to the role of PSIs is still unclear. Overall, this study provided a large amount of insightful data that requires more analysis beyond what is discussed here but served as a strong beginning point for achieving our aims.

6. References

Ahmed, S. U., Rojo, E., Kovaleva, V., Venkataraman, S., Dombrowski, J. E., Matsuoka, K., & Raikhel, N. V. (2000). The Plant Vacuolar Sorting Receptor Atelp Is Involved in Transport of Nh2-Terminal Propeptide-Containing Vacuolar Proteins in Arabidopsis thaliana. *The Journal of Cell Biology*, *149*(7), 1335. https://doi.org/10.1083/JCB.149.7.1335

Alberts, B., Johnson, A., Lewis, J., Raff, M., Roberts, K., & Walter, P. (2002). *Transport from the ER through the Golgi Apparatus*. https://www.ncbi.nlm.nih.gov/books/NBK26941/

Almeida, C. M., Pereira, C., da Costa, D. S., Pereira, S., Pissarra, J., Simões, I., & Faro, C. (2012). Chlapsin, a chloroplastidial aspartic proteinase from the green algae Chlamydomonas reinhardtii. *Planta*, *236*(1), 283–296. https://doi.org/10.1007/S00425-012-1605-2

Altan-Bonnet, N., Phair, R. D., Polishchuk, R. S., Weigert, R., & Lippincott-Schwartz, J. (2003). A role for Arf1 in mitotic Golgi disassembly, chromosome segregation, and cytokinesis. *Proceedings of the National Academy of Sciences of the United States of America*, *100*(23), 13314. https://doi.org/10.1073/PNAS.2234055100

Anelli, T., & Sitia, R. (2008). Protein quality control in the early secretory pathway. *The EMBO Journal*, *27*(2), 315. https://doi.org/10.1038/SJ.EMBOJ.7601974

Aniento, F., de Medina Hernández, V. S., Dagdas, Y., Rojas-Pierce, M., & Russinova, E. (2022). Molecular mechanisms of endomembrane trafficking in plants. *The Plant Cell*, *34*(1), 146–173. https://doi.org/10.1093/PLCELL/KOAB235

Appenzeller-Herzog, C., & Hauri, H. P. (2006). The ER-Golgi intermediate compartment (ERGIC): In search of its identity and function. *Journal of Cell Science*, *119*(11), 2173–2183. https://doi.org/10.1242/JCS.03019

Assaad, F. F., Qiu, J. L., Youngs, H., Ehrhardt, D., Zimmerli, L., Kalde, M., Wanner, G., Peck, S. C., Edwards, H., Ramonell, K., Somerville, C. R., & Thordal-Christensen, H. (2004). The PEN1 syntaxin defines a novel cellular compartment upon fungal attack and is required for the timely assembly of papillae. *Molecular Biology of the Cell*, *15*(11), 5118–5129. https://doi.org/10.1091/MBC.E04-02-0140

Athauda, S. B. P., Matsumoto, K., Rajapakshe, S., Kuribayashi, M., Kojima, M., Kubomura-Yoshida, N., Iwamatsu, A., Shibata, C., Inoue, H., & Takahashi, K. (2004). Enzymic and structural characterization of nepenthesin, a unique member

of a novel subfamily of aspartic proteinases. *The Biochemical Journal*, *381*(Pt 1), 295–306. https://doi.org/10.1042/BJ20031575

Bassham, D. C., & Blatt, M. R. (2008). SNAREs: cogs and coordinators in signaling and development. *Plant Physiology*, *147*(4), 1504–1515. https://doi.org/10.1104/PP.108.121129

Bassham, D. C., Brandizzi, F., Otegui, M. S., & Sanderfoot, A. A. (2008). The Secretory System of Arabidopsis. *The Arabidopsis Book / American Society of Plant Biologists*, *6*, e0116. https://doi.org/10.1199/TAB.0116

Becker, B., Bölinger, B., & Melkonian, M. (1995). Anterograde transport of algal scales through the Golgi complex is not mediated by vesicles. *Trends in Cell Biology*, *5*(8), 305–307. https://doi.org/10.1016/S0962-8924(00)89047-9

Bednarek, S. Y., & Raikhel, N. V. (1991). The barley lectin carboxyl-terminal propeptide is a vacuolar protein sorting determinant in plants. *The Plant Cell*, *3*(11), 1195. https://doi.org/10.1105/TPC.3.11.1195

Bernat-Silvestre, C., De Sousa Vieira, V., Sánchez-Simarro, J., Aniento, F., & Marcote, M. J. (2021). Transient Transformation of A. thaliana Seedlings by Vacuum Infiltration. *Methods in Molecular Biology (Clifton, N.J.)*, *2200*, 147–155. https://doi.org/10.1007/978-1-0716-0880-7_6

Bethke, P. C., & Jones, R. L. (2000a). Vacuoles and prevacuolar compartments. *Current Opinion in Plant Biology*, *3*(6), 469–475. https://doi.org/10.1016/S1369-5266(00)00115-1

Bethke, P. C., & Jones, R. L. (2000b). Vacuoles and prevacuolar compartments. *Current Opinion in Plant Biology*, *3*(6), 469–475. https://doi.org/10.1016/S1369-5266(00)00115-1

Béthune, J., & Wieland, F. T. (2018). Assembly of COPI and COPII Vesicular Coat Proteins on Membranes. *Annual Review of Biophysics*, *47*, 63–83. https://doi.org/10.1146/ANNUREV-BIOPHYS-070317-033259

Bock, J. B., Matern, H. T., Peden, A. A., & Scheller, R. H. (2001). A genomic perspective on membrane compartment organization. *Nature*, *409*(6822), 839–841. https://doi.org/10.1038/35057024

Bolte, S., Brown, S., & Satiat-Jeunemaitre, B. (2004). The N-myristoylated Rab-GTPase m-Rabmc is involved in post-Golgi trafficking events to the lytic vacuole in plant cells. *Journal of Cell Science*, *117*(6), 943–954. https://doi.org/10.1242/JCS.00920

Bolte, S., Lanquar, V., Soler, M. N., Beebo, A., Satiat-Jeunemaître, B., Bouhidel, K., & Thomine, S. (2011). Distinct Lytic Vacuolar Compartments are Embedded Inside the Protein Storage Vacuole of Dry and Germinating Arabidopsis thaliana Seeds. *Plant and Cell Physiology*, *52*(7), 1142–1152. https://doi.org/10.1093/PCP/PCR065

Boncompain, G., & Weigel, A. V. (2018). Transport and sorting in the Golgi complex: multiple mechanisms sort diverse cargo. *Current Opinion in Cell Biology*, *50*, 94–101. https://doi.org/10.1016/J.CEB.2018.03.002

Bonifacino, J. S., & Traub, L. M. (2003). Signals for Sorting of Transmembrane Proteins to Endosomes and Lysosomes*. *Https://Doi.Org/10.1146/Annurev.Biochem.72.121801.161800*, *72*, 395–447. https://doi.org/10.1146/ANNUREV.BIOCHEM.72.121801.161800

Boonamnaj, P., Pandey, R. B., & Sompornpisut, P. (2022). Effect of pH on stability of dimer structure of the main protease of coronavirus-2. *Biophysical Chemistry*, *287*, 106829. https://doi.org/10.1016/J.BPC.2022.106829

Boyes, D. C., Zayed, A. M., Ascenzi, R., McCaskill, A. J., Hoffman, N. E., Davis, K. R., & Görlach, J. (2001). Growth stage-based phenotypic analysis of Arabidopsis: a model for high throughput functional genomics in plants. *The Plant Cell*, *13*(7), 1499–1510. https://doi.org/10.1105/TPC.010011

Brandizzi, F., Hanton, S., Pinto DaSilva, L. L., Boevink, P., Evans, D., Oparka, K., Denecke, J., & Hawes, C. (2003). ER quality control can lead to retrograde transport from the ER lumen to the cytosol and the nucleoplasm in plants. *The Plant Journal*, *34*(3), 269–281. https://doi.org/10.1046/J.1365-313X.2003.01728.X

Braulke, T., & Bonifacino, J. S. (2009). Sorting of lysosomal proteins. *Biochimica et Biophysica Acta (BBA) - Molecular Cell Research*, *1793*(4), 605–614. https://doi.org/10.1016/J.BBAMCR.2008.10.016

Brown, R. M., Franke, W. W., Kleinig, H., Falk, H., & Sitte, P. (1970). Scale formation in chrysophycean algae: I. Cellulosic and noncellulosic wall components made by the golgi apparatus. *Journal of Cell Biology*, *45*(2), 246–271. https://doi.org/10.1083/JCB.45.2.246

Brückner, A., Polge, C., Lentze, N., Auerbach, D., & Schlattner, U. (2009). Yeast two-hybrid, a powerful tool for systems biology. *International Journal of Molecular Sciences*, *10*(6), 2763–2788. https://doi.org/10.3390/IJMS10062763

Bryksa, B. C., Bhaumik, P., Magracheva, E., De Moura, D. C., Kurylowicz, M., Zdanov, A., Dutcher, J. R., Wlodawer, A., & Yada, R. Y. (2011). Structure and Mechanism of the Saposin-like Domain of a Plant Aspartic Protease. *The Journal of Biological Chemistry*, *286*(32), 28265. https://doi.org/10.1074/JBC.M111.252619

Bryksa, B. C., Grahame, D. A., & Yada, R. Y. (2017). Comparative structure-function characterization of the saposin-like domains from potato, barley, cardoon and Arabidopsis aspartic proteases. *Biochimica et Biophysica Acta. Biomembranes*, *1859*(5), 1008–1018. https://doi.org/10.1016/J.BBAMEM.2017.02.007

Cai, H., Reinisch, K., & Ferro-Novick, S. (2007). Coats, tethers, Rabs, and SNAREs work together to mediate the intracellular destination of a transport vesicle. *Developmental Cell*, *12*(5), 671–682. https://doi.org/10.1016/J.DEVCEL.2007.04.005

Carter, C., Pan, S., Zouhar, J., Avila, E. L., Girke, T., & Raikhel, N. V. (2004). The vegetative vacuole proteome of Arabidopsis thaliana reveals predicted and unexpected proteins. *The Plant Cell*, *16*(12), 3285–3303. https://doi.org/10.1105/TPC.104.027078

Cereghino, J. L., Marcusson, E. G., & Emr, S. D. (1995). The cytoplasmic tail domain of the vacuolar protein sorting receptor Vps10p and a subset of VPS gene products regulate receptor stability, function, and localization. *Molecular Biology of the Cell*, *6*(9), 1089–1102. https://doi.org/10.1091/MBC.6.9.1089

Cevher-Keskin, B., & Cevher-Keskin, B. (2020). Endomembrane Trafficking in Plants. *Electrodialysis*. https://doi.org/10.5772/INTECHOPEN.91642

Chen, H. J., Huang, Y. H., Huang, G. J., Huang, S. S., Chow, T. J., & Lin, Y. H. (2015). Sweet potato SPAP1 is a typical aspartic protease and participates in ethephon-mediated leaf senescence. *Journal of Plant Physiology*, *180*, 1–17. https://doi.org/10.1016/J.JPLPH.2015.03.009

Chen, H., Wei, P., Huang, C., Tan, L., Liu, Y., & Lai, L. (2006). Only one protomer is active in the dimer of SARS 3C-like proteinase. *The Journal of Biological Chemistry*, *281*(20), 13894–13898. https://doi.org/10.1074/JBC.M510745200

Chen, X., Shen, J., & Prywes, R. (2002). The luminal domain of ATF6 senses endoplasmic reticulum (ER) stress and causes translocation of ATF6 from the ER to the Golgi. *The Journal of Biological Chemistry*, *277*(15), 13045–13052. https://doi.org/10.1074/JBC.M110636200

Chen, Y. F., Randlett, M. D., Findell, J. L., & Schallert, G. E. (2002). Localization of the ethylene receptor ETR1 to the endoplasmic reticulum of Arabidopsis. *The Journal of Biological Chemistry*, *277*(22), 19861–19866. https://doi.org/10.1074/JBC.M201286200

Chen, Y. N., Slabaugh, E., & Brandizzi, F. (2008). Membrane-tethered transcription factors in Arabidopsis thaliana: novel regulators in stress response and development. *Current Opinion in Plant Biology*, *11*(6), 695–701. https://doi.org/10.1016/J.PBI.2008.10.005

Cheung, L. K. Y., Dupuis, J. H., Dee, D. R., Bryksa, B. C., & Yada, R. Y. (2020). Roles of Plant-Specific Inserts in Plant Defense. *Trends in Plant Science*, *25*(7), 682–694. https://doi.org/10.1016/J.TPLANTS.2020.02.009

Chou, C. Y., Chang, H. C., Hsu, W. C., Lin, T. Z., Lin, C. H., & Chang, G. G. (2004). Quaternary structure of the severe acute respiratory syndrome (SARS) coronavirus main protease. *Biochemistry*, *43*(47), 14958–14970. https://doi.org/10.1021/BI0490237

Chrispeels, M. J. (1983). The Golgi apparatus mediates the transport of phytohemagglutinin to the protein bodies in bean cotyledons. *Planta*, *158*(2), 140–151. https://doi.org/10.1007/BF00397707

Chrispeels, M. J., & Herman, E. M. (2000). Endoplasmic reticulum-derived compartments function in storage and as mediators of vacuolar remodeling via a new type of organelle, precursor protease vesicles. *Plant Physiology*, *123*(4), 1227–1233. https://doi.org/10.1104/PP.123.4.1227

Claessen, J. H. L., Kundrat, L., & Ploegh, H. L. (2012). Protein quality control in the ER: balancing the ubiquitin checkbook. *Trends in Cell Biology*, *22*(1), 22–32. https://doi.org/10.1016/J.TCB.2011.09.010

Conceição, A. D. S., Marty-Mazars, D., Bassham, D. C., Sanderfoot, A. A., Marty, F., & Raikhel, N. V. (1997). The syntaxin homolog AtPEP12p resides on a late post-Golgi compartment in plants. *The Plant Cell*, *9*(4), 571–582. https://doi.org/10.1105/TPC.9.4.571

Cooper, A. A., & Stevens, T. H. (1996). Vps10p cycles between the late-Golgi and prevacuolar compartments in its function as the sorting receptor for multiple yeast vacuolar hydrolases. *The Journal of Cell Biology*, *133*(3), 529–541. https://doi.org/10.1083/JCB.133.3.529

Cordeiro M, P. M. B. P. (1994). Tissue-specific expression of multi- ple forms of cyprosin (aspartic proteinase) in flowers of Cynara cardunculus. *Physiologia Plantarum*, *92*, 645–653.

Costa, J., Ashford, D. A., Nimtz, M., Bento, I., Frazao, C., Esteves, C. L., Faro, C. J., Kervinen, J., Pires, E., Verissimo, P., Wlodawer, A., & Carrondo, M. A. (1997). The Glycosylation of the Aspartic Proteinases from Barley (Hordeum Vulgare L.) and Cardoon (Cynara Cardunculus L.). *European Journal of Biochemistry*, *243*(3), 695–700. https://doi.org/10.1111/J.1432-1033.1997.T01-1-00695.X

Craddock, C. P., Hunter, P. R., Szakacs, E., Hinz, G., Robinson, D. G., & Frigerio, L. (2008). Lack of a vacuolar sorting receptor leads to non-specific missorting of soluble vacuolar proteins in Arabidopsis seeds. *Traffic (Copenhagen, Denmark)*, *9*(3), 408–416. https://doi.org/10.1111/J.1600-0854.2007.00693.X

Cruz, R., Huesgen, P., Riley, S. P., Wlodawer, A., Faro, C., Overall, C. M., Martinez, J. J., & Simões, I. (2014). RC1339/APRc from Rickettsia conorii is a novel aspartic protease with properties of retropepsin-like enzymes. *PLoS Pathogens*, *10*(8). https://doi.org/10.1371/JOURNAL.PPAT.1004324

Curto, P., Lufrano, D., Pinto, C., Custódio, V., Gomes, A. C., Trejo, S. A., Bakás, L., Vairo-Cavalli, S., Faro, C., & Simõesa, I. (2014). Establishing the Yeast Kluyveromyces lactis as an Expression Host for Production of the Saposin-Like Domain of the Aspartic Protease Cirsin. *Applied and Environmental Microbiology*, *80*(1), 86. https://doi.org/10.1128/AEM.03151-13

da Costa, D. S., Pereira, S., Moore, I., & Pissarra, J. (2010). Dissecting cardosin B trafficking pathways in heterologous systems. *Planta*, *232*(6), 1517–1530. https://doi.org/10.1007/S00425-010-1276-9

DaSilva, L. L. P., Foresti, O., & Denecke, J. (2006a). Targeting of the plant vacuolar sorting receptor BP80 is dependent on multiple sorting signals in the cytosolic tail. *The Plant Cell*, *18*(6), 1477–1497. https://doi.org/10.1105/TPC.105.040394

DaSilva, L. L. P., Foresti, O., & Denecke, J. (2006b). Targeting of the Plant Vacuolar Sorting Receptor BP80 Is Dependent on Multiple Sorting Signals in the Cytosolic Tail. *The Plant Cell*, *18*(6), 1477. https://doi.org/10.1105/TPC.105.040394

DaSilva, L. L. P., Taylor, J. P., Hadlington, J. L., Hanton, S. L., Snowden, C. J., Fox, S. J., Foresti, O., Brandizzi, F., & Denecke, J. (2005a). Receptor salvage from the

prevacuolar compartment is essential for efficient vacuolar protein targeting. *The Plant Cell*, *17*(1), 132–148. https://doi.org/10.1105/TPC.104.026351

DaSilva, L. L. P., Taylor, J. P., Hadlington, J. L., Hanton, S. L., Snowden, C. J., Fox, S. J., Foresti, O., Brandizzi, F., & Denecke, J. (2005b). Receptor salvage from the prevacuolar compartment is essential for efficient vacuolar protein targeting. *The Plant Cell*, *17*(1), 132–148. https://doi.org/10.1105/TPC.104.026351

Davies, D. R. (1990). The structure and function of the aspartic proteinases. *Annual Review of Biophysics and Biophysical Chemistry*, *19*, 189–215. https://doi.org/10.1146/ANNUREV.BB.19.060190.001201

De Caroli, M., Barozzi, F., Renna, L., Piro, G., & Di Sansebastiano, G. Pietro. (2021). Actin and microtubules differently contribute to vacuolar targeting specificity during the export from the er. *Membranes*, *11*(4), 299. https://doi.org/10.3390/MEMBRANES11040299/S1

De Matteis, M. A., & Morrow, J. S. (2000). Spectrin tethers and mesh in the biosynthetic pathway. *Journal of Cell Science*, *113 (Pt 13)*(13), 2331–2343. https://doi.org/10.1242/JCS.113.13.2331

De Moura, D. C., Bryksa, B. C., & Yada, R. Y. (2014). In Silico Insights into Protein-Protein Interactions and Folding Dynamics of the Saposin-Like Domain of Solanum tuberosum Aspartic Protease. *PLOS ONE*, *9*(9), e104315. https://doi.org/10.1371/JOURNAL.PONE.0104315

Domingos, A., Cardoso, P. C., Xue, Z. T., Clemente, A., Brodelius, P. E., & Pais, M. S. (2000). Purification, cloning and autoproteolytic processing of an aspartic proteinase from Centaurea calcitrapa. *European Journal of Biochemistry*, *267*(23), 6824–6831. https://doi.org/10.1046/J.1432-1033.2000.01780.X

Donaldson, J. G., & Lippincott-Schwartz, J. (2000). Sorting and signaling at the Golgi complex. *Cell*, *101*(7), 693–696. https://doi.org/10.1016/S0092-8674(00)80881-8

Doray, B., Ghosh, P., Griffith, J., Geuze, H. J., & Kornfeld, S. (2002). Cooperation of GGAs and AP-1 in Packaging MPRs at the Trans-Golgi Network. *Science*, *297*(5587), 1700–1703. https://doi.org/10.1126/SCIENCE.1075327

Dreze, M., Monachello, D., Lurin, C., Cusick, M. E., Hill, D. E., Vidal, M., & Braun, P. (2010). High-quality binary interactome mapping. *Methods in Enzymology*, *470*(C), 281–315. https://doi.org/10.1016/S0076-6879(10)70012-4

D'Souza, S. E., Ginsberg, M. H., & Plow, E. F. (1991). Arginyl-glycyl-aspartic acid (RGD): a cell adhesion motif. *Trends in Biochemical Sciences*, *16*(7), 246–250. https://doi.org/10.1016/0968-0004(91)90096-E

Duarte, P., Pissarra, J., & Moore, I. (2008). Processing and trafficking of a single isoform of the aspartic proteinase cardosin A on the vacuolar pathway. *Planta*, *227*(6), 1255–1268. https://doi.org/10.1007/S00425-008-0697-1

Dunn, B. M. (2002). Structure and mechanism of the pepsin-like family of aspartic peptidases. *Chemical Reviews*, *102*(12), 4431–4458. https://doi.org/10.1021/CR010167Q

Dunphy, W. G., & Rothman, J. E. (1985a). Compartmental organization of the Golgi stack. *Cell*, *42*(1), 13–21. https://doi.org/10.1016/S0092-8674(85)80097-0

Dunphy, W. G., & Rothman, J. E. (1985b). Compartmental organization of the golgi stack. *Cell*, *42*(1), 13–21. https://doi.org/10.1016/S0092-8674(85)80097-0

Ebine, K., Inoue, T., Ito, J., Ito, E., Uemura, T., Goh, T., Abe, H., Sato, K., Nakano, A., & Ueda, T. (2014a). Plant vacuolar trafficking occurs through distinctly regulated pathways. *Current Biology*, *24*(12), 1375–1382. https://doi.org/10.1016/J.CUB.2014.05.004

Ebine, K., Inoue, T., Ito, J., Ito, E., Uemura, T., Goh, T., Abe, H., Sato, K., Nakano, A., & Ueda, T. (2014b). Plant vacuolar trafficking occurs through distinctly regulated pathways. *Current Biology : CB*, *24*(12), 1375–1382. https://doi.org/10.1016/J.CUB.2014.05.004

Ebine, K., Okatani, Y., Uemura, T., Goh, T., KeikoShoda, Niihama, M., Morita, M. T., Spitzer, C., Otegui, M. S., Nakano, A., & Ueda, T. (2008a). A SNARE complex unique to seed plants is required for protein storage vacuole biogenesis and seed development of arabidopsis thaliana. *Plant Cell*, *20*(11), 3006–3021. https://doi.org/10.1105/TPC.107.057711

Ebine, K., Okatani, Y., Uemura, T., Goh, T., KeikoShoda, Niihama, M., Morita, M. T., Spitzer, C., Otegui, M. S., Nakano, A., & Ueda, T. (2008b). A SNARE Complex Unique to Seed Plants Is Required for Protein Storage Vacuole Biogenesis and Seed Development of Arabidopsis thaliana. *The Plant Cell*, *20*(11), 3006–3021. https://doi.org/10.1105/TPC.107.057711

Ebine, K., Okatani, Y., Uemura, T., Goh, T., KeikoShoda, Niihama, M., Morita, M. T., Spitzer, C., Otegui, M. S., Nakano, A., & Ueda, T. (2008c). A SNARE Complex

Unique to Seed Plants Is Required for Protein Storage Vacuole Biogenesis and Seed Development of Arabidopsis thaliana. *The Plant Cell*, *20*(11), 3006–3021. https://doi.org/10.1105/TPC.107.057711

Ebine, K., Uemura, T., Nakano, A., & Ueda, T. (2012). Flowering time modulation by a vacuolar SNARE via FLOWERING LOCUS C in Arabidopsis thaliana. *PloS One*, *7*(7). https://doi.org/10.1371/JOURNAL.PONE.0042239

Egas, C., Lavoura, N., Resende, R., Brito, R. M. M., Pires, E., Pedroso De Lima, M. C., & Faro, C. (2000). The saposin-like domain of the plant aspartic proteinase precursor is a potent inducer of vesicle leakage. *The Journal of Biological Chemistry*, *275*(49), 38190–38196. https://doi.org/10.1074/JBC.M006093200

Eisenach, C., Francisco, R., & Martinoia, E. (2015). Plant vacuoles. *Current Biology : CB*, *25*(4), R136–R137. https://doi.org/10.1016/J.CUB.2014.11.056

El Kasmi, F., Krause, C., Hiller, U., Stierhof, Y. D., Mayer, U., Conner, L., Kong, L., Reichardt, I., Sanderfoot, A. A., & Jürgens, G. (2013). SNARE complexes of different composition jointly mediate membrane fusion in Arabidopsis cytokinesis. *Molecular Biology of the Cell*, *24*(10), 1593–1601. https://doi.org/10.1091/MBC.E13-02-0074

English, A. R., & Voeltz, G. K. (2013). Endoplasmic Reticulum Structure and Interconnections with Other Organelles. *Cold Spring Harbor Perspectives in Biology*, *5*(4), 1–16. https://doi.org/10.1101/CSHPERSPECT.A013227

Farquhar, M. G. (1985). Progress in unraveling pathways of Golgi traffic. *Annual Review of Cell Biology*, *1*, 447–488. https://doi.org/10.1146/ANNUREV.CB.01.110185.002311

Feijoo-Siota, L., Rama, J. L. R., Sánchez-Pérez, A., & Villa, T. G. (2018). Expression, activation and processing of a novel plant milk-clotting aspartic protease in Pichia pastoris. *Journal of Biotechnology*, *268*, 28–39. https://doi.org/10.1016/J.JBIOTEC.2018.01.006

Feraru, E., Paciorek, T., Feraru, M. I., Zwiewka, M., de Groodt, R., de Rycke, R., Kleine-Vehn, J., & Friml, J. (2012). The AP-3 β Adaptin Mediates the Biogenesis and Function of Lytic Vacuoles in Arabidopsis. *The Plant Cell*, *22*(8), 2812–2824. https://doi.org/10.1105/TPC.110.075424

Fields, S., & Song, O. K. (1989). A novel genetic system to detect protein-protein interactions. *Nature*, *340*(6230), 245–246. https://doi.org/10.1038/340245A0

Frazão, C., Bento, I., Costa, J., Soares, C. M., Veríssimo, P., Faro, C., Pires, E., Cooper, J., & Carrondo, M. A. (1999). Crystal structure of cardosin A, a glycosylated and Arg-Gly-Asp- containing aspartic proteinase from the flowers of Cynara cardunculus L. *Journal of Biological Chemistry*, *274*(39), 27694–27701. https://doi.org/10.1074/jbc.274.39.27694

Frey, M. E., D'Ippolito, S., Pepe, A., Daleo, G. R., & Guevara, M. G. (2018). Transgenic expression of plant-specific insert of potato aspartic proteases (StAP-PSI) confers enhanced resistance to Botrytis cinerea in Arabidopsis thaliana. *Phytochemistry*, *149*, 1–11. https://doi.org/10.1016/J.PHYTOCHEM.2018.02.004

Frigerio, L., & Hawes, C. (2008). The Endomembrane System: A Green Perspective. *Traffic*, *9*(10), 1563–1563. https://doi.org/10.1111/J.1600-0854.2008.00795.X

Frigerio, L., Jolliffe, N. A., Di Cola, A., Hernández Felipe, D., Paris, N., Neuhaus, J. M., Lord, J. M., Ceriotti, A., & Roberts, L. M. (2001). The internal propeptide of the ricin precursor carries a sequence-specific determinant for vacuolar sorting. *Plant Physiology*, *126*(1), 167–175. https://doi.org/10.1104/PP.126.1.167

Friml, J., & Jones, A. R. (2010a). Endoplasmic reticulum: the rising compartment in auxin biology. *Plant Physiology*, *154*(2), 458–462. https://doi.org/10.1104/PP.110.161380

Friml, J., & Jones, A. R. (2010b). Endoplasmic Reticulum: The Rising Compartment in Auxin Biology. *Plant Physiology*, *154*(2), 458. https://doi.org/10.1104/PP.110.161380

Fuji, K., Shimada, T., Takahashi, H., Tamura, K., Koumoto, Y., Utsumi, S., Nishizawa, K., Maruyama, N., & Hara-Nishimura, I. (2007a). Arabidopsis Vacuolar Sorting Mutants (green fluorescent seed) Can Be Identified Efficiently by Secretion of Vacuole-Targeted Green Fluorescent Protein in Their Seeds. *The Plant Cell*, *19*(2), 597–609. https://doi.org/10.1105/TPC.106.045997

Fuji, K., Shimada, T., Takahashi, H., Tamura, K., Koumoto, Y., Utsumi, S., Nishizawa, K., Maruyama, N., & Hara-Nishimura, I. (2007b). Arabidopsis Vacuolar Sorting Mutants (green fluorescent seed) Can Be Identified Efficiently by Secretion of Vacuole-Targeted Green Fluorescent Protein in Their Seeds. *The Plant Cell*, *19*(2), 597–609. https://doi.org/10.1105/TPC.106.045997

Ghosh, P., Dahms, N. M., & Kornfeld, S. (2003). Mannose 6-phosphate receptors: new twists in the tale. *Nature Reviews Molecular Cell Biology 2003 4:3*, *4*(3), 202–213. https://doi.org/10.1038/nrm1050

Gietz, R. D., Triggs-Raine, B., Robbins, A., Graham, K. C., & Woods, R. A. (1997). Identification of proteins that interact with a protein of interest: Applications of the yeast two-hybrid system. *Molecular and Cellular Biochemistry*, *172*(1–2), 67–79. https://doi.org/10.1023/A:1006859319926

Glathe, S., Kervinen, J., Nimtz, M., Li, G. H., Tobin, G. J., Copeland, T. D., Ashford, D. A., Wlodawer, A., & Costa, J. (1998). Transport and Activation of the Vacuolar Aspartic Proteinase Phytepsin in Barley (Hordeum vulgare L.). *Journal of Biological Chemistry*, *273*(47), 31230–31236. https://doi.org/10.1074/JBC.273.47.31230

Glick, B. S., & Nakano, A. (2009). Membrane traffic within the Golgi apparatus. *Annual Review of Cell and Developmental Biology*, *25*, 113–132. https://doi.org/10.1146/ANNUREV.CELLBIO.24.110707.175421

Goring, D. R., & Sansebastiano, G. P. Di. (2018). Protein and membrane trafficking routes in plants: conventional or unconventional? *Journal of Experimental Botany*, *69*(1), 1. https://doi.org/10.1093/JXB/ERX435

Goyal, B., & Goyal, D. (2020). Targeting the Dimerization of the Main Protease of Coronaviruses: A Potential Broad-Spectrum Therapeutic Strategy. *ACS Combinatorial Science*, *22*(6), 297–305. https://doi.org/10.1021/ACSCOMBSCI.0C00058/ASSET/IMAGES/MEDIUM/CO0C00058_0003.GIF

Grefen, C., & Blatt, M. R. (2012). A 2in1 cloning system enables ratiometric bimolecular fluorescence complementation (rBiFC). *BioTechniques*, *53*(5), 311–314. https://doi.org/10.2144/000113941/FORMAT/EPUB

Guevara, M. G., Daleo, G. R., & Oliva, C. R. (2001). Purification and characterization of an aspartic protease from potato leaves. *Physiologia Plantarum*, *112*(3), 321–326. https://doi.org/10.1034/J.1399-3054.2001.1120304.X

Guevara, M. G., Oliva, C. R., Machinandiarena, M., & Daleo, G. R. (1999). Purification and properties of an aspartic protease from potato tuber that is inhibited by a basic chitinase. *Physiologia Plantarum*, *106*(2), 164–169. https://doi.org/10.1034/J.1399-3054.1999.106203.X

Guo, R., Xu, X., Carole, B., Li, X., Gao, M., Zheng, Y., & Wang, X. (2013). Genome-wide identification, evolutionary and expression analysis of the aspartic protease gene superfamily in grape. *BMC Genomics*, *14*(1), 1–18. https://doi.org/10.1186/1471-2164-14-554/FIGURES/6

Happel, N., Höning, S., Neuhaus, J. M., Paris, N., Robinson, D. G., & Holstein, S. E. H. (2004). ArabidopsisμA-adaptin interacts with the tyrosine motif of the vacuolar sorting receptor VSR-PS1. *The Plant Journal*, *37*(5), 678–693. https://doi.org/10.1111/J.1365-313X.2003.01995.X

Hara-Nishimura, I., & Hatsugai, N. (2011). The role of vacuole in plant cell death. *Cell Death & Differentiation 2011 18:8*, *18*(8), 1298–1304. https://doi.org/10.1038/cdd.2011.70

Hara-Nishimura, I., Matsushima, R., … T. S.-P., & 2004, undefined. (n.d.). Diversity and formation of endoplasmic reticulum-derived compartments in plants. Are these compartments specific to plant cells? *Academic.Oup.ComI Hara-Nishimura, R Matsushima, T Shimada, M NishimuraPlant Physiology, 2004•academic.Oup.Com*. Retrieved September 1, 2023, from https://academic.oup.com/plphys/article-abstract/136/3/3435/6112446

Hara-Nishimura, I., Shimada, T., Hatano, K., Takeuchi, Y., & Nishimura, M. (1998). Transport of storage proteins to protein storage vacuoles is mediated by large precursor-accumulating vesicles. *Academic.Oup.ComI Hara-Nishimura, T Shimada, K Hatano, Y Takeuchi, M NishimuraThe Plant Cell, 1998•academic.Oup.Com*, *10*, 825–836. https://academic.oup.com/plcell/article-abstract/10/5/825/5999358

Hatsugai, N., Kuroyanagi, M., Yamada, K., Meshi, T., Tsuda, S., Kondo, M., Nishimura, M., & Hara-Nishimura, I. (2004). A plant vacuolar protease, VPE, mediates virus-induced hypersensitive cell death. *Science (New York, N.Y.)*, *305*(5685), 855–858. https://doi.org/10.1126/SCIENCE.1099859

Hayashi, Y., Yamada, K., Shimada, T., Matsushima, R., Nishizawa, N. K., Nishimura, M., & Hara-Nishimura, I. (2001). A Proteinase-Storing Body that Prepares for Cell Death or Stresses in the Epidermal Cells of Arabidopsis. *Plant and Cell Physiology*, *42*(9), 894–899. https://doi.org/10.1093/PCP/PCE144

Herman, E. M. (2008). Endoplasmic reticulum bodies: solving the insoluble. *Current Opinion in Plant Biology*, *11*(6), 672–679. https://www.academia.edu/81423367/Endoplasmic_reticulum_bodies_solving_the_insoluble

Herman, E. M., & Larkins, B. A. (1999a). Protein storage bodies and vacuoles. *The Plant Cell*, *11*(4), 601–613. https://doi.org/10.1105/TPC.11.4.601

Herman, E. M., & Larkins, B. A. (1999b). Protein storage bodies and vacuoles. *The Plant Cell*, *11*(4), 601–613. https://doi.org/10.1105/TPC.11.4.601

Herman, E., & Schmidt, M. (2004). Endoplasmic Reticulum to Vacuole Trafficking of Endoplasmic Reticulum Bodies Provides an Alternate Pathway for Protein Transfer to the Vacuole. *Plant Physiology*, *136*(3), 3440–3446. https://doi.org/10.1104/PP.104.051722

Hinz, G., Colanesi, S., Hillmer, S., Rogers, J. C., & Robinson, D. G. (2007). Localization of vacuolar transport receptors and cargo proteins in the Golgi apparatus of developing Arabidopsis embryos. *Traffic (Copenhagen, Denmark)*, *8*(10), 1452–1464. https://doi.org/10.1111/J.1600-0854.2007.00625.X

Hinz, G., Hillmer, S., Bäumer, M., & Hohl, I. (1999). Vacuolar storage proteins and the putative vacuolar sorting receptor BP-80 exit the golgi apparatus of developing pea cotyledons in different transport vesicles. *The Plant Cell*, *11*(8), 1509–1524. https://doi.org/10.1105/TPC.11.8.1509

Hohl, I., Robinson, D. G., Chrispeels, M. J., & Hinz, G. (1996). Transport of storage proteins to the vacuole is mediated by vesicles without a clathrin coat. *Journal of Cell Science*, *109 (Pt 10)*(10), 2539–2550. https://doi.org/10.1242/JCS.109.10.2539

Holwerda, B. C., Padgett, H. S., & Rogers, J. C. (1992). Proaleurain vacuolar targeting is mediated by short contiguous peptide interactions. *The Plant Cell*, *4*(3), 307–318. https://doi.org/10.1105/TPC.4.3.307

Hong, B., Ichida, A., Wang, Y., Gens, J. S., Pickard, B. G., & Harper, J. F. (1999). Identification of a Calmodulin-Regulated Ca2+-ATPase in the Endoplasmic Reticulum. *Plant Physiology*, *119*(4), 1165. https://doi.org/10.1104/PP.119.4.1165

Huang, A. H. C. (1996). Oleosins and Oil Bodies in Seeds and Other Organs. *Plant Physiology*, *110*(4), 1055–1061. https://doi.org/10.1104/PP.110.4.1055

Humair, D., Felipe, D. H., Neuhaus, J., & Paris, N. (2001). Demonstration in yeast of the function of BP-80, a putative plant vacuolar sorting receptor. *The Plant Cell*, *13*(4), 781–792. https://doi.org/10.1105/TPC.13.4.781

Hwang, I. (2008). Sorting and anterograde trafficking at the Golgi apparatus. *Plant Physiology*, *148*(2), 673–683. https://doi.org/10.1104/PP.108.124925

Ibl, V., & Stoger, E. (2012). The formation, function and fate of protein storage compartments in seeds. *Protoplasma*, *249*(2), 379–392. https://doi.org/10.1007/S00709-011-0288-Z

Ito, Y., Uemura, T., & Nakano, A. (2014). Formation and maintenance of the golgi apparatus in plant cells. *International Review of Cell and Molecular Biology*, *310*, 221–287. https://doi.org/10.1016/B978-0-12-800180-6.00006-2

Iwaki, T., Hosomi, A., Tokudomi, S., Kusunoki, Y., Fujita, Y., Giga-Hama, Y., Tanaka, N., & Takegawa, K. (2006). Vacuolar protein sorting receptor in Schizosaccharomyces pombe. *Microbiology*, *152*(5), 1523–1532. https://doi.org/10.1099/MIC.0.28627-0/CITE/REFWORKS

Jahn, R., & Scheller, R. H. (2006). SNAREs--engines for membrane fusion. *Nature Reviews. Molecular Cell Biology*, *7*(9), 631–643. https://doi.org/10.1038/NRM2002

Jiang, L., Phillips, T. E., Hamm, C. A., Drozdowicz, Y. M., Rea, P. A., Maeshima, M., Rogers, S. W., & Rogers, J. C. (2001). The protein storage vacuole: A unique compound organelle. *Journal of Cell Biology*, *155*(6), 991–1002. https://doi.org/10.1083/JCB.200107012

Jiang, L., Phillips, T. E., Rogers, S. W., & Rogers, J. C. (2000a). Biogenesis of the Protein Storage Vacuole Crystalloid. *The Journal of Cell Biology*, *150*(4), 755. https://doi.org/10.1083/JCB.150.4.755

Jiang, L., Phillips, T. E., Rogers, S. W., & Rogers, J. C. (2000b). Biogenesis of the Protein Storage Vacuole Crystalloid. *The Journal of Cell Biology*, *150*(4), 755. https://doi.org/10.1083/JCB.150.4.755

Jiang, L., Phillips, T. E., Rogers, S. W., & Rogers, J. C. (2000c). Biogenesis of the protein storage vacuole crystalloid. *Journal of Cell Biology*, *150*(4), 755–769. https://doi.org/10.1083/JCB.150.4.755

Jiang, L., & Rogers, J. C. (1998). Integral Membrane Protein Sorting to Vacuoles in Plant Cells: Evidence for Two Pathways. *The Journal of Cell Biology*, *143*(5), 1183. https://doi.org/10.1083/JCB.143.5.1183

Jolliffe, I. T., Trendafilov, N. T., & Uddin, M. (2012). A Modified Principal Component Technique Based on the LASSO. *Http://Dx.Doi.Org/10.1198/1061860032148*, *12*(3), 531–547. https://doi.org/10.1198/1061860032148

Jolliffe, N. A., Brown, J. C., Neumann, U., Vicré, M., Bachi, A., Hawes, C., Ceriotti, A., Roberts, L. M., & Frigerio, L. (2004). Transport of ricin and 2S albumin precursors

to the storage vacuoles of Ricinus communis endosperm involves the Golgi and VSR-like receptors. *The Plant Journal : For Cell and Molecular Biology*, *39*(6), 821–833. https://doi.org/10.1111/J.1365-313X.2004.02167.X

Jolliffe, N. A., Craddock, C. P., & Frigerio, L. (2005). Pathways for protein transport to seed storage vacuoles. *Biochemical Society Transactions*, *33*(5), 1016–1018. https://doi.org/10.1042/BST20051016

Jørgensen, M., Stensballe, A., & Welinder, K. G. (2011). Extensive post-translational processing of potato tuber storage proteins and vacuolar targeting. *The FEBS Journal*, *278*(21), 4070–4087. https://doi.org/10.1111/J.1742-4658.2011.08311.X

Jürgens, G. (2004). Membrane trafficking in plants. *Annual Review of Cell and Developmental Biology*, *20*, 481–504. https://doi.org/10.1146/ANNUREV.CELLBIO.20.082503.103057

Kervinen, J., Tobin, G. J., Costa, J., Waugh, D. S., Wlodawer, A., & Zdanov, A. (1999). Crystal structure of plant aspartic proteinase prophytepsin: inactivation and vacuolar targeting. *The EMBO Journal*, *18*(14), 3947. https://doi.org/10.1093/EMBOJ/18.14.3947

Kim, S. J., & Brandizzi, F. (2012). News and views into the SNARE complexity in Arabidopsis. *Frontiers in Plant Science*, *3*(FEB), 18488. https://doi.org/10.3389/FPLS.2012.00028/BIBTEX

Kim, W. T., Franceschi, V. R., Krishnan, H. B., & Okita, T. W. (1988). Formation of wheat protein bodies: Involvement of the Golgi apparatus in gliadin transport. *Planta*, *176*(2), 173–182. https://doi.org/10.1007/BF00392442

Kirchhausen, T. (2000). Clathrin. *Annual Review of Biochemistry*, *69*, 699–727. https://doi.org/10.1146/ANNUREV.BIOCHEM.69.1.699

Kirsch, T., Paris, N., Butler, J. M., Beevers, L., & Rogers, J. C. (1994). Purification and initial characterization of a potential plant vacuolar targeting receptor. *Proceedings of the National Academy of Sciences of the United States of America*, *91*(8), 3403. https://doi.org/10.1073/PNAS.91.8.3403

Koide, Y., Hirano, H., Matsuoka, K., & Nakamura, K. (1997). The N-terminal propeptide of the precursor to sporamin acts as a vacuole-targeting signal even at the C terminus of the mature part in tobacco cells. *Plant Physiology*, *114*(3), 863. https://doi.org/10.1104/PP.114.3.863

Koide, Y., Matsuoka, K., Ohto, M. A., & Nakamura, K. (1999). The N-terminal propeptide and the C terminus of the precursor to 20-kilo-dalton potato tuber protein can function as different types of vacuolar sorting signals. *Plant & Cell Physiology*, *40*(11), 1152–1159. https://doi.org/10.1093/OXFORDJOURNALS.PCP.A029500

Künzl, F., Früholz, S., Fäßler, F., Li, B., & Pimpl, P. (2016). Receptor-mediated sorting of soluble vacuolar proteins ends at the trans-Golgi network/early endosome. *Nature Plants*, *2*(4). https://doi.org/10.1038/NPLANTS.2016.17

Kwon, Y., Shen, J., Lee, M. H., Geem, K. R., Jiang, L., & Hwang, I. (2018). AtCAP2 is crucial for lytic vacuole biogenesis during germination by positively regulating vacuolar protein trafficking. *Proceedings of the National Academy of Sciences of the United States of America*, *115*(7), E1675–E1683. https://doi.org/10.1073/pnas.1717204115

Lam, S., Cai, Y., Hillmer, S., Robinson, D. G., & Jiang, L. (2008). SCAMPs Highlight the Developing Cell Plate during Cytokinesis in Tobacco BY-2 Cells. *Plant Physiology*, *147*(4), 1637. https://doi.org/10.1104/PP.108.119925

Lam, S., Ching, L. S., Hillmer, S., Jang, S., An, G., Robinson, D. G., & Jiang, L. (2007). Rice SCAMP1 defines clathrin-coated, trans-golgi-located tubular-vesicular structures as an early endosome in tobacco BY-2 cells. *The Plant Cell*, *19*(1), 296–319. https://doi.org/10.1105/TPC.106.045708

Lam, S. K., Tse, Y. C., Jiang, L., Oliviusson, P., Heinzerling, O., & Robinson, D. G. (2005). Plant Prevacuolar Compartments and Endocytosis. *Plant Endocytosis*, 37–61. https://doi.org/10.1007/7089_004

Lam, S. K., Tse, Y. C., Miao, Y., Li, H. Y., Wang, J., Lo, S. W., & Jiang, L. (2007). Molecular characterization of plant prevacuolar and endosomal compartments. *Journal of Integrative Plant Biology*, *49*(8), 1119–1128. https://doi.org/10.1111/J.1672-9072.2007.00517.X/PDF

Lam, S. K., Tse, Y. C., Robinson, D. G., & Jiang, L. (2007). Tracking down the elusive early endosome. *Trends in Plant Science*, *12*(11), 497–505. https://doi.org/10.1016/J.TPLANTS.2007.09.001

Langemeyer, L., Fröhlich, F., & Ungermann, C. (2018). Rab GTPase Function in Endosome and Lysosome Biogenesis. *Trends in Cell Biology*, *28*(11), 957–970. https://doi.org/10.1016/J.TCB.2018.06.007

Lousa, C. D. M., & Denecke, J. (2016). Lysosomal and vacuolar sorting: not so different after all! *Biochemical Society Transactions*, *44*(3), 891–897. https://doi.org/10.1042/BST20160050

Luo, F., Fong, Y. H., Zeng, Y., Shen, J., Jiang, L., & Wong, K. B. (2014). How vacuolar sorting receptor proteins interact with their cargo proteins: crystal structures of apo and cargo-bound forms of the protease-associated domain from an Arabidopsis vacuolar sorting receptor. *The Plant Cell*, *26*(9), 3693–3708. https://doi.org/10.1105/TPC.114.129940

Marcos Lousa, C. de, Gershlick, D. C., & Denecke, J. (2012). Mechanisms and concepts paving the way towards a complete transport cycle of plant vacuolar sorting receptors. *Plant Cell*, *24*(5), 1714–1732. https://doi.org/10.1105/TPC.112.095679/DC1

Marti, L., Fornaciari, S., Renna, L., Stefano, G., & Brandizzi, F. (2010). COPII-mediated traffic in plants. *Trends in Plant Science*, *15*(9), 522–528. https://doi.org/10.1016/J.TPLANTS.2010.05.010

Martinoia, E., Maeshima, M., & Neuhaus, H. E. (2007). Vacuolar transporters and their essential role in plant metabolism. *Journal of Experimental Botany*, *58*(1), 83–102. https://doi.org/10.1093/JXB/ERL183

Martinoia, E., Massonneau, A., & Frangne, N. (2000). Transport processes of solutes across the vacuolar membrane of higher plants. *Plant & Cell Physiology*, *41*(11), 1175–1186. https://doi.org/10.1093/PCP/PCD059

Marty, F. (1999). Plant vacuoles. *The Plant Cell*, *11*(4), 587–599. https://doi.org/10.1105/TPC.11.4.587

Maruyama, N., Mun, L. C., Tatsuhara, M., Sawada, M., Ishimoto, M., & Utsumi, S. (2006). Multiple vacuolar sorting determinants exist in soybean 11S globulin. *The Plant Cell*, *18*(5), 1253–1273. https://doi.org/10.1105/TPC.105.036376

Matsuoka, K., & Neuhaus, J. M. (1999a). Cis-elements of protein transport to the plant vacuoles. *Journal of Experimental Botany*, *50*(331), 165–174. https://doi.org/10.1093/JXB/50.331.165

Matsuoka, K., & Neuhaus, J. M. (1999b). Cis-elements of protein transport to the plant vacuoles. *Journal of Experimental Botany*, *50*(331), 165–174. https://doi.org/10.1093/JXB/50.331.165

Matsushima, R., Hayashi, Y., Kondo, M., Shimada, T., Nishimura, M., & Hara-Nishimura, I. (2002). An endoplasmic reticulum-derived structure that is induced under stress conditions in Arabidopsis. *Plant Physiology*, *130*(4), 1807–1814. https://doi.org/10.1104/PP.009464

Matsushima, R., Hayashi, Y., Yamada, K., Shimada, T., Nishimura, M., & Hara-Nishimura, I. (2003). The ER Body, a Novel Endoplasmic Reticulum-Derived Structure in Arabidopsis. *Plant and Cell Physiology*, *44*(7), 661–666. https://doi.org/10.1093/PCP/PCG089

Maxfield, F. R., & McGraw, T. E. (2004). Endocytic recycling. *Nature Reviews Molecular Cell Biology 2004 5:2*, *5*(2), 121–132. https://doi.org/10.1038/nrm1315

Mazorra-Manzano, M. A., Tanaka, T., Dee, D. R., & Yada, R. Y. (2010). Structure-function characterization of the recombinant aspartic proteinase A1 from Arabidopsis thaliana. *Phytochemistry*, *71*(5–6), 515–523. https://doi.org/10.1016/J.PHYTOCHEM.2009.12.005

Mazorra-Manzano, M. A., & Yada, R. Y. (2008). Expression and characterization of the recombinant aspartic proteinase A1 from Arabidopsis thaliana. *Phytochemistry*, *69*(13), 2439–2448. https://doi.org/10.1016/J.PHYTOCHEM.2008.07.012

McMahon, H. T., & Boucrot, E. (2011). Molecular mechanism and physiological functions of clathrin-mediated endocytosis. *Nature Reviews. Molecular Cell Biology*, *12*(8), 517–533. https://doi.org/10.1038/NRM3151

McNew, J. A., Parlatl, F., Fukuda, R., Johnston, R. J., Paz, K., Paumet, F., Söllner, T. H., & Rothman, J. E. (2000). Compartmental specificity of cellular membrane fusion encoded in SNARE proteins. *Nature*, *407*(6801), 153–159. https://doi.org/10.1038/35025000

Meents, M. J., Motani, S., Mansfield, S. D., & Lacey Samuels, A. (2019). Organization of xylan production in the Golgi during secondary cell wall biosynthesis. *Plant Physiology*, *181*(2), 527–546. https://doi.org/10.1104/PP.19.00715

Meldolesi, J., & Pozzan, T. (1998). The Heterogeneity of ER Ca2+ Stores Has a Key Role in Nonmuscle Cell Signaling and Function. *The Journal of Cell Biology*, *142*(6), 1395. https://doi.org/10.1083/JCB.142.6.1395

Melkonian, M., Becker, B., & Becker, D. (1991). Scale formation in algae. *Journal of Electron Microscopy Technique*, *17*(2), 165–178. https://doi.org/10.1002/JEMT.1060170205

Mellman, I., & Warren, G. (2000). The road taken: past and future foundations of membrane traffic. *Cell*, *100*(1), 99–112. https://doi.org/10.1016/S0092-8674(00)81687-6

Meusser, B., Hirsch, C., Jarosch, E., & Sommer, T. (2005). ERAD: the long road to destruction. *Nature Cell Biology*, *7*(8), 766–772. https://doi.org/10.1038/NCB0805-766

Michael Lord, J., & Spooner, R. A. (2011). Ricin trafficking in plant and mammalian cells. *Toxins*, *3*(7), 787–801. https://doi.org/10.3390/TOXINS3070787

Milisavljevic, M. D., Timotijevic, G. S., Radovic, S. R., Konstantinovic, M. M., & Maksimovic, V. R. (2008). Two types of aspartic proteinases from buckwheat seed – Gene structure and expression analysis. *Journal of Plant Physiology*, *165*(9), 983–990. https://doi.org/10.1016/J.JPLPH.2007.03.016

Mizushima, N., Yoshimori, T., & Ohsumi, Y. (2011). The Role of Atg Proteins in Autophagosome Formation. *Https://Doi.Org/10.1146/Annurev-Cellbio-092910-154005*, *27*, 107–132. https://doi.org/10.1146/ANNUREV-CELLBIO-092910-154005

Molina, M., Otegui, M., of, S. P.-E. J., & 2006, undefined. (n.d.). Sunflower storage proteins are transported in dense vesicles that contain proteins homologous to the pumpkin vacuolar sorting receptor PV 72. *SciELO ChileMI Molina, M Otegui, S PetruccelliElectronic Journal of Biotechnology, 2006•SciELO Chile*. Retrieved September 1, 2023, from https://www.scielo.cl/scielo.php?pid=S0717-34582006000300029&script=sci_arttext&tlng=pt

Moore, P. J., Swords, K. M. M., Lynch, M. A., & Staehelin, L. A. (1991a). Spatial organization of the assembly pathways of glycoproteins and complex polysaccharides in the Golgi apparatus of plants. *The Journal of Cell Biology*, *112*(4), 589–602. https://doi.org/10.1083/JCB.112.4.589

Moore, P. J., Swords, K. M. M., Lynch, M. A., & Staehelin, L. A. (1991b). Spatial organization of the assembly pathways of glycoproteins and complex polysaccharides in the Golgi apparatus of plants. *The Journal of Cell Biology*, *112*(4), 589–602. https://doi.org/10.1083/JCB.112.4.589

Morita, M. T., & Shimada, T. (2014). The Plant Endomembrane System—A Complex Network Supporting Plant Development and Physiology. *Plant and Cell Physiology*, *55*(4), 667–671. https://doi.org/10.1093/PCP/PCU049

Muñoz, F. F., Mendieta, J. R., Pagano, M. R., Paggi, R. A., Daleo, G. R., & Guevara, M. G. (2010). The swaposin-like domain of potato aspartic protease (StAsp-PSI) exerts antimicrobial activity on plant and human pathogens. *Peptides*, *31*(5), 777–785. https://doi.org/10.1016/J.PEPTIDES.2010.02.001

Muñoz, F., Palomares-Jerez, M. F., Daleo, G., Villalaín, J., & Guevara, M. G. (2011). Cholesterol and membrane phospholipid compositions modulate the leakage capacity of the swaposin domain from a potato aspartic protease (StAsp-PSI). *Biochimica et Biophysica Acta - Molecular and Cell Biology of Lipids*, *1811*(12), 1038–1044. https://doi.org/10.1016/J.BBALIP.2011.08.013

Muñoz, F., Palomares-Jerez, M. F., Daleo, G., Villalaín, J., & Guevara, M. G. (2014). Possible mechanism of structural transformations induced by StAsp-PSI in lipid membranes. *Biochimica et Biophysica Acta*, *1838*(1 Pt B), 339–347. https://doi.org/10.1016/J.BBAMEM.2013.08.004

Müntz, K. (1998). Deposition of storage proteins. *Plant Molecular Biology*, *38*(1–2), 77–99. https://doi.org/10.1007/978-94-011-5298-3_4/COVER

Murphy, K. A., Kuhle, R. A., Fischer, A. M., Anterola, A. M., & Grimes, H. D. (2005). The functional status of paraveinal mesophyll vacuoles changes in response to altered metabolic conditions in soybean leaves. *Functional Plant Biology : FPB*, *32*(4), 335–344. https://doi.org/10.1071/FP05006

Mutlu, A., & Susannah, G. (1999). Plant aspartic proteinases: Enzymes on the way to a function. *Physiologia Plantarum*, *105*(3), 569–576. https://doi.org/10.1034/J.1399-3054.1999.105324.X

Nakamura, K., & Matsuoka, K. (1993). Protein targeting to the vacuole in plant cells. *Plant Physiology*, *101*(1), 1. https://doi.org/10.1104/PP.101.1.1

Nakano, R. T., Yamada, K., Bednarek, P., Nishimura, M., & Hara-Nishimura, I. (2014). ER bodies in plants of the Brassicales order: Biogenesis and association with innate immunity. *Frontiers in Plant Science*, *5*(MAR), 80528. https://doi.org/10.3389/FPLS.2014.00073/BIBTEX

Nebenführ, A. (2002). Vesicle traffic in the endomembrane system: A tale of COPs, Rabs and SNAREs. *Current Opinion in Plant Biology*, *5*(6), 507–512. https://doi.org/10.1016/S1369-5266(02)00303-5

Neuhaus, J. M., & Rogers, J. C. (1998a). Sorting of proteins to vacuoles in plant cells. *Plant Molecular Biology*, *38*(1–2), 127–144.

Neuhaus, J. M., & Rogers, J. C. (1998b). Sorting of proteins to vacuoles in plant cells. *Plant Molecular Biology*, *38*(1–2), 127–144. https://doi.org/10.1007/978-94-011-5298-3_7

Neuhaus, J. M., Sticher, L., Meins, F., & Boller, T. (1991). A short C-terminal sequence is necessary and sufficient for the targeting of chitinases to the plant vacuole. *Proceedings of the National Academy of Sciences of the United States of America*, *88*(22), 10362. https://doi.org/10.1073/PNAS.88.22.10362

Niihama, M., Takemoto, N., Hashiguchi, Y., Tasaka, M., & Morita, M. T. (2009). ZIP Genes Encode Proteins Involved in Membrane Trafficking of the TGN–PVC/Vacuoles. *Plant and Cell Physiology*, *50*(12), 2057–2068. https://doi.org/10.1093/PCP/PCP137

Niihama, M., Uemura, T., Saito, C., Nakano, A., Sato, M. H., Tasaka, M., & Terao Morita, M. (2005). Conversion of Functional Specificity in Qb-SNARE VTI1 Homologues of Arabidopsis. *Current Biology*, *15*, 555–560. https://doi.org/10.1016/j.cub.2005.02.021

Nishizawa, K., Maruyama, N., & Utsumi, S. (2006). The C-terminal region of alpha' subunit of soybean beta-conglycinin contains two types of vacuolar sorting determinants. *Plant Molecular Biology*, *62*(1–2), 111–125. https://doi.org/10.1007/S11103-006-9007-0

Ohtomo, I., Ueda, H., Shimada, T., Nishiyama, C., Komoto, Y., Hara-Nishimura, I., & Takahashi, T. (2005). Identification of an allele of VAM3/SYP22 that confers a semi-dwarf phenotype in Arabidopsis thaliana. *Plant & Cell Physiology*, *46*(8), 1358–1365. https://doi.org/10.1093/PCP/PCI146

Okita, T. W., & Rogers, J. C. (1996a). COMPARTMENTATION OF PROTEINS IN THE ENDOMEMBRANE SYSTEM OF PLANT CELLS. *Annual Review of Plant Physiology and Plant Molecular Biology*, *47*(1), 327–350. https://doi.org/10.1146/ANNUREV.ARPLANT.47.1.327

Okita, T. W., & Rogers, J. C. (1996b). COMPARTMENTATION OF PROTEINS IN THE ENDOMEMBRANE SYSTEM OF PLANT CELLS. *Annual Review of Plant Physiology and Plant Molecular Biology*, *47*(1), 327–350. https://doi.org/10.1146/ANNUREV.ARPLANT.47.1.327

Olbrich, A., Hillmer, S., Hinz, G., Oliviusson, P., & Robinson, D. G. (2007). Newly formed vacuoles in root meristems of barley and pea seedlings have characteristics of both

protein storage and lytic vacuoles. *Plant Physiology*, *145*(4), 1383–1394. https://doi.org/10.1104/PP.107.108985

Oliveira, A., Pereira, C., Costa, D. S. da, Teixeira, J., Fidalgo, F., Pereira, S., & Pissarra, J. (2010). Characterization of aspartic proteinases in C. cardunculus L. callus tissue for its prospective transformation. *Plant Science*, *178*(2), 140–146. https://doi.org/10.1016/J.PLANTSCI.2009.11.008

Orci, L., Glick, B. S., & Rothman, J. E. (1986). A new type of coated vesicular carrier that appears not to contain clathrin: Its possible role in protein transport within the Golgi stack. *Cell*, *46*(2), 171–184. https://doi.org/10.1016/0092-8674(86)90734-8

Paez Valencia, J., Goodman, K., & Otegui, M. S. (2016). Endocytosis and Endosomal Trafficking in Plants. *Annual Review of Plant Biology*, *67*, 309–335. https://doi.org/10.1146/ANNUREV-ARPLANT-043015-112242

Paris, N., & Neuhaus, J. M. (2002). BP-80 as a vacuolar sorting receptor. *Plant Molecular Biology*, *50*(6), 903–914. https://doi.org/10.1023/A:1021205715324/METRICS

Paris, N., Rogers, S. W., Jiang, L., Kirsch, T., Beevers, L., Phillips, T. E., & Rogers, J. C. (1997). Molecular cloning and further characterization of a probable plant vacuolar sorting receptor. *Plant Physiology*, *115*(1), 29–39. https://doi.org/10.1104/PP.115.1.29

Paris, N., Stanley, C. M., Jones, R. L., & Rogers, J. C. (1996). Plant cells contain two functionally distinct vacuolar compartments. *Cell*, *85*(4), 563–572. https://doi.org/10.1016/S0092-8674(00)81256-8

Payie, K. G., Tanaka, T., Gal, S., & Yada, R. Y. (2003). Construction, expression and characterization of a chimaeric mammalian-plant aspartic proteinase. *The Biochemical Journal*, *372*(Pt 3), 671–678. https://doi.org/10.1042/BJ20021126

Peixoto, B., Pereira, S., Pereira, C., & Pissarra, J. (2018). Vacuolar Sorting Determinants: Isolation and Study. *Methods in Molecular Biology (Clifton, N.J.)*, *1789*, 21–31. https://doi.org/10.1007/978-1-4939-7856-4_3

Peixoto, B., Pereira, S., & Pissarra, J. (2016). *Plant Vacuolar Sorting: An Overview*. 67–94. https://doi.org/10.1007/124_2016_6

Pereira, C., Pereira, S., & Pissarra, J. (2014). Delivering of Proteins to the Plant Vacuole-An Update. *Int. J. Mol. Sci*, *15*, 7611–7623. https://doi.org/10.3390/ijms15057611

Pereira, C., Pereira, S., Satiat-Jeunemaitre, B., & Pissarra, J. (2013). Cardosin A contains two vacuolar sorting signals using different vacuolar routes in tobacco epidermal cells. *The Plant Journal : For Cell and Molecular Biology*, *76*(1), 87–100. https://doi.org/10.1111/TPJ.12274

Pereira, C. S., Da Costa, D. S., Pereira, S., De Moura Nogueira, F., Albuquerque, P. M., Teixeira, J., Faro, C., & Pissarra, J. (2008). Cardosins in postembryonic development of cardoon: towards an elucidation of the biological function of plant aspartic proteinases. *Protoplasma*, *232*(3–4), 203–213. https://doi.org/10.1007/S00709-008-0288-9

Pissarra, J., Pereira, C., Soares Da Costa, D., Figueiredo, R., Duarte, P., Teixeira, J., & Pereira, S. (2007). *From Flower to Seed Germination in Cynara cardunculus: A Role for Aspartic Proteinases.* https://repositorio-aberto.up.pt/handle/10216/82523

Pompa, A., De Marchis, F., Pallotta, M. T., Benitez-Alfonso, Y., Jones, A., Schipper, K., Moreau, K., Žárský, V., Di Sansebastiano, G. Pietro, & Bellucci, M. (2017). Unconventional Transport Routes of Soluble and Membrane Proteins and Their Role in Developmental Biology. *International Journal of Molecular Sciences*, *18*(4). https://doi.org/10.3390/IJMS18040703

PORTER, K. R. (1961). The Ground Substance; Observations from Electron Microscopy. *The Cell*, 621–675. https://doi.org/10.1016/B978-0-12-123302-0.50016-2

Pratelli, R., Sutter, J. U., & Blatt, M. R. (2004). A new catch in the SNARE. *Trends in Plant Science*, *9*(4), 187–195. https://doi.org/10.1016/J.TPLANTS.2004.02.007

Qi, X., & Grabowski, G. A. (2001). Differential Membrane Interactions of Saposins A and C: IMPLICATIONS FOR THE FUNCTIONAL SPECIFICITY. *Journal of Biological Chemistry*, *276*(29), 27010–27017. https://doi.org/10.1074/JBC.M101075200

Raiborg, C., Rusten, T. E., & Stenmark, H. (2003). Protein sorting into multivesicular endosomes. *Current Opinion in Cell Biology*, *15*(4), 446–455. https://doi.org/10.1016/S0955-0674(03)00080-2

Raimbault, A. K., Zuily-Fodil, Y., Soler, A., & Cruz de Carvalho, M. H. (2013). A novel aspartic acid protease gene from pineapple fruit (Ananas comosus): cloning, characterization and relation to postharvest chilling stress resistance. *Journal of Plant Physiology*, *170*(17), 1536–1540. https://doi.org/10.1016/J.JPLPH.2013.06.007

Ramalho-Santos, M., Pissarra, J., Veríssimo, P., Pereira, S., Salema, R., Pires, E., & Faro, C. J. (1997). Cardosin A, an abundant aspartic proteinase, accumulates in protein storage vacuoles in the stigmatic papillae of Cynara cardunculus L. *Planta*, *203*(2), 204–212. https://doi.org/10.1007/S004250050183

Ramalho-Santos, M., Verissimo, P., Cortes, L., Samyn, B., Beeumen, J. V., Pires, E., & Faro, C. (1998). Identification and proteolytic processing of procardosin A. *European Journal of Biochemistry*, *255*(1), 133–138. https://doi.org/10.1046/J.1432-1327.1998.2550133.X

Robinson, D. G. (2020). Plant Golgi ultrastructure. *Journal of Microscopy*, *280*(2), 111–121. https://doi.org/10.1111/JMI.12899

Robinson, D. G., Hinz, G., & Holstein, S. E. H. (1998). The molecular characterization of transport vesicles. *Plant Molecular Biology*, *38*(1–2), 49–76. https://doi.org/10.1007/978-94-011-5298-3_3

Robinson, D. G., Jiang, L., & Schumacher, K. (2008). The Endosomal System of Plants: Charting New and Familiar Territories. *Plant Physiology*, *147*(4), 1482–1492. https://doi.org/10.1104/PP.108.120105

Robinson, D. G., & Neuhaus, J. M. (2016). Receptor-mediated sorting of soluble vacuolar proteins: myths, facts, and a new model. *Journal of Experimental Botany*, *67*(15), 4435–4449. https://doi.org/10.1093/JXB/ERW222

Robinson, D. G., Oliviusson, P., & Hinz, G. (2005). Protein sorting to the storage vacuoles of plants: a critical appraisal. *Traffic (Copenhagen, Denmark)*, *6*(8), 615–625. https://doi.org/10.1111/J.1600-0854.2005.00303.X

Robinson, D. G., & Pimpl, P. (2014). Clathrin and post-Golgi trafficking: a very complicated issue. *Trends in Plant Science*, *19*(3), 134–139. https://doi.org/10.1016/J.TPLANTS.2013.10.008

Robinson, D., Hoh, B., Hinz, G., physiology, B. J.-J. of plant, & 1995, undefined. (n.d.). One vacuole or two vacuoles: do protein storage vacuoles arise de novo during pea cotyledon development? *Elsevier*. Retrieved September 1, 2023, from https://www.sciencedirect.com/science/article/pii/S0176161711812782

Rogers, J. C. (2008). Multiple vacuoles in plant cells. *Plant Physiology*, *146*(3), 1024–1025. https://doi.org/10.1104/PP.107.900248

Rojo, E., & Denecke, J. (2008). What Is Moving in the Secretory Pathway of Plants? *Plant Physiology*, *147*(4), 1493–1503. https://doi.org/10.1104/PP.108.124552

Rothman, J. E. (2002). The machinery and principles of vesicle transport in the cell. *Nature Medicine*, *8*(10), 1059–1062. https://doi.org/10.1038/NM770

Rothman, J. E., & Wieland, F. T. (1996). Protein sorting by transport vesicles. *Science (New York, N.Y.)*, *272*(5259), 227–234. https://doi.org/10.1126/SCIENCE.272.5259.227

Rouillé, Y., Rohn, W., & Hoflack, B. (2000). Targeting of lysosomal proteins. *Seminars in Cell & Developmental Biology*, *11*(3), 165–171. https://doi.org/10.1006/SCDB.2000.0168

RUNEBERG-ROOS, P., TÖRMÄKANGAS, K., & ÖSTMAN, A. (1991). Primary structure of a barley-grain aspartic proteinase. *European Journal of Biochemistry*, *202*(3), 1021–1027. https://doi.org/10.1111/J.1432-1033.1991.TB16465.X

Saito, C., & Ueda, T. (2009a). Chapter 4: functions of RAB and SNARE proteins in plant life. *International Review of Cell and Molecular Biology*, *274*(C), 183–233. https://doi.org/10.1016/S1937-6448(08)02004-2

Saito, C., & Ueda, T. (2009b). Chapter 4 Functions of RAB and SNARE Proteins in Plant Life. *International Review of Cell and Molecular Biology*, *274*(C), 183–233. https://doi.org/10.1016/S1937-6448(08)02004-2

Sampaio, M. (2020). *Dissect the PSIs' interaction network involved in conventional and unconventional sorting routes*. Faculty of Sciences of Porto.

Sanderfoot, A. (2007). Increases in the Number of SNARE Genes Parallels the Rise of Multicellularity among the Green Plants. *Plant Physiology*, *144*(1), 6–17. https://doi.org/10.1104/PP.106.092973

Sanderfoot, A. A., Assaad, F. F., & Raikhel, N. V. (2000). The Arabidopsis genome. An abundance of soluble N-ethylmaleimide-sensitive factor adaptor protein receptors. *Plant Physiology*, *124*(4), 1558–1569. https://doi.org/10.1104/PP.124.4.1558

Sanderfoot, A. A., Kovaleva, V., Bassham, D. C., & Raikhel, N. V. (2001a). Interactions between Syntaxins Identify at Least Five SNARE Complexes within the Golgi/Prevacuolar System of the Arabidopsis Cell. *Molecular Biology of the Cell*, *12*(12), 3733. https://doi.org/10.1091/MBC.12.12.3733

Sanderfoot, A. A., Kovaleva, V., Bassham, D. C., & Raikhel, N. V. (2001b). Interactions between Syntaxins Identify at Least Five SNARE Complexes within the Golgi/Prevacuolar System of the Arabidopsis Cell. *Molecular Biology of the Cell*, *12*(12), 3733. https://doi.org/10.1091/MBC.12.12.3733

Sanderfoot, A. A., Kovaleva, V., Bassham, D. C., & Raikhel, N. V. (2001c). Interactions between Syntaxins Identify at Least Five SNARE Complexes within the Golgi/Prevacuolar System of the Arabidopsis Cell. *Molecular Biology of the Cell*, *12*(12), 3733. https://doi.org/10.1091/MBC.12.12.3733

Sanderfoot, A. A., Kovaleva, V., Zheng, H., & Raikhel, N. V. (1999). The t-SNARE AtVAM3p resides on the prevacuolar compartment in Arabidopsis root cells. *Plant Physiology*, *121*(3), 929–938. https://doi.org/10.1104/PP.121.3.929

Sanderfoot, A. A., Pilgrim, M., Adam, L., & Raikhel, N. V. (2001). Disruption of Individual Members of Arabidopsis Syntaxin Gene Families Indicates Each Has Essential Functions. *The Plant Cell*, *13*(3), 659. https://doi.org/10.1105/TPC.13.3.659

Sanderfoot, A. A., & Raikhel, N. V. (1999). The specificity of vesicle trafficking: coat proteins and SNAREs. *The Plant Cell*, *11*(4), 629–641. https://doi.org/10.1105/TPC.11.4.629

Sanmartín, M., Ordóñez, A., Sohn, E. J., Robert, S., Sánchez-Serrano, J. J., Surpin, M. A., Raikhel, N. V., & Rojo, E. (2007). Divergent functions of VTI12 and VTI11 in trafficking to storage and lytic vacuoles in Arabidopsis. *Proceedings of the National Academy of Sciences*, *104*(9), 3645–3650. https://doi.org/10.1073/PNAS.0611147104

Sato, M. H., Nakamura, N., Ohsumi, Y., Kouchi, H., Kondo, M., Hara-Nishimura, I., Nishimura, M., & Wada, Y. (1997). The AtVAM3 encodes a syntaxin-related molecule implicated in the vacuolar assembly in Arabidopsis thaliana. *The Journal of Biological Chemistry*, *272*(39), 24530–24535. https://doi.org/10.1074/JBC.272.39.24530

Schmitz, A., & Herzog, V. (2004). Endoplasmic reticulum-associated degradation: exceptions to the rule. *European Journal of Cell Biology*, *83*(10), 501–509. https://doi.org/10.1078/0171-9335-00412

Schneider, C. A., Rasband, W. S., & Eliceiri, K. W. (2012). NIH Image to ImageJ: 25 years of image analysis. *Nature Methods*, *9*(7), 671–675. https://doi.org/10.1038/NMETH.2089

Schröder, M., & Kaufman, R. J. (2005a). ER stress and the unfolded protein response. *Mutation Research*, *569*(1–2), 29–63. https://doi.org/10.1016/J.MRFMMM.2004.06.056

Schröder, M., & Kaufman, R. J. (2005b). The mammalian unfolded protein response. *Annual Review of Biochemistry*, *74*, 739–789. https://doi.org/10.1146/ANNUREV.BIOCHEM.73.011303.074134

Schroeder, M. R., Borkhsenious, O. N., Matsuoka, K., Nakamura, K., & Raikhel, N. V. (1993). Colocalization of barley lectin and sporamin in vacuoles of transgenic tobacco plants. *Plant Physiology*, *101*(2), 451. https://doi.org/10.1104/PP.101.2.451

Seaman, M. N. J. (2005). Recycle your receptors with retromer. *Trends in Cell Biology*, *15*(2), 68–75. https://doi.org/10.1016/j.tcb.2004.12.004

Shimada, T., … M. N.-P. and cell, & 1994, undefined. (n.d.). Small GTP-binding proteins are associated with the vesicles that are targeted to vacuoles in developing pumpkin cotyledons. *Academic.Oup.ComT Shimada, M Nishimura, I Hara-NishimuraPlant and Cell Physiology, 1994•academic.Oup.Com*. Retrieved September 1, 2023, from https://academic.oup.com/pcp/article-abstract/35/7/995/1846148

Shimada, T., Fuji, K., Tamura, K., Kondo, M., Nishimura, M., & Hara-Nishimura, I. (2003a). Vacuolar sorting receptor for seed storage proteins in Arabidopsis thaliana. *Proceedings of the National Academy of Sciences of the United States of America*, *100*(26), 16095–16100. https://doi.org/10.1073/PNAS.2530568100

Shimada, T., Fuji, K., Tamura, K., Kondo, M., Nishimura, M., & Hara-Nishimura, I. (2003b). Vacuolar sorting receptor for seed storage proteins in Arabidopsis thaliana. *Proceedings of the National Academy of Sciences of the United States of America*, *100*(26), 16095. https://doi.org/10.1073/PNAS.2530568100

Shimada, T., Takagi, J., Ichino, T., Shirakawa, M., & Hara-Nishimura, I. (2018). Plant Vacuoles. *Https://Doi.Org/10.1146/Annurev-Arplant-042817-040508*, *69*(6), 123–145. https://doi.org/10.1146/ANNUREV-ARPLANT-042817-040508

Shirakawa, M., Ueda, H., Shimada, T., Koumoto, Y., Shimada, T. L., Kondo, M., Takahashi, T., Okuyama, Y., Nishimura, M., & Hara-Nishimura, I. (2010). Arabidopsis Qa-SNARE SYP2 proteins localized to different subcellular regions function redundantly in vacuolar protein sorting and plant development. *The Plant Journal : For Cell and Molecular Biology*, *64*(6), 924–935. https://doi.org/10.1111/J.1365-313X.2010.04394.X

Shirakawa, M., Ueda, H., Shimada, T., Nishiyama, C., & Hara-Nishimura, I. (2009). Vacuolar SNAREs Function in the Formation of the Leaf Vascular Network by

Regulating Auxin Distribution. *Plant and Cell Physiology*, *50*(7), 1319–1328. https://doi.org/10.1093/PCP/PCP076

Shivhare, D., Musialak-Lange, M., Julca, I., Gluza, P., & Mutwil, M. (2021). Removing auto-activators from yeast-two-hybrid assays by conditional negative selection. *Scientific Reports 2021 11:1*, *11*(1), 1–9. https://doi.org/10.1038/s41598-021-84608-9

Simões, I., & Faro, C. (2004). Structure and function of plant aspartic proteinases. *European Journal of Biochemistry*, *271*(11), 2067–2075. https://doi.org/10.1111/J.1432-1033.2004.04136.X

Simões, I., Faro, R., Bur, D., Kay, J., & Faro, C. (2011). Shewasin A, an active pepsin homolog from the bacterium Shewanella amazonensis. *The FEBS Journal*, *278*(17), 3177–3186. https://doi.org/10.1111/J.1742-4658.2011.08243.X

Soares, A., Ribeiro Carlton, S. M., & Simões, I. (2019). Atypical and nucellin-like aspartic proteases: emerging players in plant developmental processes and stress responses. *Journal of Experimental Botany*, *70*(7), 2059–2076. https://doi.org/10.1093/JXB/ERZ034

Söllner, T., Whiteheart, S. W., Brunner, M., Erdjument-Bromage, H., Geromanos, S., Tempst, P., & Rothman, J. E. (1993). SNAP receptors implicated in vesicle targeting and fusion. *Nature 1993 362:6418*, *362*(6418), 318–324. https://doi.org/10.1038/362318a0

Souza Cândido, E., Pinto, M. F. S., Pelegrini, P. B., Lima, T. B., Silva, O. N., Pogue, R., Grossi-de-Sá, M. F., & Franco, O. L. (2011). Plant storage proteins with antimicrobial activity: novel insights into plant defense mechanisms. *FASEB Journal : Official Publication of the Federation of American Societies for Experimental Biology*, *25*(10), 3290–3305. https://doi.org/10.1096/FJ.11-184291

Sparkes, I. A., Ketelaar, T., De Ruijter, N. C. A., & Hawes, C. (2009). Grab a golgi: Laser trapping of golgi bodies reveals in vivo interactions with the endoplasmic reticulum. *Traffic*, *10*(5), 567–571. https://doi.org/10.1111/J.1600-0854.2009.00891.X

Staehelin, L. A. (1997a). The plant ER: a dynamic organelle composed of a large number of discrete functional domains. *The Plant Journal*, *11*(6), 1151–1165. https://doi.org/10.1046/J.1365-313X.1997.11061151.X

Staehelin, L. A. (1997b). The plant ER: a dynamic organelle composed of a large number of discrete functional domains. *The Plant Journal : For Cell and Molecular Biology*, *11*(6), 1151–1165. https://doi.org/10.1046/J.1365-313X.1997.11061151.X

Staehelin, L. A. (1997c). The plant ER: a dynamic organelle composed of a large number of discrete functional domains. *The Plant Journal : For Cell and Molecular Biology*, *11*(6), 1151–1165. https://doi.org/10.1046/J.1365-313X.1997.11061151.X

Stefan, C. J., Manford, A. G., & Emr, S. D. (2013). ER–PM connections: sites of information transfer and inter-organelle communication. *Current Opinion in Cell Biology*, *25*(4), 434. https://doi.org/10.1016/J.CEB.2013.02.020

Stefano, G., Hawes, C., & Brandizzi, F. (2014a). ER - the key to the highway. *Current Opinion in Plant Biology*, *22*, 30–38. https://doi.org/10.1016/J.PBI.2014.09.001

Stefano, G., Hawes, C., & Brandizzi, F. (2014b). ER - the key to the highway. *Current Opinion in Plant Biology*, *22*, 30–38. https://doi.org/10.1016/J.PBI.2014.09.001

Stigliano, E., Faraco, M., Neuhaus, J. M., Montefusco, A., Dalessandro, G., Piro, G., & Di Sansebastiano, G. Pietro. (2013). Two glycosylated vacuolar GFPs are new markers for ER-to-vacuole sorting. *Plant Physiology and Biochemistry : PPB*, *73*, 337–343. https://doi.org/10.1016/J.PLAPHY.2013.10.010

Strasser, R. (2016). Plant protein glycosylation. *Glycobiology*, *26*(9), 926–939. https://doi.org/10.1093/GLYCOB/CWW023

Strasser, R. (2018). Protein Quality Control in the Endoplasmic Reticulum of Plants. *Annual Review of Plant Biology*, *69*, 147–172. https://doi.org/10.1146/ANNUREV-ARPLANT-042817-040331

Suda, Y., & Nakano, A. (2012). The Yeast Golgi Apparatus. *Traffic*, *13*(4), 505–510. https://doi.org/10.1111/J.1600-0854.2011.01316.X

Suen, P. K., Shen, J., Sun, S. S. M., & Jiang, L. (2010). Expression and characterization of two functional vacuolar sorting receptor (VSR) proteins, BP-80 and AtVSR4 from culture media of transgenic tobacco BY-2 cells. *Plant Science*, *179*(1–2), 68–76. https://doi.org/10.1016/J.PLANTSCI.2010.04.008

Sun, Z., & Brodsky, J. L. (2019). Protein quality control in the secretory pathway. *The Journal of Cell Biology*, *218*(10), 3171–3187. https://doi.org/10.1083/JCB.201906047

Surpin, M., & Raikhel, N. (2004). Traffic jams affect plant development and signal transduction. *Nature Reviews. Molecular Cell Biology*, *5*(2), 100–109. https://doi.org/10.1038/NRM1311

Surpin, M., Zheng, H., Morita, M. T., Saito, C., Avila, E., Blakeslee, J. J., Bandyopadhyay, A., Kovaleva, V., Carter, D., Murphy, A., Tasaka, M., & Raikhel, N. (2003). The VTI Family of SNARE Proteins Is Necessary for Plant Viability and Mediates Different Protein Transport Pathways. *The Plant Cell*, *15*(12), 2885. https://doi.org/10.1105/TPC.016121

Swanson, S. J., & Jones, R. L. (1996). Gibberellic Acid Induces Vacuolar Acidification in Barley Aleurone. *The Plant Cell*, *8*(12), 2211–2221. https://doi.org/10.1105/TPC.8.12.2211

Teckman, J. H., & Perlmutter, D. H. (2000). Retention of mutant α1-antitrypsin Z in endoplasmic reticulum is associated with an autophagic response. *American Journal of Physiology - Gastrointestinal and Liver Physiology*, *279*(5 42-5). https://doi.org/10.1152/AJPGI.2000.279.5.G961/ASSET/IMAGES/LARGE/H31100158013.JPEG

Terauchi, K., Asakura, T., Nishizawa, N., Matsumoto, I., & Abe, K. (2004). Characterization of the genes for two soybean aspartic proteinases and analysis of their different tissue-dependent expression. *Planta*. https://doi.org/10.1007/S00425-003-1179-0

Terauchi, K., Asakura, T., Ueda, H., Tamura, T., Tamura, K., Matsumoto, I., Misaka, T., Hara-Nishimura, I., & Abe, K. (2006). Plant-specific insertions in the soybean aspartic proteinases, soyAP1 and soyAP2, perform different functions of vacuolar targeting. *Journal of Plant Physiology*, *163*(8), 856–862. https://doi.org/10.1016/J.JPLPH.2005.08.007

Törmäkangas, K., Hadlington, J. L., Pimpl, P., Hillmer, S., Brandizzi, F., Teeri, T. H., & Denecke, J. (2001). A Vacuolar Sorting Domain May Also Influence the Way in Which Proteins Leave the Endoplasmic Reticulum. *The Plant Cell*, *13*(9), 2021–2032. https://doi.org/10.1105/TPC.13.9.2021

Tse, Y. C., Mo, B., Hillmer, S., Zhao, M., Lo, S. W., Robinson, D. G., & Jiang, L. (2004). Identification of Multivesicular Bodies as Prevacuolar Compartments in Nicotiana tabacum BY-2 Cells. *The Plant Cell*, *16*(3), 672. https://doi.org/10.1105/TPC.019703

Ueda, H., Nishiyama, C., Shimada, T., Koumoto, Y., Hayashi, Y., Kondo, M., Takahashi, T., Ohtomo, I., Nishimura, M., & Hara-Nishimura, I. (2006). AtVAM3 is required for normal specification of idioblasts, myrosin cells. *Plant & Cell Physiology*, *47*(1), 164–175. https://doi.org/10.1093/PCP/PCI232

Uemura, T., Morita, M. T., Ebine, K., Okatani, Y., Yano, D., Saito, C., Ueda, T., & Nakano, A. (2010). Vacuolar/pre-vacuolar compartment Qa-SNAREs VAM3/SYP22 and PEP12/SYP21 have interchangeable functions in Arabidopsis. *The Plant Journal : For Cell and Molecular Biology*, *64*(5), 864–873. https://doi.org/10.1111/J.1365-313X.2010.04372.X

Vaccaro, A. M., Salvioli, R., Tatti, M., & Ciaffoni, F. (1999). Saposins and their interaction with lipids. *Neurochemical Research*, *24*(2), 307–314. https://doi.org/10.1023/A:1022530508763

Van der Wilden, W., Herman, E. M., & Chrispeels, M. J. (1980). Protein bodies of mung bean cotyledons as autophagic organelles. *Proceedings of the National Academy of Sciences*, *77*(1), 428–432. https://doi.org/10.1073/PNAS.77.1.428

Vembar, S. S., & Brodsky, J. L. (2008). One step at a time: endoplasmic reticulum-associated degradation. *Nature Reviews. Molecular Cell Biology*, *9*(12), 944–957. https://doi.org/10.1038/NRM2546

Veríssimo, P., Faro, C., Moir, A. J. G., Lin, Y., Tang, J., & Pires, E. (1996). Purification, characterization and partial amino acid sequencing of two new aspartic proteinases from fresh flowers of Cynara cardunculus L. *European Journal of Biochemistry*, *235*(3), 762–768. https://doi.org/10.1111/J.1432-1033.1996.00762.X

Vieira, M., Pissarra, J., Veríssimo, P., Castanheira, P., Costa, Y., Pires, E., & Faro, C. (2001). Molecular cloning and characterization of cDNA encoding cardosin B, an aspartic proteinase accumulating extracellularly in the transmitting tissue of Cynara cardunculus L. *Plant Molecular Biology*, *45*(5), 529–539. https://doi.org/10.1023/A:1010675015318/METRICS

Vieira, V., Peixoto, B., Costa, M., Pereira, S., Pissarra, J., & Pereira, C. (2019a). N-Linked Glycosylation Modulates Golgi-Independent Vacuolar Sorting Mediated by the Plant Specific Insert. *Plants 2019, Vol. 8, Page 312*, *8*(9), 312. https://doi.org/10.3390/PLANTS8090312

Vieira, V., Peixoto, B., Costa, M., Pereira, S., Pissarra, J., & Pereira, C. (2019b). N-Linked Glycosylation Modulates Golgi-Independent Vacuolar Sorting Mediated by

the Plant Specific Insert. *Plants (Basel, Switzerland)*, *8*(9). https://doi.org/10.3390/PLANTS8090312

Viotti, C., Bubeck, J., Stierhof, Y. D., Krebs, M., Langhans, M., van den Berg, W., van Dongen, W., Richter, S., Geldner, N., Takano, J., Jürgens, G., de Vries, S. C., Robinson, D. G., & Schumacher, K. (2010). Endocytic and secretory traffic in Arabidopsis merge in the trans-golgi network/early endosome, an independent and highly dynamic organelle. *Plant Cell*, *22*(4), 1344–1357. https://doi.org/10.1105/TPC.109.072637

Vision, T. J., Brown, D. G., & Tanksley, S. D. (2000). The origins of genomic duplications in Arabidopsis. *Science (New York, N.Y.)*, *290*(5499), 2114–2117. https://doi.org/10.1126/SCIENCE.290.5499.2114

Vitale, A., & Denecke, J. (1999). The endoplasmic reticulum-gateway of the secretory pathway. *The Plant Cell*, *11*(4), 615–628. https://doi.org/10.1105/TPC.11.4.615

Vitale, A., & Hinz, G. (2005). Sorting of proteins to storage vacuoles: How many mechanisms? *Trends in Plant Science*, *10*(7), 316–323. https://doi.org/10.1016/J.TPLANTS.2005.05.001

Vitale, A., & Raikhel, N. V. (1999). What do proteins need to reach different vacuoles? *Trends in Plant Science*, *4*(4), 149–155. https://doi.org/10.1016/S1360-1385(99)01389-8

Wallis, J. G., & Browse, J. (2010). Lipid biochemists salute the genome. *The Plant Journal : For Cell and Molecular Biology*, *61*(6), 1092–1106. https://doi.org/10.1111/J.1365-313X.2010.04125.X

Wang, T., Li, L., & Hong, W. (2017). SNARE proteins in membrane trafficking. *Traffic (Copenhagen, Denmark)*, *18*(12), 767–775. https://doi.org/10.1111/TRA.12524

Wenzel, D., Schauermann, G., Lüpke, A., Traffic, G. H.-, & 2005, undefined. (2005). The cargo in vacuolar storage protein transport vesicles is stratified. *Wiley Online LibraryD Wenzel, G Schauermann, A Lüpke, G HinzTraffic, 2005•Wiley Online Library*, *6*(1), 45–55. https://doi.org/10.1111/j.1600-0854.2004.00243.x

Wolfenstetter, S., Wirsching, P., Dotzauer, D., Schneider, S., & Sauer, N. (2012). Routes to the Tonoplast: The Sorting of Tonoplast Transporters in Arabidopsis Mesophyll Protoplasts. *The Plant Cell*, *24*(1), 215–232. https://doi.org/10.1105/TPC.111.090415

Xia, B., & Kang, X. (2011). Activation and maturation of SARS-CoV main protease. *Protein & Cell*, *2*(4), 282–290. https://doi.org/10.1007/S13238-011-1034-1

Xiang, L., Etxeberria, E., & Van Den Ende, W. (2013a). Vacuolar protein sorting mechanisms in plants. *FEBS Journal*, *280*(4), 979–993. https://doi.org/10.1111/FEBS.12092

Xiang, L., Etxeberria, E., & Van Den Ende, W. (2013b). Vacuolar protein sorting mechanisms in plants. *The FEBS Journal*, *280*(4), 979–993. https://doi.org/10.1111/FEBS.12092

Xie, Z., & Klionsky, D. J. (2007). Autophagosome formation: core machinery and adaptations. *Nature Cell Biology 2007 9:10*, *9*(10), 1102–1109. https://doi.org/10.1038/ncb1007-1102

Yamada, K., Hara-Nishimura, I., & Nishimura, M. (2011). Unique defense strategy by the endoplasmic reticulum body in plants. *Plant & Cell Physiology*, *52*(12), 2039–2049. https://doi.org/10.1093/PCP/PCR156

Yano, D., Sato, M., Saito, C., Sato, M. H., Terao Morita, M., & Tasaka, M. (2003a). A SNARE complex containing SGR3/AtVAM3 and ZIG/VTI11 in gravity-sensing cells is important for Arabidopsis shoot gravitropism. *Proceedings of the National Academy of Sciences of the United States of America*, *100*(14), 8589–8594. https://doi.org/10.1073/PNAS.1430749100

Yano, D., Sato, M., Saito, C., Sato, M. H., Terao Morita, M., & Tasaka, M. (2003b). A SNARE complex containing SGR3/AtVAM3 and ZIG/VTI11 in gravity-sensing cells is important for Arabidopsis shoot gravitropism. *Proceedings of the National Academy of Sciences of the United States of America*, *100*(14), 8589–8594. https://doi.org/10.1073/PNAS.1430749100

Zeng, Y., Liang, Z., Liu, Z., Li, B., Cui, Y., Gao, C., Shen, J., Wang, X., Zhao, Q., Zhuang, X., Erdmann, P. S., Wong, K. B., & Jiang, L. (2023). Recent advances in plant endomembrane research and new microscopical techniques. *New Phytologist*, *240*(1), 41–60. https://doi.org/10.1111/NPH.19134

Zhang, G. F., & Staehelin, L. A. (1992). Functional compartmentation of the Golgi apparatus of plant cells: Immunocytochemical analysis of high-pressure frozen- and freeze-substituted sycamore maple suspension culture cells. *Plant Physiology*, *99*(3), 1070–1083. https://doi.org/10.1104/PP.99.3.1070

Zhang, Y., & Hughson, F. M. (2021). Chaperoning SNARE Folding and Assembly. *Annual Review of Biochemistry*, *90*, 581–603. https://doi.org/10.1146/ANNUREV-BIOCHEM-081820-103615

Zhao, X., Tian, J. J., Yu, H., Bryksa, B. C., Dupuis, J. H., Ou, X., Qian, Z., Song, C., Wang, S., & Yada, R. Y. (2020). Insights into the mechanism of membrane fusion induced by the plant defense element, plant-specific insert. *Journal of Biological Chemistry*, *295*(43), 14548–14562. https://doi.org/10.1074/JBC.RA120.014311/ATTACHMENT/F201FD35-78A5-4772-A90A-418880117A24/MMC4.PDF

Zheng, H., & Andrew Staehelin, L. (2011). Protein storage vacuoles are transformed into lytic vacuoles in root meristematic cells of germinating seedlings by multiple, cell type-specific mechanisms. *Plant Physiology*, *155*(4), 2023–2035. https://doi.org/10.1104/PP.110.170159

Zouhar, J., Muñoz, A., & Rojo, E. (2010). Functional specialization within the vacuolar sorting receptor family: VSR1, VSR3 and VSR4 sort vacuolar storage cargo in seeds and vegetative tissues. *The Plant Journal : For Cell and Molecular Biology*, *64*(4), 577–588. https://doi.org/10.1111/J.1365-313X.2010.04349.X

Zouhar, J., Rojo, E., & Bassham, D. C. (2009). AtVPS45 is a positive regulator of the SYP41/SYP61/VTI12 SNARE complex involved in trafficking of vacuolar cargo. *Plant Physiology*, *149*(4), 1668–1678. https://doi.org/10.1104/PP.108.134361

Zwiewka, M., Feraru, E., Möller, B., Hwang, I., Feraru, M. I., Kleine-Vehn, J., Weijers, D., & Friml, J. (2011). The AP-3 adaptor complex is required for vacuolar function in Arabidopsis. *Cell Research 2011 21:12*, *21*(12), 1711–1722. https://doi.org/10.1038/cr.2011.99

7. Attachments

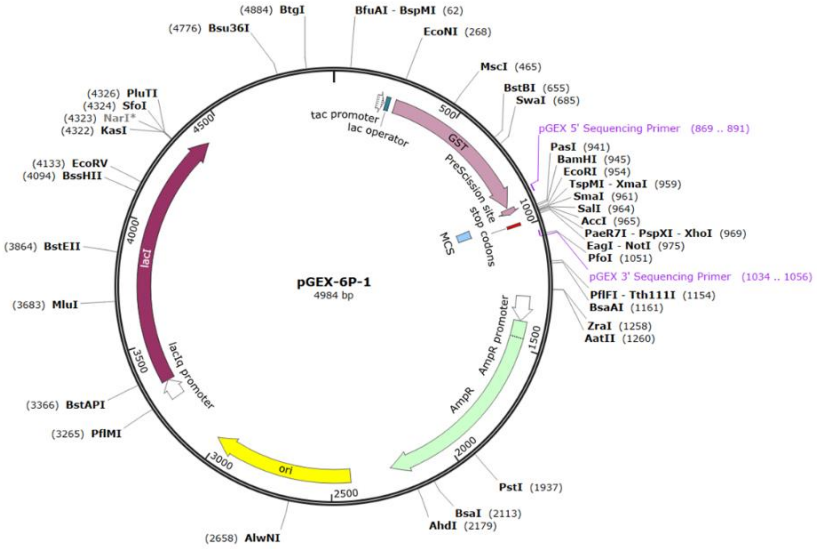

Supplementary figure 34. pGEX-6p-1 empty plasmid map.

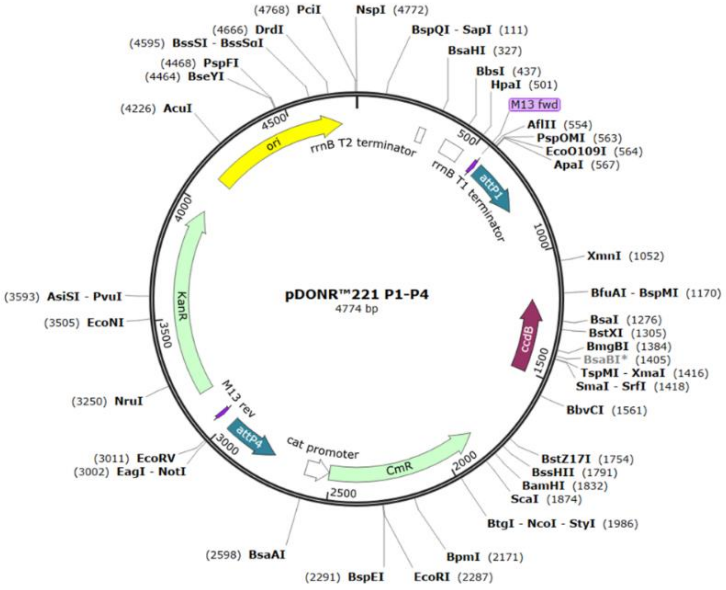

Supplementary figure 35. pDONR221-P1P4 empty plasmid map.

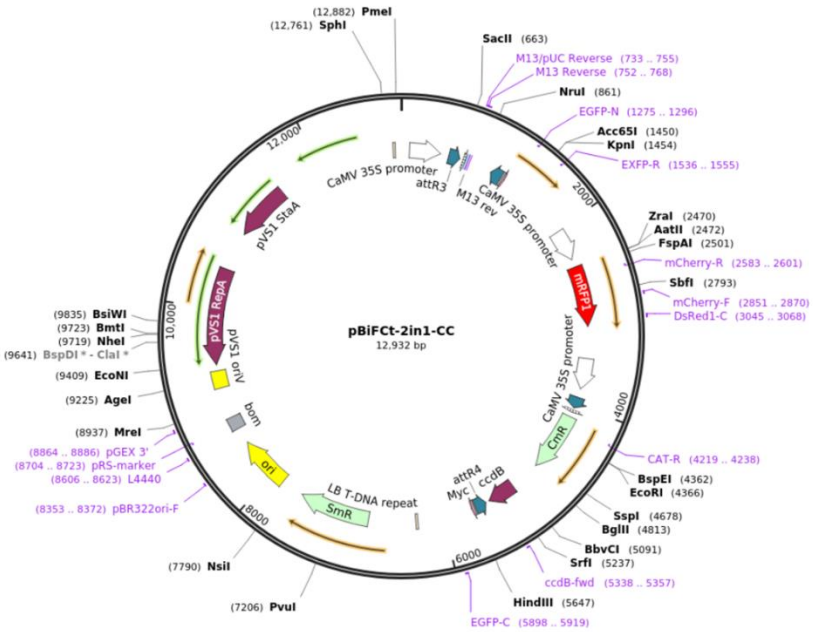

Supplementary figure 36. pBiFC-2 CC empty plasmid map.

Strains Used

AH109: MATa, trp1-901, leu2-3, 112, ura3-52, his3-200, gal4Δ, gal80Δ, LYS2: : $GAL1_{UAS}$- $GAL1_{TATA}$-HIS3, $GAL2_{UAS}$-$GAL2_{TATA}$-ADE2, URA3 : : $MEL1_{UAS}$-$MEL1_{TATA}$-lacZ

Y187: MATα, ura3-52, his3-200, ade2-101, trp1-901, leu2-3, 112, gal4Δ, met–, gal80Δ, URA3:: $GAL1_{UAS}$-$GAL1_{TATA}$-lacZ

Plasmid	Antibiotic Resistance	Y2H Strain	SM Plate
Bait plasmid pGBKT7	Kanamycin	AH109	SM (-) Trp
Prey Plasmid pGADT7	Ampicillin	Y187	SM (-) Leu

Plasmids Used

pGADT7 T-antigen – positive prey plasmid

pGADT7 empty - prey vector

pGBKT7 p53 - positive bait interactor with T-antigen

pGBKT7 empty - bait vector

Supplementary figure 37. Prey and bait Y2H plasmids.